UNIVERSITY OF PADUA

Department of Physics and Astronomy "Galileo Galilei"

Master Degree in Astrophysics and Cosmology

Outward Migration of Two Planets in Resonance

Thesis supervisor:

Prof. Francesco Marzari

Candidate:

Carlo Rizza

Academic Year 2022-23

Outward Migration of Two Planets in Resonance

Rizza Carlo[1]

[1]Department of Physics and Astronomy, University of Padova

Abstract

Studies of planet migration due to the interaction of the planets with the parent circumstellar disk are of paramount importance to understand the evolution of the orbital elements of exoplanets. It was shown that planet migration can lead to resonance capture, during which the planets exert a regular and periodic gravitational influence on each other. Depending on the details of the resonance process, this phenomenon can either stabilize or destabilize the orbits of the involved bodies. The case of a Jupiter-Saturn system shows the occurrence of a two-stage migration, based on the coupling between planet migration due to the interaction with the gaseous disk and a 3:2 mean motion resonance. In this work it was chosen to investigate via numerical modeling the effects of the model resolution on the migration of a Jupiter-Saturn pair locked in resonance. The choice of this type of analysis follows from the results obtained by recent 2-dimensional preliminary simulations performed with the hydrodynamical code FARGO3D. It was found that by increasing the resolution of the grid firstly by a factor of 2 and subsequently by a factor of 3, the results are different compared to the low-resolution case. In the high resolution case, it seems to be the second-order 5:3 mean motion resonance to drive the outward migration of the two-planets and not the usual 3:2 commensurability. The medium resolution case shows an intermediate behaviour, with a temporary capture in the 5:3 mean motion resonance and a final arrangement in the 3:2 commensurability. The obtained results raise several questions regarding whether the observed outcomes are due to an intrinsic issue within the FARGO3D code or if the resolution of the model indeed influences the type of resonance capable of driving the outward planet migration. In order to explore further this problem, an alternative hydrodynamical code, namely PLUTO, is employed to investigate the coupled evolution of a Jupiter-Saturn pair within its parent protoplanetary disk.

Contents

1 Introduction

The study of planet migration within circumstellar disks has revolutionized the understanding of planetary system formation and evolution, becoming a fundamental topic in the field of astrophysics. Over the past decades, numerous exoplanetary systems were discovered, revealing a rich diversity of planetary architectures and orbital configurations. In order to explain the complexity of these findings, the interaction between the planets and their parent gaseous disk represents one of the key processes that is able to cause large variations in the orbital elements of the planets. However, planet-planet and star-planet interactions are also needed to account for the diversity of the observed planetary systems, leading to significant changes in the semi-major axis, eccentricity and inclination of the involved bodies.

Among all these phenomena, the migration of a pair of planets in resonance within a circumstellar disk has attracted considerable attention, due to its relevance to the long-term stability and orbital architectures of planetary systems. Orbital resonances occur when two or more celestial bodies exert regular and periodic gravitational influences on each other, thus reinforcing or dampening their orbital motions. In particular, the most important resonance is the mean-motion resonance, which takes place when the orbital periods of the planets are commensurate, i.e. when they have a simple integer ratio. This process can significantly affect the orbital evolution of the involved bodies, as it can cause both resonant trapping, where planets maintain a stable configuration, and resonant destabilization, characterized by close encounters or even collisions.

The migration of resonant planet pairs within their parent circumstellar disks is a complex process governed by the interplay between tidal interactions, gravitational perturbations and disk-planet interactions. As a consequence, understanding the underlying mechanisms and the resulting dynamics is crucial for unraveling the formation and dynamical evolution of planetary systems.

In recent years, significant progress was made in theoretical modeling and numerical simulations aimed at studying the migration of resonant planet pairs in circumstellar disks. In particular, a study conducted by Masset & Snellgrove [31] has shown that a system composed of two closely spaced giant planets orbiting around a central star has the ability to migrate outwards within the parent disk, once the two planets are captured in resonance. Within this context, numerical simulations carried out by D'Angelo & Marzari [13] have demonstrated that the most favorable conditions for successful joint outward migration occur when the mass ratio between the inner and outer planets closely resembles that of Jupiter and Saturn. It follows that the Jupiter-Saturn system serves as a template for studying other planetary systems beyond the solar one and to interpret the observations of a multitude of exoplanets. According to these studies, the most accepted theory to

explain the formation, migration and dynamics of Jupiter and Saturn is the occurrence of a two-stage migration, based on the coupling between planet migration due to the interaction with the disk and a 3:2 mean motion resonance. Firstly, Jupiter underwent an initial inward migration, until it was caught up by Saturn. Once they get captured in resonance, both planets started to migrate outwards together, until the dispersion of the parent gaseous disk [58].

In this work, it was chosen to investigate via numerical modeling the effects of the model resolution on the migration of two planets locked in resonance. The choice of this type of analysis is due to the results obtained by recent 2-dimensional preliminary simulations performed with the hydrodynamical code FARGO3D. It was found that by increasing the resolution of the grid firstly by a factor of 2 and subsequently by a factor of 3, the results are different compared to the low-resolution case. In particular, in the high resolution case, it seems to be the second-order 5:3 mean motion resonance to drive the outward migration of the two-planets and not the usual 3:2 commensurability. The medium resolution case instead shows an intermediate behaviour, with a temporary capture in the 5:3 mean motion resonance and a final arrangement in the 3:2 commensurability. The obtained results raise several questions regarding whether the observed outcomes are due to an intrinsic issue within the FARGO3D code or if the resolution of the model indeed influences the type of resonance capable of driving the outward planet migration. In order to explore this further, an alternative hydrodynamical code, namely PLUTO, is employed to investigate the coupled evolution of a Jupiter-Saturn pair within its parent protoplanetary disk.

The work is organized as follows: in Section 2, a theoretical framework is provided for understanding the process of planet formation. Section 3 discusses the several interaction mechanisms between the planets and their gaseous parent disk. In section 4, the FARGO3D code is presented, together with the results of the preliminary simulations that inspired this work. Section 5 provides an illustration of the PLUTO code, with particular attention to the related configuration files and a comparison with the FARGO3D code. In section 6 the results of the simulations obtained with the PLUTO code are presented and discussed, including the effects of the model resolution on planets migration. Finally, in Section 7, the conclusions are summarized and avenues for future research are highlighted.

2 The Standard Model of Planet Formation

The standard model of planet formation, also known as the core accretion model, is a widely accepted framework that was developed in order to explain the origin of the Solar System and in particular the process by which planets form in circumstellar disks around young stars.

This model proposes a sequential series of steps that lead to the formation of planets. It starts with a molecular cloud made of gas and dust, which gravitationally collapses into a protostar. Since the infalling material possesses some amount of angular momentum, its conservation results in the formation of a rotating circumstellar disk of gas and dust that continues to feed the central young star.

As the disk gradually cools down, a dust sedimentation process takes place along the middle plane of the disk. From this dust, pebbles and planetesimals grow, giving rise to objects with dimensions larger than $1-100\ km$. Subsequently, collisions and gravitational accumulation occur, leading to the formation of terrestrial planets and the core of giants. Finally, the infall of gas on the core produces giant planets and the disk dissipates. A graphical representation of the various stages characterizing the standard model of planet formation is provided in Fig. 1.
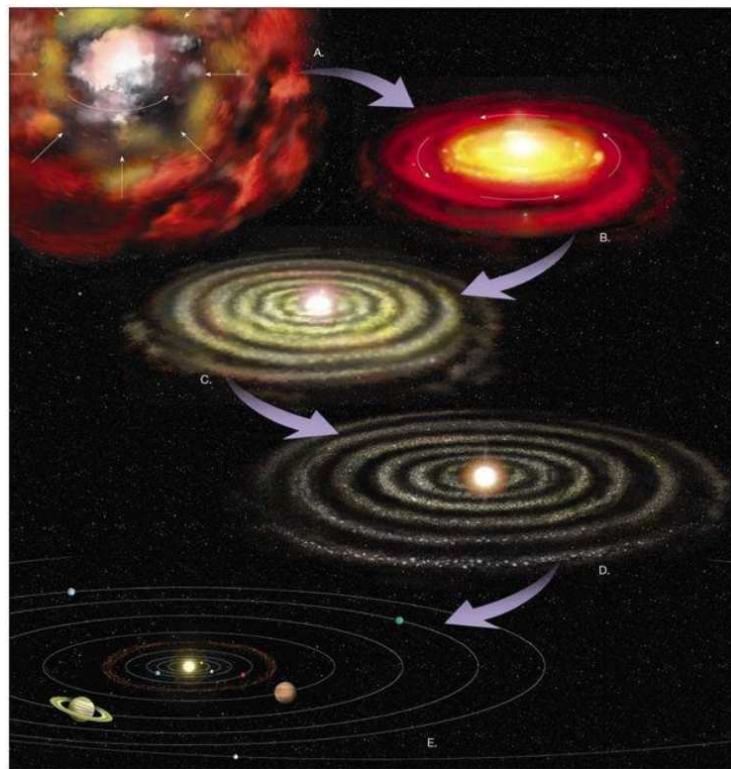

Figure 1: Graphical representation of the different steps that characterize the standard model of planet formation. Credit to Pearson Prentice Hall, Inc.

2.1 Circumstellar Disks

It was seen in Sec. 2 that a disk of rotating circumstellar material usually forms around a growing protostar as a consequence of angular momentum conservation during the cloud collapse.

Circumstellar disks, also known as protoplanetary disks, play a crucial role in the formation of planetary systems and they are believed to be the birthplaces of planets. These structures are made of gas and dust, with the latter being usually a fraction of the order of $\sim 1/100$ with respect to the other component. Note that the density of gas and dust in circumstellar disks decreases with increasing distance from the central star. The initial evolution of the disk is quite turbulent, due to the infall of dust and gas from the envelope and to the presence of jets in form of bipolar outflows. However, this phase is followed by a more quiet state, during which the dust settles towards the middle plane of the circumstellar disk [30].

Circumstellar disks are assumed to be in thermal equilibrium, due to the presence of three main mechanisms, i.e. viscous heating, star irradiation and radiative cooling. As a consequence of star irradiation, a temperature gradient is present within the disk, with higher temperatures in the inner regions. The so-called snow line marks the radial distance at which the disk temperature drops below the condensation temperature of a particular ice. This means that within this line the ices cannot condense and the only particles that are able to do it are mainly silicates and iron compounds. On the other hand, in the outer regions of the disk ices and gases are able to condense.

These structures can be detected mainly in two ways, i.e. by studying the infrared excess in the star spectrum or through direct imaging. In particular, the infrared excess is due to the fact that the dust present in the disk emits at a lower temperature with respect to the star, with a blackbody radiation falling within the infrared spectral range. Therefore, the presence of a disk is deduced by this additional infrared emission, as it is shown in Fig. 2. The infrared excess changes according to the disk evolution, since as the disk evolves the density and temperature profiles are different. This means that by measuring the infrared excess, it is possible to get information about the density and temperature profiles of the circumstellar disk.

The standard power-law disk model proposed by Beckwith et al. [4] provides the following expression for the superficial density profile of the disk ($\Sigma_0 \approx 10^2 - 10^4 \; g/cm^2$):

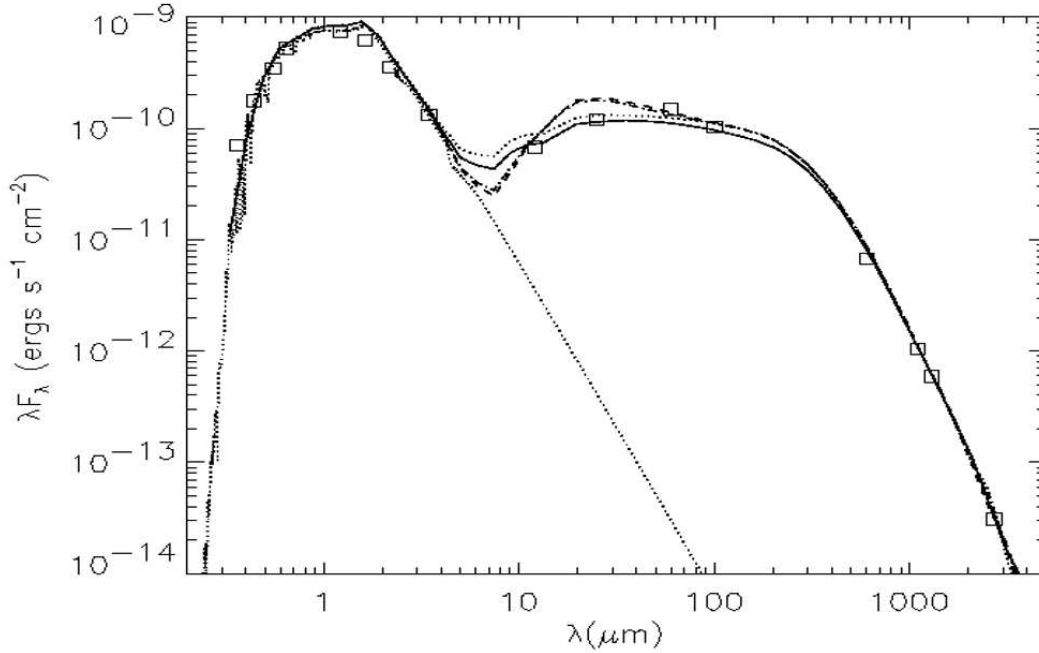$$\Sigma = \Sigma_0 \left(\frac{R}{R_0} \right)^{-p}$$

Figure 2: Spectral energy distribution (SED) of GM Aurigae, a classical T Tauri star. It shows a large infrared excess indicating the presence of a disk. From Schneider et al. [51].

Similarly, the temperature profile of the disk is given by ($T_0 \approx 1000 - 2000\ K$):

$$T(R) = T_0 \left(\frac{R}{R_0}\right)^{-q}$$

In these two expressions the quantity R_0 and the two coefficients q and p depend on the type of the star. By fitting the infrared excess it is possible to derive approximate values for Σ_0, T_0, q and p.

The vertical structure of the disk is described through the scale height $h = \frac{H}{R}$, where H is the height of the disk surface at radius R. The value of the scale height is constant in the flat disk model, being usually of the order of $h \approx 0.05$, while it grows going outwards in the flared disk model.

Regarding instead direct imaging observations, with the arrival of ALMA (Atacama Large Millimiter Array) high resolution images have become possible. They highlighted the fact that circumstellar disks are not regular structures, but they often present many different features. As shown in Fig 3, circumstellar disks can be characterized by the presence of gaps, spirals, inner holes and different gas and dust distributions. Thanks to ALMA it was possible to obtain a large sample of disks, thus leading to a statistical estimate of the

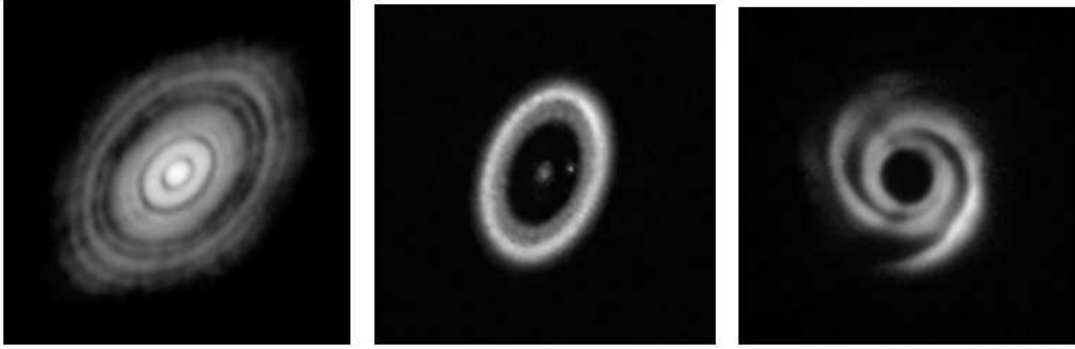fraction of stars with disk and of their lifetime.

Figure 3: Three examples of circumstellar disks imaged with ALMA. Credit to ALMA, ESO/NAOJ/NRAO.

Observations in the spectrum of several stars have shown that the viscous evolution of the disk leads to mass accretion onto the star, causing a transfer of angular momentum towards the outer regions. The accretion rate covers a wide range of values, being of the order of $\dot{M} \approx 10^{-12} \ M_\odot/yr$ for low mass stars up to $\dot{M} \approx 10^{-7} \ M_\odot/yr$ for more massive stars. According to the magnetospheric accretion model, the material on the inner border of the disk is ionized by the star radiation and it impacts the star following the magnetic disk lines, i.e. it impacts on a region around the two poles of the star if a dipole magnetic field is assumed. Therefore, accretion onto the star is deduced from the ultraviolet and optical excess at the shock, where the disk material impacts the star surface at a temperature of about $T \approx 10^4 \ K$. An example of ultraviolet emission is shown in Fig. 4. Within this context, it is worth to mention the work done by Hartmann et al. [20], who found a strong correlation between the mass of the star and the disk accretion rate:

$$\log(\dot{M}_{acc}) = -7.9 + 2.1 \log(M_s)$$

The long term evolution of a disk is determined by its viscous evolution, by photoevaporation and by planet formation. Let's assume to deal with a thin, axis-symmetric disk and to adopt the isothermal approximation. Moreover, let's suppose to have vertical equilibrium and that the radial velocity equals the Keplerian velocity. Under these hypotheses, the one-dimensional approximated continuity equation gives (ν is the viscosity, $\dot{\Sigma}_{PE}$ represents the photoevaporation term):

$$\frac{\partial \Sigma}{\partial t} - \frac{3}{r} \frac{\partial}{\partial r} \left(r^{\frac{1}{2}} \frac{\partial}{\partial r} |\Sigma \nu| \right) = -\dot{\Sigma}_{PE}$$
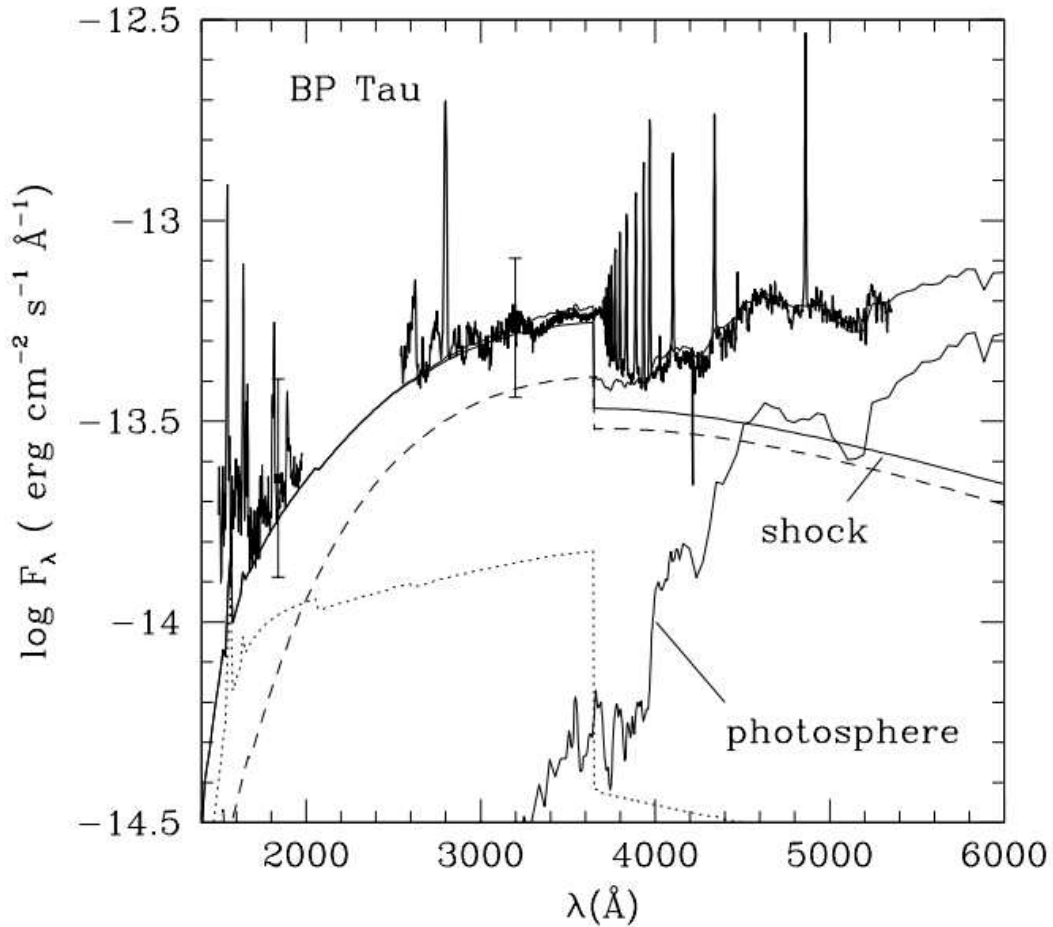
6

Figure 4: Ultraviolet emission of BP Tau. The mass accretion onto the star is deduced from the shock contribution to the spectral energy distribution (SED). From Gullbring et al. [19].

As a consequence of this evolution, disks have a finite lifetime, which appears to be of the order of $3 - 10\ Myr$. Moreover, younger regions are expected to have more massive disks as it is confirmed by comparing star forming regions of different ages. The central region of circumstellar disks in an advanced stage of evolution is characterized by the formation of a hole in the gas and dust density. At this stage, we talk about transition disks, which can be identified thanks to the infrared excess and in particular to the presence of a gap in the spectrum.

To conclude, the study of the properties and evolution of circumstellar disks is essential for understanding the processes that shape the different planetary architectures observed in the Universe. By investigating these structures, it is possible to gain insights into the mechanisms and conditions necessary for planet formation.

2.2 Planetesimal Formation

Planetesimal formation is a crucial process in the early stages of planetary formation within protoplanetary disks. The term planetesimals refers to solid bodies that serve as building blocks for planets, typically ranging from several kilometers to hundreds of kilometers in diameter. Once planetesimals have formed, they can merge and accrete more material to eventually form planets. However, the process of planetesimal formation is still an open problem in astrophysics, in particular concerning the mechanisms that built them up and their initial size distribution.

It was seen in Sec. 2.1 that during the quiet phase of the disk evolution, the dust settles towards the middle plane of the disk and it grows into larger bodies. This fact is due to the gas drag acting on the dust particles. In order to better understand this mechanism, let's assume the dust grains to be spherical, with a radius s smaller than the mean free path of the gas particles. The thermal velocity of the gas v_{th} is given by:

$$v_{th} = \sqrt{\frac{8k_B T}{\pi \mu m_H}}$$

In this expression, k_B is the Boltzmann constant, T is the absolute temperature defined by the ideal gas law, while the quantity μm_H gives the average molecular weight in terms of the hydrogen atom mass. If a dust grain moves with respect to the gas with velocity v, the frequency with which they collide head-on is equal to (ρ_g is the density of gas particles):

$$f = \pi s^2 \left(\frac{1}{3} v_{th} + v \right) \frac{\rho_g}{\mu m_H}$$

On the other hand, the same quantity computed in the opposite direction gives:

$$b = \pi s^2 \left(\frac{1}{3} v_{th} - v \right) \frac{\rho_g}{\mu m_H}$$

By assuming that $v_{th} \gg v$, each collision releases a momentum Δp equal to:

$$\Delta p = 2\mu m_H \frac{1}{3} v_{th}$$

It follows that a net force will act on the dust grain, due to its movement through the gas. This is the drag force F_D, which is by definition the force component in the direction of the flow velocity. The drag equation is also known as the Epstein drag law and it gives:

$$\vec{F}_D = -(f - b)\Delta p = -\frac{4}{3} \pi s^2 \rho_g v_{th} \vec{v} = F \vec{v}$$

The gravity force F_G is then opposed by the drag force F_D, so the motion of the dust grain in a viscous regime is described by the following expression:

$$ma = F_G - F_D = F_G - Fv \longrightarrow v(t) = \frac{F_G}{F}\left(1 - e^{-\frac{F}{m}t}\right)$$

In the limit $t \to \infty$, the previous equation becomes $v = \frac{F_G}{F}$. Therefore, the sedimentation speed in the median plane of a circumstellar disk is given by:

$$v_{settle} = \frac{F_G}{F} = \frac{GMmz}{r^3}\frac{3}{4\pi s^2 v_{th}\rho_g} = \frac{GM\rho_d zs}{r^3 v_{th}\rho_g}$$

By assuming that $z = 1\ AU$, the time required by the dust to sediment on the median plane is equal to:

$$t_{settle} = \frac{z}{v_{settle}} \approx 10^5\ yr$$

Instead, when the size of the dust grain is larger than the mean free path of the gas particles, the gas is treated as a fluid acting on the particle. In this case the drag force F_D is given by:

$$\vec{F}_D = -\frac{C_D}{2}\pi s^2 \rho_g v\vec{v}$$

In this expression the coefficient C_D depends on the Reynolds number[1] $\mathcal{R}$ and it is of the order of $C_D \approx 0.44$ at a distance of $1\ AU$.

As a result of the dust sedimentation process, the increased density of dust in the middle plane of the disk can facilitate the growth of larger bodies through coagulation and gravitational instabilities. Therefore, this process plays an important role in the evolution of protoplanetary disks and planetesimal formation.

In general, it is possible to trace a theoretical transition from dust particles to planetesimals when the drag of the gas becomes a perturbation with respect to the dominant Keplerian motion. This transition typically occurs at sizes of the order of $10\ km$ in diameter. For smaller sizes, the evolution is dominated by the gas and the motion is not Keplerian, i.e. when a particle moves around the star, it does not cross the median plane of the disk, but it is confined within the gas. On the other hand, for larger sizes the motion is Keplerian and planetesimals perform an orbit with a given inclination, thus crossing the median plane of the disk at the nodal line. Obviously, a sharp cut in size is not possible and there will be a slow transition from one kind of motion to the other depending on the size of the body.

Until not long ago, it was believed that the progressive accumulation of dust particles

---

[1]The Reynolds number is a dimensionless quantity used in fluid dynamics to characterize the flow of a fluid in different situations. In particular, it is defined as the ratio between the inertial forces and the viscous forces.

into larger bodies led directly to planetesimals through a series of two-body collisions. However, it was seen that there are many possible outcomes of dust particle collisions. According to Zsom et al. [63] and to what is described in Fig. 5, two particles may be subject to sticking (with partial or total mass transfer), bouncing (with partial or null mass transfer), fragmentation or erosion. The final outcome of collisions is strongly dependent on the mutual impact velocity between the two particles. In particular, if it is too high, fragmentation and erosion will dominate and the dust accumulation process is halted.
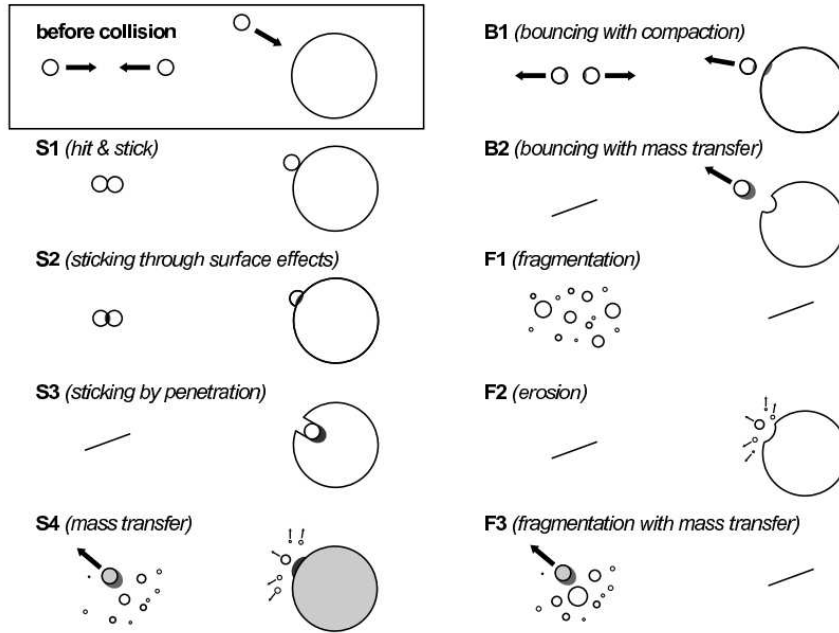

Figure 5: Different types of collision between dust particles. From Zsom et al. [63].

The relative velocity is determined by several contributes, i.e. the Brownian motion of the two particles, their differential vertical settling, their differential radial shift and the presence of turbulence. By combining all these contributions, the estimated relative velocity profile shows a sudden jump around pebble-size particles, as it is shown in Fig. 6. Laboratory experiments with these impact velocities performed by Wurm & Blum [9] have shown that accretion appears not to be possible for objects larger than about $10\ cm$, since in this case mass loss dominates, leading to the erosion or fragmentation of the bodies.

An additional negative factor for direct accumulation of dust particles into planetesimals is the so called meter-size barrier. This term refers to the fact that the interaction with the gas component of the disk leads to a fast spiraling of bodies of about $1\ m$ in size, although notable drift will begin already in the millimeter and centimeter size regimes. In particular, the inward radial velocity v_{rad} becomes comparable to the Keplerian velocity
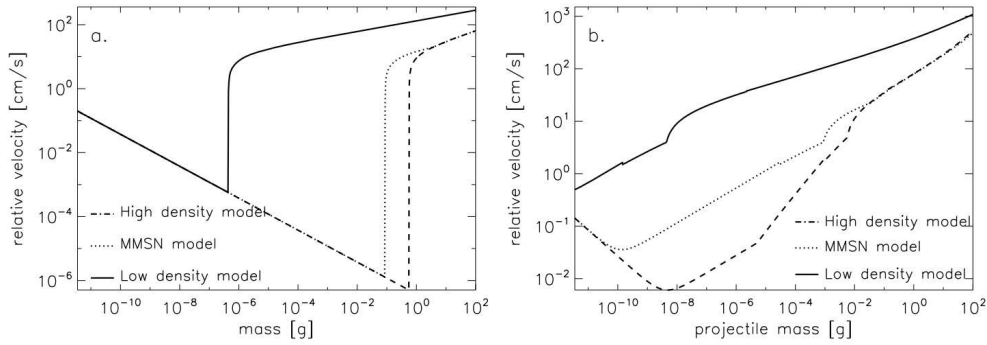
Figure 6: Combined relative velocities between dust particles caused by Brownian motion, radial drift, and turbulence in three different disk models for equal-sized particles (panel a) and for different-sized particles with a mass ratio of 100 (panel b). From Zsom et al. [63].

v_K, leading to a radial redistribution of matter:

$$v_{rad} = -0.5\eta v_K$$

As a consequence, the timescale to drift towards the star becomes of the order of $100 - 1000\ yr$. It follows that planetesimal formation must be rapid in order to occur, otherwise a further accumulation of dust particles may be prevented.

Alternative models on planetesimal formation with respect to the continuous growth of dust particles directly into larger bodies were proposed, by assuming a strong interaction with the gas. A first attempt supposes that the dust settles in the middle plane of the disk, where gravitational instabilities lead to the direct formation of planetesimals. However, this model does not consider the Kelvin-Helmholtz instability due to the back-reaction of dust on the gas, which creates turbulence that diffuses the dust particles and reduces the density below the value needed for gravitational instability to be effective.

A second attempt considers the streaming instability, i.e. a different type of instability that may lead to the clumping of a large number of dust particles into planetesimals. According to a study provided by Johansen & Youdin [23], the streaming instability predicts the formation of dense filaments in the gas, which trap the dust and become unstable to self-gravity. In this way, it creates a planetesimal size distribution, directly leading from centimeter size pebbles to the formation of large bodies with dimensions of the order of $100 - 200\ km$, skipping the $1 - 10\ km$ size phase. In order for this phenomenon to occur, it requires a high density in the middle plane for the back-reaction to be important, typically a dust-to-gas mass ratio of the order of ~ 1. It is interesting to note that the key ingredient for the streaming instability is the occurrence of pressure bumps where the dust is trapped, which in general can be produced by any kind of gas instability. The formation

11

of dense filaments in the gas due to the streaming instability is shown in the four different snapshots provided in Fig. 7
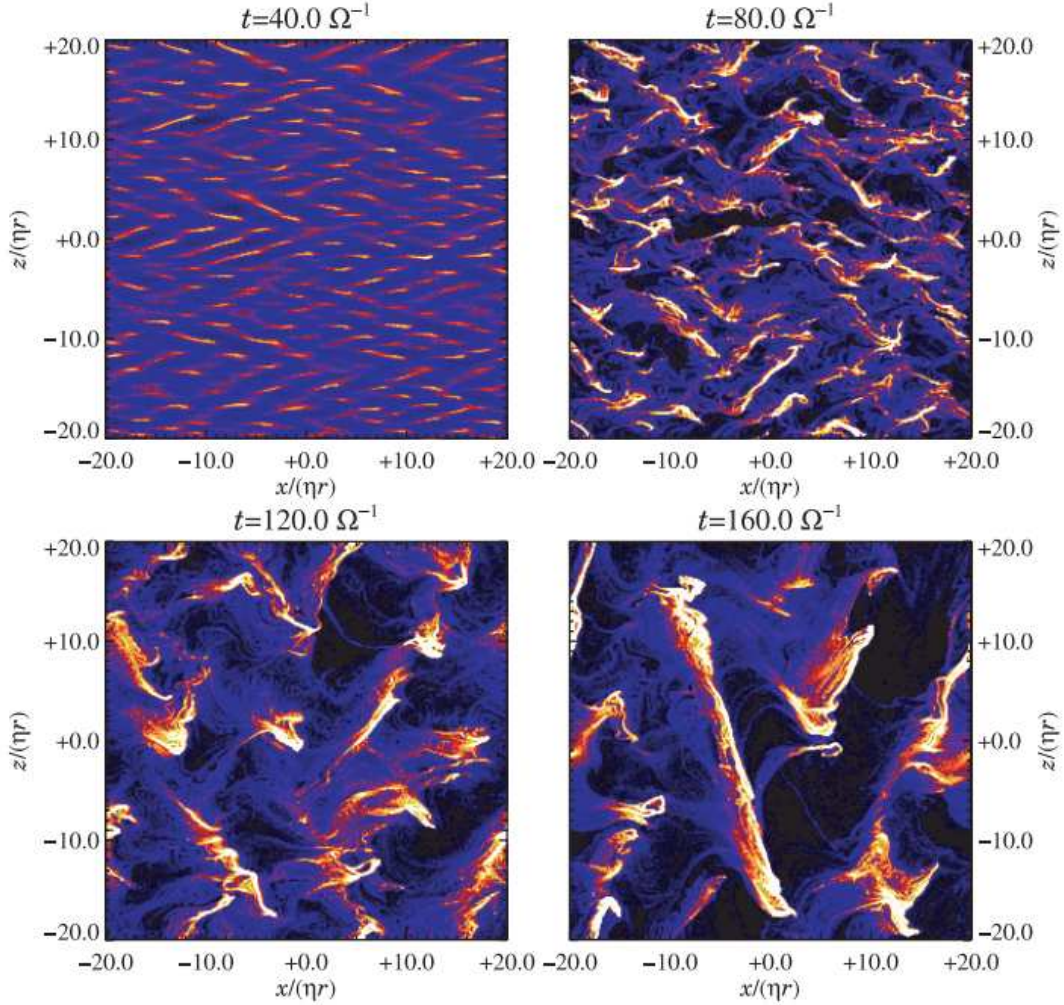
Figure 7: Four particle density snapshots. The evident linear wavelength in the top left panel results from the streaming instability feeding off the drift of the particles through the gas. Subsequent panels document the consequences of a self-consistently generated turbulence, i.e. the non-linear cascade of dense particle clumps into larger filaments. From Johansen & Youdin [23].

There are also other mechanisms which are able to trap dust particles into a restricted volume and trigger the gravitational instability needed to form planetesimals. For example, Drazkowska & Alibert [14] found that large icy grains coming from the outer regions of the disk may be trapped at the snow line and shrink due to evaporation. This would cause a slow down of the inward drift velocity, thus leading to a higher dust density. Alternatively, if magneto-rotational instability is responsible for the viscosity in the disk, a gas bump can form at the edges of a dead zone of low ionization and trap the dust, as studied

by Dzyurkevich et al. [15]. Finally, Pinilla et al. [48] found that as giant planets produce a gap in the gas, at the edges of these gaps dust accumulates because of the pressure bump and this can favor clumping.

2.3   Planet Formation

The process of planet formation refers to the planetesimal gravitational accumulation through mutual collisions. Once billions of planetesimals have formed around the protostar, they start to collide, forming bigger bodies if the condition of low relative velocity is satisfied. Otherwise, if the relative velocity between the colliding objects is large, they will undergo cratering in case of small mass ratio, or fragmentation in case of high mass ratio.

Planetesimal accretion can be divided in three different stages, i.e. the runaway growth, the oligarchic growth and the giant impacts phase (or chaotic growth). During the runaway growth phase, some planetesimals outrun the others and grow at a faster pace. This behaviour was studied thanks to the planet building code, which is a numerical model used to simulate planetesimal evolution and to estimate the timescale of planetesimal accumulation. From this model, it appears that after about $1\ Myr$ a large fraction of the initial mass is in a few bodies more massive than the remnant population, i.e. a family of protoplanets has formed. This phenomenon is shown in the three plots provided in Fig. 8.

The transition from runaway growth to oligarchic growth occurs when the protoplanets become massive enough to affect the random velocities of the other planetesimals. This typically happens when their mass is about 100 times the average mass of the total planetesimal population. At this point the protoplanets excite the eccentricities and inclinations of the planetesimals, thus increasing the relative velocity between the two types of objects. As a consequence, the growth regime switches to a slower one, although the mass ratio between protoplanets and planetesimals continues to increase with time. N-body simulations have shown that protoplanets tend to keep a typical orbital separation of 10 Hill's radius[2]. It follows that protoplanets grow oligarchically and no substantial accretion between the remaining planetesimals occurs. This fact was studied by Kokubo & Ida [26], who found the formation of a bi-modal mass distribution, composed of a large number of small planetesimals and a small number of protoplanets dominating the planetesimal system. After reaching a limit mass value that depends on their orbital separation,

---

[2]The Hill's sphere is the region where an astronomical body dominates the attraction of its satellites. This is a fundamental condition to differentiate between planets and moons, since a satellite must have an orbit that lies within the Hill's sphere of the planet in order to be considered a planet itself. By defining as m the mass of the satellite, as M the mass of the central body and as a the semi-major axis of the satellite, the Hill's radius is defined as $R_H = \left(\frac{m}{3M}\right)^{\frac{1}{3}} a$.
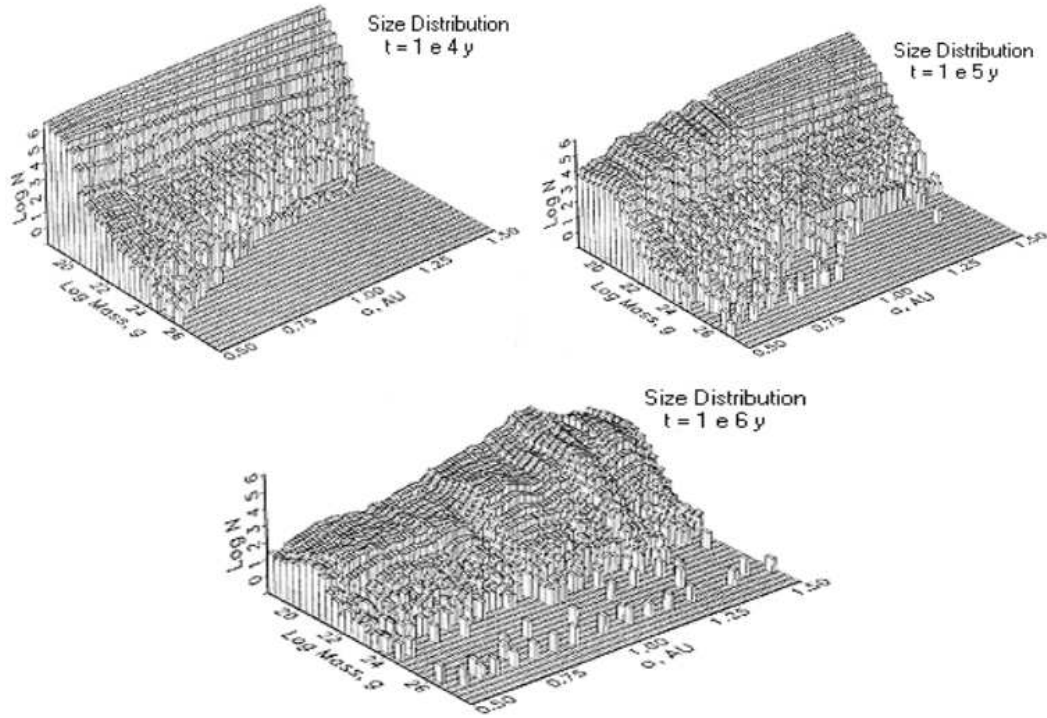
Figure 8: Planetesimal accumulation modelled with the planet-building code. An initial population of planetesimals is evolved through collisions until runaway growth occurs after approximately $1\ Myr$. On the x-axis there is the distance of the planetesimals from the star, on the y-axis their mass and on the z-axis the number of bodies with the values of mass and radial distance given in the (x, y)-axes. From Weidenschilling et al. [61].

on the dust density of the circumstellar disk and on the fraction of icy solid material, the protoplanets end up dynamically isolated and they do not grow further. An example of oligarchic growth is given in Fig. 9.

The giant impacts phase starts when the dynamical friction of smaller planetesimals via repeated close encounters is no longer sufficient to damp the protoplanets eccentricities. According to Kenyon & Bromley [24], the protoplanets mutually excite their orbits and the evolution becomes chaotic, with frequent close encounters and giant collisions. The result is the formation of larger bodies, with dimensions similar to those of the Earth and Venus.

Finally, if a protoplanet reaches a mass of the order of $10-30\ M_{Earth}$, a fast mass infall of gas onto the the rocky-icy core occurs. In this way, after about $10^3-10^4\ yr$, the final mass of the giant planet is achieved. Note that the formation of a gas giant planet is influenced by the rate of gas infall and by the availability of gas in the protoplanetary disk.
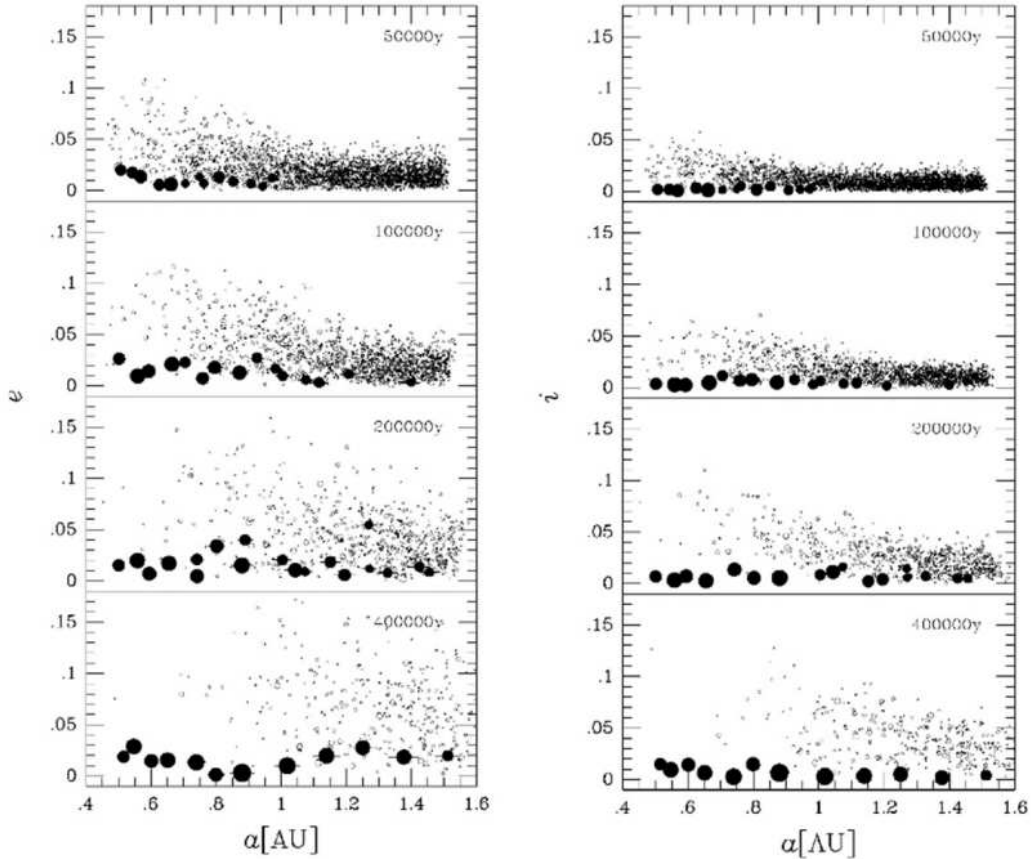
Figure 9: Example of oligarchic growth computed via an N-body numerical simulation in the $a - e$ (left panel) and $a - i$ (right panel) planes. Initially, the bodies have a mass of $2.5 \cdot 10^{-4} \ M_{Earth}$ and they grow by mutual collisions. From Kokubo & Ida [26].

2.4   Pebble Accretion

It was seen in Sec. 2.1 that circumstellar disks dissipate with a timescale of the order of $3 - 10 \ Myr$, as their evolution is driven by viscosity, photoevaporation and planet formation. This means that planetesimal and planet formation must be rapid to occur, otherwise there will be not enough material available to grow further. This fact is particularly important for giant planets, which must have time to reach a more massive core with respect to terrestrial planets (i.e. of the order of $10 - 30 \ M_{Earth}$) and to successfully capture the surrounding gas.

The pebble accretion model provides a solution to this problem. It states that not all the dust ends up into planetesimals, but that a significant amount of mass can stay in the form of pebbles, i.e. decimeter size rocky-icy bodies. Due to the friction exercised by the surrounding gas, these pebbles slow down and can be captured by the gravity of a growing protoplanet. In this regard, a study conducted by Ormel & Klahr [44] has indeed shown

that the cross section for pebble impacts on a protoplanet is strongly enhanced by the gas drag on the pebbles. As a consequence, pebble accretion significantly contributes to the planet growth and speeds up the planet formation timescale with respect to the planetesimal only scenario.

According to a study conducted by Chatterjee & Tan [10], pebbles drift from the outer region of the disk towards the inner one, until they find the end of the dead zone[3]. At this point, pebbles collect due to the presence of a pressure trap, thus forming a pebble ring that persists until it either becomes gravitationally unstable enough to form a planet or it induces gradual planet formation via core accretion. After the first planet is formed, the inner edge of the dead zone gets farther out, since the disk dissipates and more regions are ionized. This process repeats at the location of the new pressure trap, always requiring the existence of a dead zone. A schematic overview of this phenomenon is provided in Fig. 10.
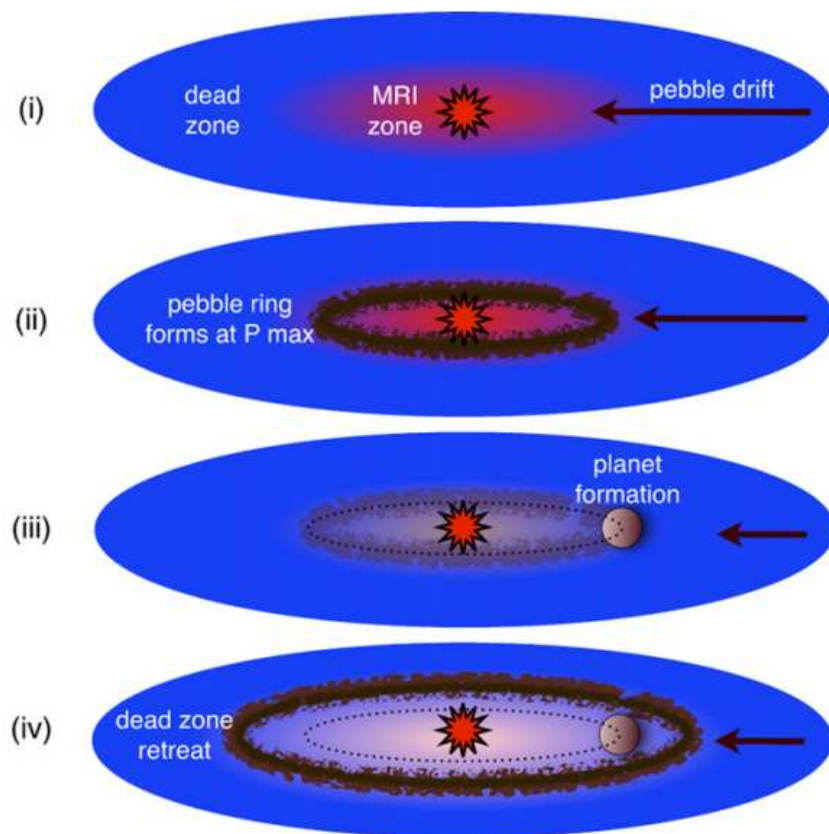
Figure 10: Schematic overview of the stages of the inside-out planet formation scenario. From Chatterjee et al. [10].

---

[3]In the outer regions of the disk, where the radiation from the star is weaker, the ionization level decreases significantly. As a result, the gas becomes less turbulent and less effective at transporting angular momentum. This region is known as the dead zone, whose reduced activity can make it challenging for planetesimals and dust grains to accumulate and form larger objects like planets.

It is worth to note that pebbles can be either primordial or the outcome of planetesimal collisions. In fact, during the runaway growth phase, most of the pebbles are lost due to radial drift. Therefore, planetesimal collisions are necessary to produce a second generation of pebbles.

3 Planet-Disk Interaction

The term exoplanet refers to a planet not belonging to the Solar System. Since the detection of the first exoplanet by Mayor & Queloz [33], i.e. the gaseous giant 51 Peg b, more than 5000 extrasolar planets were discovered to date. This goal was achieved thanks to the development of several detection methods, i.e. radial velocity, transit photometry, microlensing, astrometry, direct imaging and orbital brightness modulation.

The radial velocity method allows to indirectly detect the presence of a planet from the motion of the star around the barycenter of the planet-star system. In particular, it measures the oscillation of the absorption lines due to the Doppler effect, providing the planet mass, semi-major axis and eccentricity[4].

The transit or occultation method takes advantage of the fact that when the planet passes in front of the star, the brightness of the star decreases. The transit data provide the orbital period and radius of the planet from the star dimming, while its eccentricity is deduced from the duration of the transit.

The microlensing method is based on the gravitational lens effect and it allows to compute the mass and semi-major axis of a planet, even if it is located very far away from the observer.

Astrometry computes the orbit of the star around the barycenter of the planet-star system by making precise measurements of its position in the sky. This method preferentially detects planets with large orbits, giving their semi-major axis, eccentricity and mass[5].

Direct imaging efficiently detects young planets located far from the star, since they emit at infrared wavelengths where the star light is dimmer. It is worth to note that this method works better for face-on planetary orbits.

Finally, the orbital brightness modulation method is based either on the change in the star light due to the phases of a bright planet, or on the change in the shape of the star due to planetary tides.

The inclination of the planet orbit can be computed thanks to a synergy between radial velocity and transit observations. When the planet passes in front of a star during a transit, it first shades one limb and then the other one. Since the star is rotating, the limbs are affected by the Doppler effect and this appears in the radial velocity curve. It follows that from the shape of the signal it is possible to estimate the inclination of the planet orbit with respect to the star spin. This phenomenon is known as the Rossiter-McLaughlin ef-

---

[4]The semi-major axis of the planet is computed from the period of the oscillation, while the eccentricity is obtained from the shape of the radial velocity curve. The amplitude of the radial velocity oscillation instead gives the quantity $m \cdot \sin i$, where m is the mass of the planet and i is the inclination of the orbital plane with respect to the line of sight.

[5]As in the case of the radial velocity method, astrometry computes the mass with a $\sin i$ uncertainty, i.e. it gives the quantity $m \cdot \sin i$.
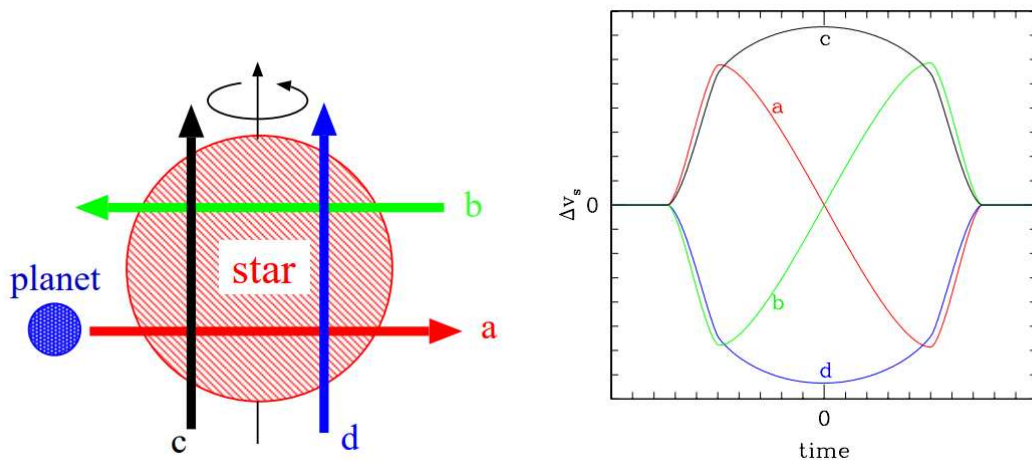
fect and it is illustrated in Fig. 11.

Figure 11: Schematic illustration of the velocity curve anomaly due to the Rossiter-McLaughlin effect. The four different paths of a planet in the left panel correspond to the velocity curves in the right panel. From Ohta et al. [43].

What emerges from the many exoplanet observations made thanks to these detection methods is that the Solar System seems to be quite unique. Indeed, it is composed of terrestrial planets in the inner region and giant planets in the outer one, all of them having nearly circular orbits that lie near the plane of the Earth's orbit, which is called the ecliptic. Conversely, most of the extrasolar systems discovered show a large number of gaseous giants orbiting very close to their stars, with periods ranging from a few to some days. They were termed Hot or Warm Jupiters[6] and it is thought that they formed in the outer regions of the circumstellar disk (so beyond the frost line) and then migrated inwards to their current positions. Measurements of the Rossiter-McLaughlin effect have revealed that the orbits of several Hot Jupiters are characterized by a high misalignment with respect to the equatorial plane of the star [1], suggesting that exoplanets have a broad distribution of inclination. Furthermore, many planets present very high eccentricities, despite having formed from a disk which should give origin to planets on circular orbits. The fact that exoplanets present a broad distribution of eccentricity was studied by Takeda & Rasio [54], who found a median value of the order of $e \approx 0.3$.

It is clear that in order to include these findings in the standard model for planet formation, some additional dynamical mechanisms must be included. One of these key processes is the interaction between the planets and their parent protoplanetary disk, which is able

---

[6]The name hot or warm Jupiter derives from the fact that it refers to giant planets warmer than our system's gas giant Jupiter, being located very close to their parent stars.

to cause large variations in the orbital elements of the planets. However, planet-planet and star-planet interactions are also needed to account for the diversity of exoplanetary systems [2], leading to significant changes not only in the semi-major axis, but also in the eccentricity and inclination. In the following paragraph, some of the major ingredients in shaping the architecture of observed planetary systems will be presented. These are planet migration by interaction with the gaseous disk, periods of dynamical instability characterized by close approaches between the planets (i.e. planet-planet scattering), tidal interaction between the planet and the star and mean motion resonances.

3.1   Planet Migration by Interaction with the Gaseous Disk

Planet migration by interaction with the gaseous disk is an important process in the standard model of planet formation. In particular, it refers to the movement of a forming planet within the protoplanetary disk due to gravitational interactions and exchange of angular momentum with the surrounding gas.

It is possible to divide this phenomenon into two regimes, i.e. type I and type II migration, depending on the mass of the planet. Specifically, type I migration occurs when the planet is relatively small compared to the surrounding gaseous disk, having a mass of the order of $1-50\ M_{Earth}$. In this case, the perturbations in the disk induced by the planet are small and the disk structure does not change significantly. These perturbations are commonly divided into two parts, as it is illustrated in Fig. 12:

- A wave part, in which the disk responds by generating spiral density waves that propagate across the entire disk from the planet's position.

- Another part localized within a narrow zone that surrounds the planet's orbital radius, known as the planet's horseshoe region. Within this region, the material in the disk makes u-turns as it interacts with the planet.

Dealing with the wave part, Goldreich & Tremaine [18] found that a planet exerting its gravitational force to the disk has the ability to initiate waves at Lindblad resonances. This type of resonances occur at locations where the azimuthal velocity of the gas relative to the planet matches the phase velocity[7] of acoustic waves in the azimuthal direction [2]. The combination of the waves generated at Lindblad resonances results in the formation of a spiral density wave with a single-arm pattern, which is known as the wake [42]. The inner part of the spiral wave rotates faster than the planet, thus exerting a gravitational torque that tends to dampen the planet's eccentricity and inclination, while transferring

---

[7]The phase velocity of acoustic waves depends on the azimuthal wavenumber, on the sound speed and on the epicyclic frequency [2], i.e. the oscillation frequency of a particle in the disk that is subject to a small radial displacement [60].
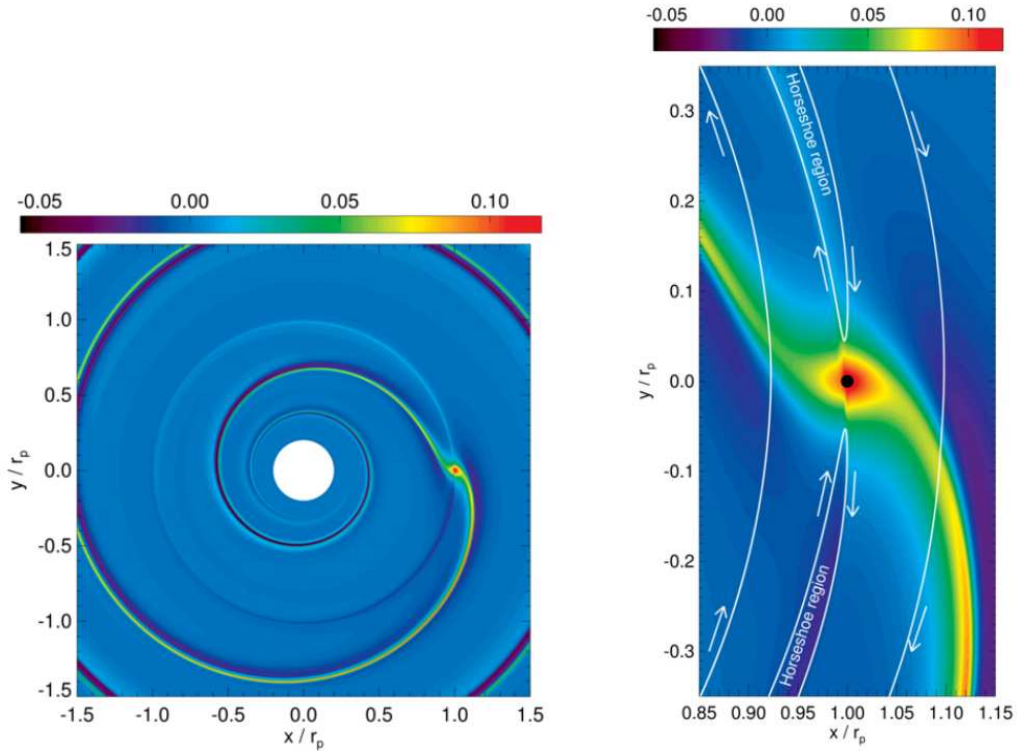
Figure 12: Relative perturbation of the surface density of a gaseous protoplanetary disk perturbed by a planet with mass $M = 5 \ M_{Earth}$, located at $x = r_p$ and $y = 0$. The planet induces a one-armed spiral density wave that propagates throughout the disk and density perturbations confined in the planet's horseshoe region. From Baruteau et al. [2].

angular momentum from the planet to the disk. As a consequence of this positive torque, the planet is accelerated and forced to migrate outwards. Conversely, the outer part of the spiral wave rotates slower than the planet, thus leading to a gravitational torque that tends to excite the planet's eccentricity and inclination, while transferring angular momentum from the disk to the planet. It follows that a negative torque is exerted on the planet, slowing it down and causing an inward migration. In most cases, the two torques are unbalanced, with the outer one being greater. This means that the sum of the two torques, i.e. the differential Lindblad torque, is negative and causes an inward migration on timescales of the order of a few $10^5 \ yr$. These timescales are significantly shorter compared to the expected lifetime of the disk, being it typically of the order of $10^6 - 10^7 \ yr$. As a consequence, this type of migration appears to be excessively efficient, making it highly challenging for planets to survive on orbits spanning several AU.

An expression for the total torque acting on the planet can be obtained by adding up all the torques at the Lindblad resonances. Let's denote as Σ the surface density of the disk, as q the planet-to-star mass ratio, as Ω the angular velocity of the disk, as r the radial distance of the planet from the star, as $h = \frac{H}{r}$ the disk aspect ratio and as γ the ratio between the

specific heats. According to the work done by Paardekooper & Papaloizou [46], the total wave torque Γ_L exerted on the planet in a non-isothermal, adiabatic and two-dimensional disk is given by:

$$\gamma\Gamma_L = -(2.5 + 1.7\beta - 0.1\alpha)\frac{q^2}{h^2}\Sigma_p r_p^4 \Omega_p^2 = -(2.5 + 1.7\beta - 0.1\alpha)\Gamma_0$$

It is immediate to note that the migration rate is proportional to both the mass of the planet M_p and the surface gas density Σ. In this expression the quantities with subscript p refer to the location of the planet, Γ_0 is a normalization factor, while the parameters α and β represent respectively the exponents of the density power-law and of the temperature profile:

$$\Sigma \propto r^{-\alpha} \qquad\qquad T \propto r^{-\beta}$$

In general, the two parameters α and β are positive, since both the surface density Σ and the temperature T decrease moving outwards. From the normalization factor Γ_0 it is possible to compute the timescale for type I migration in case of planets on circular orbits. By denoting as M_* the mass of the central star, it gives:

$$\tau_0 = \frac{r_p}{\left|\frac{dr_p}{dt}\right|} = \frac{1}{2}\frac{h^2}{q}\frac{M_*}{\Sigma_p r_p^2}\Omega_p^{-1}$$

An additional contribution to type I migration comes from corotation torques exerted by gas particles that on average corotate with the planet. In a rotating reference frame moving with the planet, these gas particles perform horseshoe orbits, reversing the direction of their motion when they approach the planet from ahead or from behind. After having spent some time in this horseshoe region, the particles will move to the region inside the planet. The exchange of angular momentum between the gas and the planet due to these orbits depends on the temperature and density profiles of the disk and on viscosity. Generally, this leads to an outward migration, thus slowing down or even reversing the inward migration due to the Lindblad resonances[8].

It is worth to note that while density waves carry away angular momentum from the planet, the horseshoe region can only operate under a finite amount of available angular momentum. This means that in order to sustain the corotation torque, it is necessary to consider an inflow of angular momentum into the horseshoe region, otherwise the corotation torque is prone to saturation [2].

A study conducted by Tanaka et al. [55] found that wave torques always dominate over corotation torques, with the exception of disks with extreme surface density profiles. Ac-

---

[8]Within this context, it is worth to mention the work done by Nelson [40]. He found that large scale turbulence can cause a stochastic migration of planets that may overcome the Lindblad torques.

cording to Paardekooper et al. [45] a numerical value for the corotation torque Γ_c can be obtained by solving the linearized disk equation. For a non-isothermal, two-dimensional disk, it gives:

$$\gamma\Gamma_c = \left[0.7\left(\frac{3}{2} - \alpha - \frac{2\zeta}{\gamma}\right) + 2.2\zeta\right]\frac{q^2}{h^2}\Sigma_p r_p^4 \Omega_p^2 = \left[0.7\left(\frac{3}{2} - \alpha - \frac{2\zeta}{\gamma}\right) + 2.2\zeta\right]\Gamma_0$$

In this expression $\zeta = \beta - (\gamma - 1)\alpha$ refers to the power-law exponent of the specific entropy. It was demonstrated that in case of an isothermal disk, $\zeta = 0$ and the linear corotation torque scales with the local gradient in vortensity[9] [18]. As a result, corotation torques exhibit a stronger dependence on gradients in the background surface density compared to wave torques.

An alternative formulation for the corotation torque was derived by Ward [59], by examining the behavior of gas particles on horseshoe orbits with respect to the planet. For an isothermal disk, he found that the torque exercised on the planet by these particles scales with the vortensity gradient similarly to what was shown by the linear corotation torque. Being corotation torques very sensitive to the viscosity and thermal properties of the disk, it was already mentioned that they may be able to counterbalance the negative wave torque, thus leading to a global outward migration. In this framework, Bitsch & Kley [7] conducted numerical simulations on small eccentric planets, demonstrating how the corotation torque decreases as the eccentricity increases. This limitation restricts the possibility of outward migration to planets with eccentricities below a few percent. According to Fendyke & Nelson [16], the reason behind this phenomenon can be attributed to the narrowing of the width of the horseshoe region as the eccentricity increases. Furthermore, Papaloizou & Larwood [47] found that the Lindblad torque becomes more positive with increasing eccentricities, a fact that further accentuates the previous limitation. Studies on low-mass inclined planets have instead shown that they can only migrate outwards if their inclination remains below a few degrees [6]. In fact, the larger the inclination, the smaller the duration of the planet's interaction with the gas near the mid-plane of the disk. Consequently, the corotation torque and the migration rate will decrease accordingly.

To conclude, it is interesting to note that type I planet migration leads to a system characterized by circular orbits, since small eccentricity variations are dumped by the gas [17][32]. An analogous reasoning applies to planetary inclinations, as they are gradually attenuated over time by planet-disk interactions [56]. Within this context, Tanaka & Ward [56] obtained an expression for the timescales of eccentricity and inclination damping in

---

[9]The vortensity, or specific vorticity, is defined as the vorticity divided by the surface density.

three-dimensional systems:

$$\tau_e = \frac{e}{\left|\frac{de}{dt}\right|} \approx 2.6h^2\tau_0 \qquad\qquad \tau_i = \frac{i}{\left|\frac{di}{dt}\right|} \approx 3.7h^2\tau_0$$

Since the factor h^2 is very small, the damping of both the eccentricity and inclination occurs at a significantly faster rate compared to migration. As a result, a single low-mass planet is expected to migrate while maintaining a circular and coplanar orbit.

Dealing now with type II migration, it occurs when the planet is massive enough to open a gap in the protoplanetary disk. The formation of a gap is due to the tidal torque exerted by the planet on the disk, which transfers angular momentum from the planet to the gas outside its orbit, while doing the opposite to the gas located inside. When the torque exerted by the planet exceeds the magnitude of the viscous torque responsible for the spreading of the disk, it results in the creation of an annular gap that encircles the planet's orbit [28]. Otherwise, the viscous torque occurring close to the planet's orbit will be able to contrast this effect, by resupplying gas and smoothing the density gradient.

The depth of the gap is defined as the distance from the planet at which the planet torque and the viscous torque achieve equilibrium [57]. However, a study conducted by Crida et al. [12] showed that the disk material close to the planet experiences an additional pressure torque, arising from the non-axisymmetric density perturbations induced by the planet. In a state of equilibrium, the three torques balance each other, ultimately determining the profile of the gap. From a semi-analytic study of this torque balance, they found the following gap-opening criterion:

$$\mathcal{P} = \frac{3}{4}\frac{H}{r_H} + \frac{50}{q\mathcal{R}} \leq 1$$

In this expression $\mathcal{P}$ is a dimensionless quantity, while r_H is the planet's Hill radius. It is possible to solve the equation $\mathcal{P} = 1$ analytically, obtaining the minimum planet-to-star mass ratio to open a deep gap in the disk. By introducing the quantity $X = \sqrt{1 + \frac{3\mathcal{R}h^3}{800}}$, it gives:

$$q_{min} = \frac{100}{\mathcal{R}}\left[(X+1)^{\frac{1}{3}} - (X-1)^{\frac{1}{3}}\right]^{-3}$$

As an annular gap develops around a planet, it divides the protoplanetary disk into two distinct regions, i.e. an inner disk and an outer disk. Both of them exert repulsive forces on the planet, thus pushing it towards the center of the gap. Since the gaseous disk is moving inwards due to viscous accretion, it will force the planet to migrate with it along the same direction [28]. Therefore, the migration of the planet follows the viscous evolution of the

disk, with a timescale equal to the viscous accretion time:

$$\tau_\nu = \frac{r_p^2}{\nu}$$

In this expression the quantity ν is the disk's kinematic viscosity, whose value is often computed by exploiting the alpha prescription for the disk viscosity. In general, the timescale for type II migration appears to be of the of the order of $10^5 - 10^6 \ yr$.

However, if the planet's mass is significantly larger than that of the gas surrounding the gap, the planet will slow down the viscous accretion of the disk [2]. This situation arises when the following condition is fulfilled:

$$M_p > 4\pi\Sigma_0 r_p^2$$

In this expression Σ_0 represents the surface density of the outer disk immediately outside the gap. In such scenarios, the inner disk continues to accrete material onto the central star, while the outer disk is controlled by the gravitational influence of the planet. As a result, it occurs a partial or complete emptying of the inner disk, while the migration timescale τ will be determined by the equilibrium between the viscous torque and the inertia of the planet:

$$\tau = \tau_\nu \cdot \frac{M_p}{4\pi\Sigma_0 r_p^2}$$

Finally, it must be considered that the gas residing within the gap exerts a positive corotation torque on the planet. As a consequence, the migration of planets that barely meet the condition for gap formation can proceed at a slower pace compared to the conventional type II migration. Specifically, if the gap density reaches a significant level, the corotation torque can overcome the viscous torque, thus leading to a global outward migration of the planet [11][2].

As it was said for type I migration, planet-disk interactions tend to dump the eccentricity and inclination also in the case of massive planets that have created gaps in the surrounding disk [8]. Therefore, type II migration is expected to produce hot Jupiters that are characterized by circular orbits and low inclinations.

3.2 Planet-Planet Scattering

It was seen in Sec. 3.1 that the eccentricities of planets forming within a circumstellar disk are kept low by the gas perturbations. However, once the gas dissipates, a multi-planet system may become unstable, allowing the eccentricities to grow. As a consequence, the planets may be subject to close encounters, thus leading to a period of chaotic evolution,

where the orbital elements of the planets show steep changes.

This instability develops on a timescale that depends on the initial mutual distance between the planets, ending when one or more planets are ejected out of the system on hyperbolic orbits. As a result, the surviving planets are placed into highly eccentric orbits, both closer and farther from the star [62].

Numerical simulations of planet-planet scattering involving three giant planets with Jupiter mass around a solar type star show the occurrence of this type of instability and the subsequent ejection of one of the planets on a hyperbolic orbit. Since the trajectory of the ejected planet has positive energy, the conservation of the total energy of the system implies that the inner surviving planet is injected on an orbit that is closer to the star. Specifically, at the beginning of the simulation, the energy of the system is given by:

$$E = -\frac{GM_s}{2}\left(\frac{m_1}{a_1} + \frac{m_2}{a_2} + \frac{m_3}{a_3}\right)$$

In this expression M_s is the mass of the star, m_1, m_2 and m_3 are the masses of the three planets, while a_1, a_2 and a_3 are the semi-major axis of the correspondent orbits. Conversely, at the end of the simulation most of the energy of the system is given by the closer planet. It follows that this planet must present a very high eccentricity, being its semi-major axis of the order of $a_{fin,1} \approx \frac{GM_s m_i}{2E}$.

It is safe to conclude that the gravitational interaction among planets can exert a remarkable influence on the final architecture and stability of planetary systems. In particular, close encounters can break resonant configurations, leading to the planets being released from their resonance or even reversing the order of planets in the chain.

3.3 Tidal Interaction

Tidal forces depend on the gradient of a gravitational field, arising from the unequal distribution of the gravitational attraction on different parts of an object.

In exoplanetary systems where the planet orbits close enough to the star, the two objects can tidally interact with each other. This means that there will be a tide raised by the planet on the star and a tide raised by the star on the planet. It is possible to define different kinds of tidal interaction:

- The equilibrium tide is typical of rocky bodies having an orbit characterized by a small eccentricity and it foresees the formation of an equilibrium bulge. In this case, the dissipation of energy is caused by the time variation of the tidal bulge.

- The dynamical tide is typical of gaseous bodies with high eccentricities. In this case, the body is assumed to be an oscillator, with a number of modes that are

26

excited when the companion passes at the pericenter.

The most important effect of tidal interaction is the circularization of the planet orbit, which in case of an eccentric planetary orbit it drags the planet closer to the star. In order to understand this phenomenon, let's consider the expression for the conservation of the angular momentum. By denoting as m_p and m_s the masses of the planet and the star, as M the total mass of the system, as a the semi-major axis of the planet's orbit and as e its eccentricity, it yields:

$$L = \frac{m_p m_s}{m_p + m_s} \sqrt{GMa(1 - e^2)} = constant$$

It follows that the quantity $a(1 - e^2)$ must not change in time, thus giving:

$$a(1 - e^2) = a(1 - e)(1 + e) \approx 2a(1 - e) = constant \longrightarrow a(1 - e) = constant$$

Therefore, if the eccentricity e decreases, so must do the semi-major axis a. In the limit in which $e \to 0$, the final semi-major axis will be equal to twice the initial pericenter distance of the orbit, being it $p = a(1 - e)$.

As a consequence of this fact, the coupling between tidal interaction of the planet with the star and planet-planet scattering is able to explain the existence of Hot/Warm Jupiters. By referring to what was said in Sec. 3.2, the occurrence of planet-planet scattering in case of three giant planets orbiting around a star implies that the inner surviving planet must have a high eccentricity [62]. This means that the planet passes very close to the star, thus causing a strong tidal interaction that leads to the circularization of the orbit to twice the initial pericenter of the planet. As a result, if the eccentricity e is initially high, then the final semi-major axis a of the orbit will be much smaller that the initial one.

This situation was studied by Nagasawa et al. [39], who carried out orbital integrations of three giant planets with Jupiter mass directly including the effect of tidal circularization. In their work, they adopted the formulas derived by Ivanov & Papaloizou [22] to compute the amount of tidal angular momentum ΔL_{tide} and energy ΔE_{tide} gained during a single pericenter passage, which are given by:

$$\Delta L_{tide} \approx -\frac{32\sqrt{2}}{15} \bar{w}_0^2 \bar{Q}^2 \zeta e^{-\frac{4\sqrt{2}}{3}w+\zeta} \left[1 - \frac{9}{2^{14}(\bar{w}_0\zeta)^4} e^{\frac{4\sqrt{2}}{3}\bar{\sigma}\zeta} \right] L_{pl}$$

$$\Delta E_{tide} \approx -\frac{16\sqrt{2}}{15} \bar{w}_0^3 \bar{Q}^2 \zeta e^{-\frac{4\sqrt{2}}{3}w+\zeta} \left[1 + \frac{3}{2^7(\bar{w}_0\zeta)^2} e^{\frac{2\sqrt{2}}{3}\bar{\sigma}\zeta} \right]^2 E_{pl}$$

In these two expressions, $L_{pl} = m(GmR)^{\frac{1}{2}}$ and $E_{pl} = \frac{Gm^2}{R}$ are the orbital angular momentum and orbital energy. Moreover, by denoting as $p = a(1-e)$ the pericenter distance,

as Ω_r the angular velocity of the planet rotation, as $\bar{w}_0$ a dimensionless frequency of fundamental mode and as $\bar{Q}$ a dimensionless overlap integral depending on the planetary interior model, then $\zeta = (mp^3)^{\frac{1}{2}}(m_* R^3)^{-\frac{1}{2}}$, $w_+ = \bar{w}_0 \left(\frac{Gm}{R^3}\right)^{\frac{1}{2}} + \Omega_r$ and $\bar{\sigma} = \frac{2\Omega_r}{\left(\frac{Gm}{R^3}\right)^{\frac{1}{2}}}$ [39]. Note that for a non-rotating planet, the previous two equations are simplified to:

$$\Delta L_{tide} \approx -\frac{32\sqrt{2}}{15} \bar{w}_0^2 \bar{Q}^2 \zeta e^{-\frac{4\sqrt{2}}{3}w_0\zeta} L_{pl}$$

$$\Delta E_{tide} \approx -\frac{16\sqrt{2}}{15} \bar{w}_0^3 \bar{Q}^2 \zeta e^{-\frac{4\sqrt{2}}{3}w_0\zeta} E_{pl}$$

This model is applicable only to fully convective planets in highly eccentric orbits, as it considers the $l = 2$ fundamental modes of tidal dissipation and it uses the impulse approximation. In fact, oscillation modes are excited within the planetary interior due to the tidal force exerted by the star near the pericenter. It is assumed that the energy of these modes dissipates, while the angular momentum is transferred to the orbital angular momentum before the subsequent pericenter passage. By supposing that the orbital changes during each approach are negligible, the orbit of the planet is changed impulsively at the moment of the pericenter passage. Since the pericenter passage occurs every Keplerian time T_{Kep}, the evolution timescales of the semi-major axis a and eccentricity e are given by ($\gamma = \frac{1-e^2}{e^2}$):

$$\tau_a = -\frac{a}{\dot{a}} = -\frac{Gmm_*}{2a}\frac{T_{Kep}}{\Delta E_{tide}}$$

$$\tau_e = -\frac{e}{\dot{e}} = Gmm_*T_{Kep}\left(-a\gamma\Delta E_{tide} + \sqrt{\frac{\gamma Gm_*}{ae^2}}\Delta L_{tide}\right)^{-1}$$

Therefore, the timescale for tidal damping is proportional to the mass and radius of the planet.

As shown in figure 13, at the end of the simulation a system of three-planet scattering usually ends with the ejection of one planet and the system entering a stable state. In particular, one planet is left on an outer orbit, while the inner one is tidally driven to a circular orbit closer to the star. It is safe to conclude that planet-planet scattering and tidal interaction with the star are able to explain the observed orbits of most Hot/Warm Jupiters without invoking planet migration by interaction with the gaseous disk, even though additional dynamical mechanisms may cause a change in their orbital elements.

3.4 Resonances

Orbital resonances arise when two or more celestial bodies exert regular and periodic gravitational influences on each other, reinforcing or dampening their orbital motions.
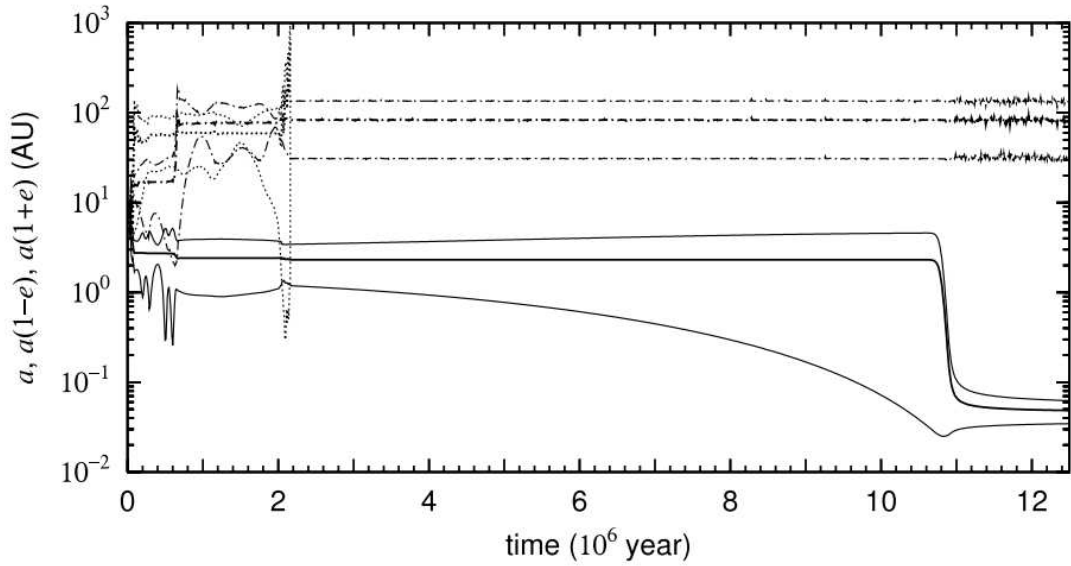
Figure 13: Evolution of the semi-major axes (middle), apocenter (outer) and pericenter (inner) of three planets. In particular, the dotted line refers to the ejected planet, the dash-dotted line to the planet left on an outer orbit, while the solid line to the planet injected on a closer orbit. From Nagasawa et al. [39].

The most important resonance is the mean-motion resonance, which occurs when the orbital periods of the involved planets have a simple integer ratio.

In order to understand the properties of the mean-motion resonance, let's consider a system of two planets that undergo migration within their parent disk. When the migration drift rates of the two planets cause them to move apart, i.e. when a divergent migration takes place, the effects of planet-planet interactions are small and resonant capture does not occur [2]. On the other hand, resonant capture takes place during convergent migration, where the planets migrate towards each other. In this case, the planets may approach a state in which their orbital periods are the ratio of two integers. As a consequence, the orbital eccentricities of the planets can be excited, thus leading to a possible resonant capture.

The occurrence of resonant capture depends on the time the two planets take to cross the resonance. In particular, the timescale of convergent migration must be longer than the timescale of libration associated with the width of the resonance [52], otherwise the two planets will not have enough time to excite the resonance and they will pass through it without being captured [38].

By denoting as Ω_1 and Ω_2 the angular velocity of the inner and outer planets, the condition

for the manifestation of a mean-motion resonance is:

$$(p + q)\Omega_2 - p\Omega_1 = 0$$

In this expression q and p are two positive integers, with q denoting the order of the resonance [2]. The same condition written in terms of the semi-major axes of the two planets gives:

$$\frac{a_2}{a_1} = \left(\frac{p + q}{p}\right)^{\frac{2}{3}}$$

When this criterion is satisfied, the system is considered to be in a $p + q : p$ mean motion resonance. As a result, at least one of the resonant angles will exhibit libration, thus showing a limited dynamical range that will be smaller than 2π.

Let's denote as λ_1 and λ_2 the mean longitudes of the inner and outer planets, while as $\bar{\omega}_1$ and $\bar{\omega}_2$ the longitude of their pericentres. The resonant angles ϕ_1 and ϕ_2 are then defined by the following combination of the mean longitudes of the two planets:

$$\phi_{1,2} = (p + q)\lambda_2 - p\lambda_1 - q\bar{\omega}_{1,2}$$

Therefore, when the two planets are captured in resonance, the resonant angles exhibit libration. In this case the system is said to be in apsidal corotation [2], since the two apsidal lines of the resonant planets are always aligned or maintain a fixed angle between them [25].

The specific resonance into which the system may ultimately settle depends on several factors, such as the masses of the planets, their initial separation and the relative speed of their migration [41]. Nevertheless, since the convergent migration speed is quite low, it is common for two initially distant planets to be captured in the 2:1 resonance, being it the first first-order resonance they encounter [2].

After being captured in resonance, the two planets migrate together, while maintaining a constant ratio between the orbital periods. Moreover, they experience an increase in their eccentricities, which will continue to rise in absence of an adequate damping mechanism. This may lead the eccentricities to reach extremely large values, thus giving rise to instabilities within the system.

The rate at which the eccentricity is damped by the surrounding disk, which is denoted as $\dot{e}$, is frequently parameterized with respect to the migration rate $\dot{a}$:

$$\left|\frac{\dot{e}}{e}\right| = K \left|\frac{\dot{a}}{a}\right|$$

In this expression the quantity K refers to a dimensionless constant. According to Baruteau et al. [2], for low-mass planets the eccentricity damping takes place at a significantly faster rate compared to migration. Conversely, the creation of a gap in the disk considerably reduces the eccentricity damping in the case of high-mass planets.

A fully analytical and integrable treatment of resonant phenomena was provided by Batygin & Morbidelli [3], who tried to construct an approximation to the first order resonant motion of two massive planets orbiting around a central star. According to their work, let's denote as M the mass of the star, as m_1 and m_2 the masses of the inner and outer bodies, as p_1 and p_2 their barycentric linear momenta, as r_1 and r_2 their distance from the star and as Δ_{12} the relative distance between them. The exact Hamiltonian $\mathcal{H}$ that governs the gravitational three-body problem in its heliocentric formulation is then given by:

$$\mathcal{H} = \frac{M + m_1}{2M} \frac{p_1^2}{m_1} + \frac{M + m_2}{2M} \frac{p_2^2}{m_2} - \frac{GMm_1}{r_1} - \frac{GMm_2}{r_2} + \frac{p_1 \cdot p_2}{M} - G\frac{m_1 m_2}{\Delta_{12}}$$

In order to obtain a suitable approximation to this expression, it is more practical to employ the classical perturbation method instead of directly dealing with the Hamiltonian. By noting that the first four terms of the Hamiltonian define the Keplerian motion of the two planets, it is possible to write the Keplerian part in terms of the orbital elements [37][36], specifically by exploiting their semi-major axes a_1 and a_2:

$$\mathcal{H}_{Kep} = -\frac{GMm_1}{2a_1} - \frac{GMm_2}{2a_2}$$

The remaining terms in the Hamiltonian account for planet-planet interactions. Since their magnitudes are significantly smaller compared to $\mathcal{H}_{Kep}$, these terms are often referred to as the disturbing function, which introduces minor perturbations to the integrable Hamiltonian.

Let's now expand the disturbing function into a Fourier series in terms of the orbital angles and a power series of the planetary eccentricities and inclinations [27]. This procedure allows to identify the presence of resonant[10] and secular terms within the disturbing function. However, the dominant secular terms in the expansion are of the order of $O(e^2, i^2)$, where e represents the eccentricity and i denotes the inclination. As a consequence, in the development of a first-order resonant theory, these terms will be neglected, along with all the resonant terms of higher order in eccentricity and inclination. The approximated Hamiltonian can thus be written as:

$$\mathcal{H} \approx \mathcal{H}_{Kep} + \mathcal{H}_{res} + O(e^2, i^2)$$

---

[10]Resonant terms are harmonics that exhibit variations on a timescale significantly longer than the orbital timescale in the vicinity of exact commensurability [3].

Within this context, the perturbation caused by the $k : k - 1$ resonance to the Keplerian motion reads:

$$\mathcal{H}_{res} = -\frac{Gm_1m_2}{a_2}(f_{res}^{(1)}e_1\cos(k\lambda_2 - (k-1)\lambda_1 - \bar{\omega}_1) + f_{res}^{(2)}e_2\cos(k\lambda_2 - (k-1)\lambda_1 - \bar{\omega}_2))$$

In this expression the quantities $f_{res}^{(1)}$ and $f_{res}^{(2)}$ are of the order of unity, being them weakly sensitive to the semi-major axes ratio $\frac{a_1}{a_2}$ only. On the other hand, $\bar{\omega}$ and λ refer respectively to the longitude of perihelion and mean longitude of the two planets.

The subsequent manipulation of the Hamiltonian is quite tricky. By means of several transformations, the number of degrees of freedom of the Hamiltonian is reduced from the initial value of six to one, providing a simple integrable expression for the Hamiltonian:

$$\mathcal{H} = \delta(\Omega + \Psi_1 + \Psi_2) - (\Omega + \Psi_1 + \Psi_2)^2 - \sqrt{2\Psi_1}\cos(\psi_1)$$

Without dwelling on the meaning of the different variables, it is still immediate to note how the Hamiltonian under consideration is equivalent to the second fundamental model of resonance developed by Henrard & Lemaitre [21], thus showing qualitative similarities to the pendulum model for resonance. Despite being only accurate at low eccentricities, this theory provides useful insights into the global dynamics of the unrestricted, first order resonant three-body problem [3]. In fact, by making use of the different constants of motion that have emerged during the computation of the final integrable Hamiltonian, it is possible to construct a geometrical characterization of the resonant motion.

3.5   The Jupiter-Saturn Case

A study conducted by Masset & Snellgrove [31] has investigated the coupled evolution of a system composed of two closely spaced giant gaseous planets orbiting around a central star. In particular, they considered a system composed of a giant planet embedded in a protoplanetary disk, which is caught up by a lighter outer giant planet before having migrated all the way to the central star.

In order to study the long-term behaviour of this system, they used two different hydrodynamical codes based on fixed Eulerian grids. The 2-dimensional simulations are conducted in a non-inertial, non-rotating frame centered on the star, which is assumed to resemble the Sun. The two planets have respectively the same masses of Jupiter and Saturn and they start their evolution with semi-major axis $a_j = 1\ AU$ and $a_s = 2\ AU$. The disk aspect ratio is assumed to be uniform and constant, being it equal to $h = \frac{H}{r} = 0.04$. The disk surface density is also uniform and it corresponds to two Jupiter masses inside the Jupiter's orbit. The adopted grid resolution is $N_r = 122$ and $N_\theta = 300$, while the grid

outer boundary is set at $R_{max} = 5\ AU$ and the inner boundary is at $R_{min} = 0.4\ AU$. It is worth to note how the outer boundary of the computational grid is set at a sufficiently high distance from the planets, preventing any inflow or outflow. This choice ensures that the spiral density waves launched by the planets are damped before reaching the outer boundary. Conversely, the inner boundary of the grid allows for outflow, thus enabling the accretion of disk material onto the central star. Finally, the viscosity is assumed to be uniform through the disk, corresponding to a value of $\alpha = 6 \cdot 10^{-3}$ near the inner planet's orbit.

All the simulations gave very similar results, showing the ability of the two-planets system to migrate outwards within the parent disk. In this scenario, the mass of the inner planet is sufficiently large to create a deep gap around its orbit, thus leading to a type II migration. On the other hand, the outer planet has a lower mass, so it only opens a partial gap in the disk. As a consequence, the outer planet migrates inward at a faster pace than the inner planet. Let's consider the case in which the convergent migration occurs rapidly enough for the planets to cross the 2:1 mean-motion resonance and become locked in the 3:2 resonance. In this situation the two planets will merge their gaps and they will start migrating together [2]. Since the inner planet is more massive than the outer one, the positive torque exerted by the inner disk overtakes the negative torque exerted by the outer disk. As a result, the two planets will move outwards in their migration.

This mechanism depends on the presence of an asymmetric density distribution across the common gap that surrounds the two planets. It follows that the joint outward migration of a resonant planet pair is influenced by the aspect ratio and viscosity of the disk, as well as the mass ratio between the two planets, being these factors affecting the density profile within the gap.

Within this context, D'Angelo & Marzari [13] carried out hydrodynamical simulations in both two and three dimensions to examine the circumstances under which the outward migration of a pair of resonant-orbit planets can be effective. Referring to the 2-dimensional simulations, they adopted a reference frame centred on the star, which is again assumed to have the same mass of the Sun. The disk is supposed to be locally isothermal, so that the temperature depends only on the radial distance r. The aspect ratio is constant through the disk, being of the order of $h = \frac{H}{r} = 0.04$. The adopted grid resolution is $N_r = 678$ and $N_\theta = 700$, ranging in radius from $R_{min} = 0.25\ AU$ to $R_{max} = 7\ AU$. The two planets have the same masses of Jupiter and Saturn and they are assumed to be fully-formed since the beginning of the calculations and non-accreting. In particular, their initial conditions are $a_j = 1.5\ AU$ and $a_s = 2\ AU$. They applied wave-damping boundary conditions for regions within $r = 0.3\ AU$ and beyond $r = 6.65\ AU$, which are appropriate for planets far enough from the boundaries. The surface density is set to $\Sigma = 50\ g/cm^2$ at $r = 1\ AU$.

This follows from disk evolution calculations, which showed that around 50% of disks have $\Sigma \leq 50\ g/cm^2$ at $r = 1\ AU$ after $\approx 1\ Myr$, i.e. at a time in which planets have already formed. The kinematic viscosity is supposed to be constant throughout the disk, being it of the order of $\nu = 4 \cdot 10^{-6}$.

Thanks to these numerical simulations, the authors have demonstrated that the most favorable conditions for successful joint outward migration with a 3:2 ratio of commensurability occur when the mass ratio between the inner and outer planets closely resembles that of Jupiter and Saturn. This commensurability represents the first encountered first-order mean motion resonance, but the second-order 5:3 commensurability may provide another possibility. Conversely, in the case of more massive planets by a factor of about three, an outward migration may be promoted by a 2:1 ratio of commensurability.

Therefore, it is possible to explain the present-day orbits of Jupiter and Saturn through the occurrence of a two-stage migration, based on the coupling between planet migration due to the interaction with the disk and a 3:2 mean motion resonance [31]. This explanation provides the most accepted theory to explain the formation, migration and dynamics of Jupiter and Saturn. The Jupiter and Saturn resonant configuration is shown in Fig. 14.

Finally, it is worth to mention the so-called Grand Tack scenario, which was proposed by Walsh et al. [58]. The authors conducted hydrodynamical simulations to show that Jupiter and Saturn can undergo a two-stage, inward-then-outward, migration within their parent protoplanetary disk. The amount of gas at any distance within the disk is multiplied by an exponentially-decaying function of time, in order to imitate the gradual dissipation of the disk as the planets are in motion. In particular, the gas surface density is set to be equal to $100\ g/cm^2$ at $r = 15\ AU$. The adopted aspect ratio is constant through the disk, being of the order of $h = \frac{H}{r} = 0.05$. Jupiter is assumed to be fully-formed since the beginning of the calculations and it starts at $3.5\ AU$. The choice of this location is considered to be highly favorable for giant planet formation due to the presence of the snow-line[11]. Saturn instead starts at $4.5\ AU$ with half of its final mass and remains stationary for about $10^5\ yr$, growing its mass as Jupiter migrates inwards. Once Saturn reaches its final mass, its inward migration begins and it is much faster than that of the fully grown Jupiter. As a consequence, Saturn catches Jupiter, they merge their gaps and they get trapped in the 3:2 mean motion resonance, which occurs when Jupiter is located approximately at $1.5\ AU$. At this point, the direction of migration is reversed and the two giant planets start migrating outwards together until the dispersion of the gaseous disk. At the end of the migration,

---

[11]A quite recent research has indicated the presence of two equilibrium radii within the disk, where the migration of cores comes to a halt [29]. The innermost equilibrium position is closely linked to the snow-line, which is estimated to be around $3 - 5\ AU$. This location, where core migration ceases, was identified as a favorable site for core growth [35][50]. As a consequence, the cores are expected to develop in the proximity of an equilibrium radius, on non-migrating orbits and locked in mutual resonances with each another [58].
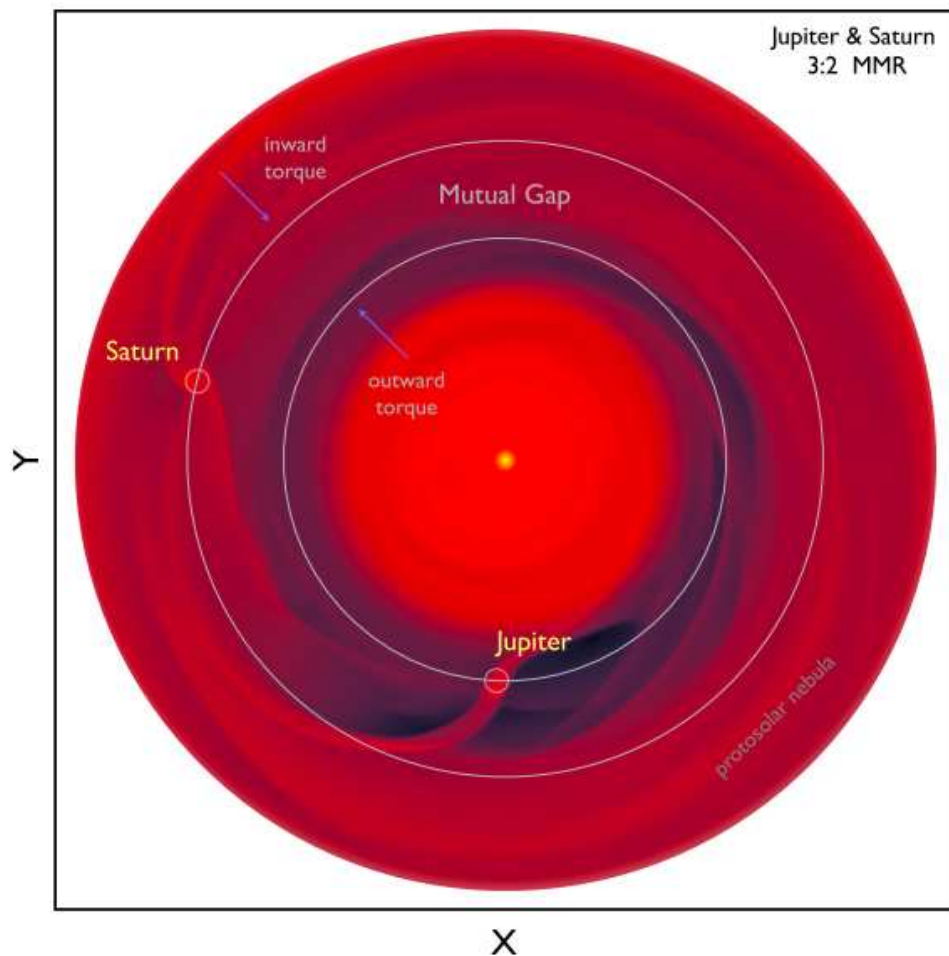
Figure 14: Jupiter and Saturn in a resonant configuration. The two planets are locked in a 3:2 mean motion resonance, having opened a mutual gap in the protoplanetary disk. As a consequence, the planetary migration direction is reversed to point outwards. The snapshot shows the orbital state of Jupiter and Saturn at a time when Jupiter is at $4.3\ AU$. From Masset & Snellgrove [31], Morbidelli & Crida [11].

Jupiter is located approximately at $5.4\ AU$ from the central star.

Once the gas is removed, the giant planets continue to experience gravitational interactions with the planetesimals present in the disk. Over time, these interactions lead to the disruption of the mutual resonances between the giant planets. This leads the planets to enter an unstable phase, which is characterized by mutual close encounters. During this phase, Jupiter and Saturn undergo significant changes in their orbital eccentricities and inclinations, ultimately acquiring their current values. N-body simulations have indeed demonstrated that the giant planet instability phase serves as the dynamical connection between the current configuration of the planets and the resonant orbital arrangement that the giant planets had at the end of the gas-disk phase.

It is worth to note that the rate of outward migration depends on the depth of the partial

gap formed by Saturn. This is in turn influenced by the characteristics of the disk, such as the scale height and the viscosity. In particular, in case of thick disks the migration proceeds at a very low pace, resulting in the planets maintaining a relatively constant distance from the central star. Conversely, in case of disks with diminishing thickness, the outward migration progressively accelerates.

To conclude, the study of the Jupiter-Saturn system is very important as it serves as a template for studying other planetary systems beyond the solar one and to interpret the observations of a multitude of exoplanets. The reversal of the migration direction between two planets in resonance appears to occur exclusively when the outer planet has a lower mass than the inner planet, with the optimal mass ratio falling between $\frac{1}{4}$ and $\frac{1}{2}$. For Jupiter-Saturn mass planets, the resonance capable of driving outward migration is the 3:2 resonance. On the other hand, for more massive planets with three times the mass of Jupiter and Saturn, the resonant configuration for outward migration is the 2:1 resonance. Finally, if the planets have similar masses or if the outer planet is more massive, the resonant planets migrate inwards.

4 The FARGO3D Code

FARGO3D is a widely-used hydrodynamical and magnetohydrodynamical code, which is specifically designed for simulating astrophysical accretion disks in the context of planet formation and migration. This code employs a finite-difference method to solve the equations of fluid dynamics on an Eulerian mesh, which can be either Cartesian, cylindrical or spherical [5]. Despite being it created to solve three-dimensional problems, it can also be used in lower dimensions.

More specifically, FARGO3D solves the hydrodynamical equations by using a time-explicit method that employs operator splitting and upwind techniques on the Eulerian mesh. The discretization of some differential equations is achieved through finite differences, while others are solved utilizing finite volume methods.

In order to understand how the operator splitting technique works, let's consider the following problem:

$$\frac{\partial U}{\partial t} + \mathcal{A}(U) = 0 \qquad\qquad U(0) = U_0$$

If it is possible to decompose the quantity $\mathcal{A}$ into $\mathcal{A} = \mathcal{A}_1 + \mathcal{A}_2$, then the solution of the previous equation can be obtained by taking the linear combination of the solutions of:

$$\frac{\partial U_1}{\partial t} + \mathcal{A}_1(U_1) = 0$$

$$\frac{\partial U_2}{\partial t} + \mathcal{A}_2(U_2) = 0$$

In a finite difference scheme, the correspondent approximate solutions can be expressed in the following form:

$$\frac{U^1 - U^0}{\Delta t} = -A_1(U^0)$$

$$\frac{U^2 - U^1}{\Delta t} = -A_2(U^1)$$

Generally, by denoting as U a set of conservative quantities, as $T(U)$ a rank 2 tensor representing the fluxes of each component of U and as $S(U)$ the source terms, a system of conservation laws is written as:

$$\frac{\partial U}{\partial t} = -\nabla \cdot T(U) + S(U)$$

In this case, applying the operator splitting technique gives:

$$A_1 = -S(U) \qquad\qquad A_2 = \nabla \cdot T(U)$$

Therefore, the operator splitting technique divides the problem into two partial ones, i.e. the source step and the transport step [53]. The equations associated with the two partial problems can be expressed as follows:

$$\partial_t Q = S(U)$$

$$\partial_t Q = -\nabla \cdot T(U)$$

It follows that a complete time step must be composed of two sequential updates. Firstly, there is a partial update from $Q(t_0) = Q^0 \rightarrow Q^1$, which is accomplished through the source step $\partial_t Q = S(U)$. This is followed by a subsequent update from $Q^1 \rightarrow Q^2 = Q(t_0 + \Delta t)$ through the transport step $\partial_t Q = -\nabla \cdot T(U)$. This technique improves computational efficiency by addressing different physical processes separately.

In the source step, the effects of external forces, such as gravity and viscous forces, are accounted for. By following the procedure of Stone & Norman [53], the source step is divided into three sub-steps:

- In sub-step 1, the velocity field is updated by incorporating pressure gradients and gravitational forces.

- In sub-step 2, an artificial von Neumann-Richtmyer viscosity is introduced along with the corresponding heating terms.

- In sub-step 3, the work done by pressure forces is added to the system.

The transport step handles instead the advection or movement of material due to the rotation of the gas. In particular, the transport step consists in solving a conservation law for the quantity Q. By assuming that the control volume V does not have an explicit dependence on time, the time variations of Q within the control volume are solely attributed to the flux across its boundary ∂V. It is worth to note that the update of the frame's angular velocity does not occur during the entire transport sub-step. As a consequence, the new velocities do not reflect the change in the frame's rotation rate. This means that after updating the frame's angular velocity, it is necessary to explicitly correct the azimuthal velocities.

The evaluation of the flux is accomplished by using an upwind method, which estimates the value of the quantity Q^* at the face center during the half-time step. While many astrophysical fluid dynamics codes use the Riemann problem to evaluate the fluxes at the interface, the FARGO3D code employs the staggering of the velocity field to express the flux in a simpler way. In most of the sub-steps, a zone-wise linear reconstruction exploiting the van Leer's slopes is employed to obtain the interpolated value of Q. In this way,

the interface values of density, energy and momenta are computed at the cell interfaces. The conservation of momenta is maintained up to machine accuracy during the transport step. In Godunov-based codes, the pressure at the interface between zones is incorporated into the momenta fluxes, thus ensuring the conservation of momenta throughout a complete update. Conversely, in FARGO3D the pressure gradient is handled separately in the source step. Therefore, it is necessary to separately address the conservation of momenta under the action of this source term [5]. Note that in Fig. 15 it is given a flow chart of all the operations performed by the FARGO3D code during a full update.

The FARGO3D code possesses several key properties that contribute to its effectiveness in simulating astrophysical systems:

- It employs high-order numerical schemes for accurate and precise calculations, which enable reliable time integration and minimize numerical errors.

- It supports the adaptive mesh refinement (AMR), allowing for enhanced resolution in regions of interest. This capability enables the simulations to capture detailed features and structures within the system.

- It can incorporate various physical processes, leading to more comprehensive and realistic simulations of astrophysical systems.

- It is designed to take advantage of parallel computing architectures, allowing to do faster simulations by distributing the computational tasks across multiple processors or nodes.

- It provides tools for data analysis and visualization, allowing users to extract relevant information from simulation results and gain insights into the simulated system.

These properties collectively contribute to the ability of FARGO3D to accurately simulate astrophysical systems, making it a valuable tool for investigating various phenomena in protoplanetary disks and other relevant astrophysical environments.

4.1 FARGO3D Simulations

As it was said in section 3.5, several studies were conducted in recent years to investigate the coupled evolution of a system composed of two closely spaced giant planets orbiting around a central star. It was found that a system of two giant planets with masses equal to that of Jupiter and Saturn has the ability to migrate outwards within its parent protoplanetary disk. In particular, the long-term evolution of this system shows the occurrence of
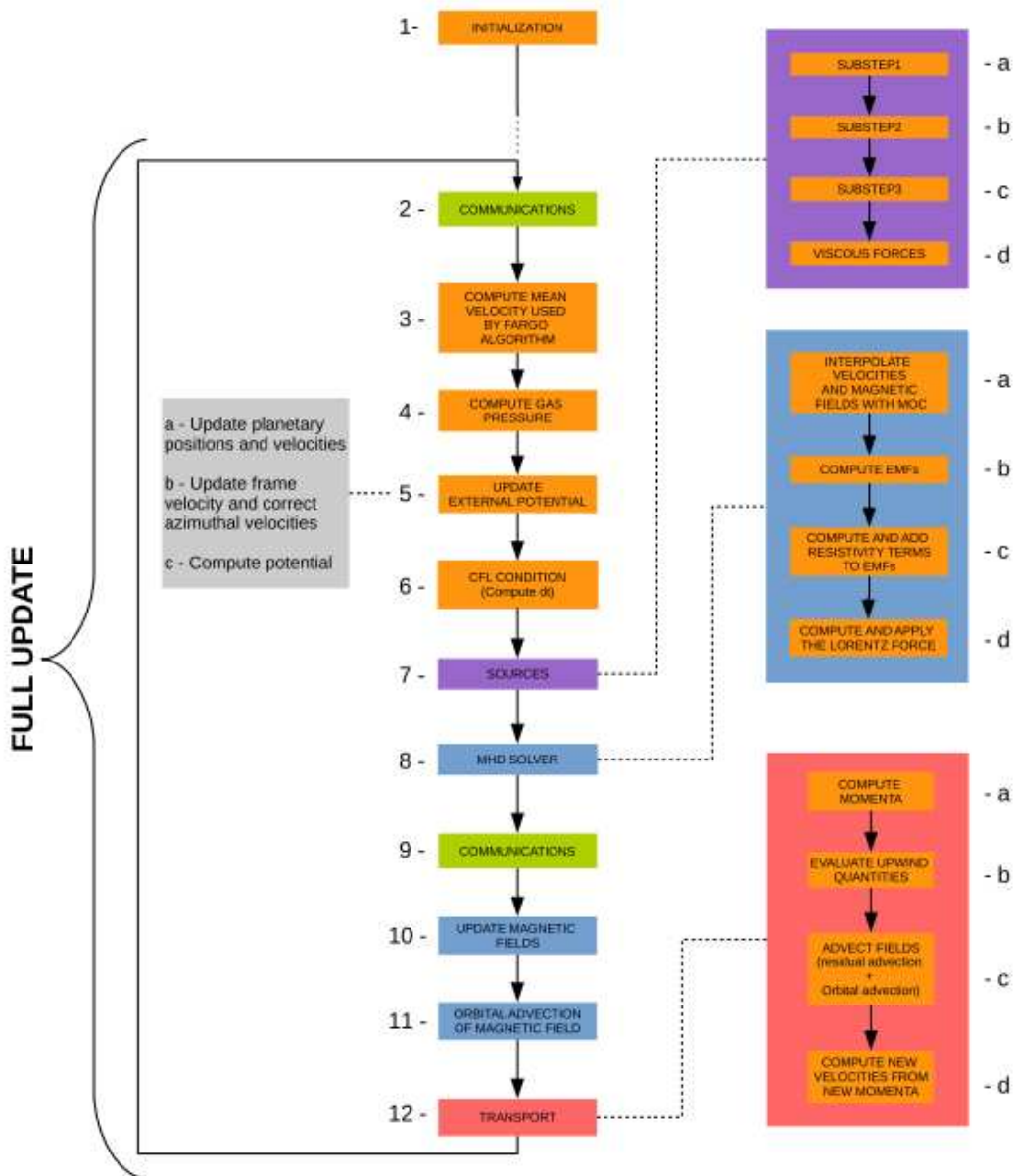
Figure 15: Flow chart of the operations performed in succession in FARGO3D during a full update. Note that the boxes with blue background are specific to the MHD case. From Benitez et al. [5].

a two-stage migration, inward-then-outward, based on the coupling between planet migration due to the interaction with the disk and a 3:2 mean motion resonance. This ratio of commensurability represents the first encountered first-order mean motion resonance for a Jupiter-Saturn pair, although the second-order 5:3 commensurability may provide another possibility [13].

Recently, preliminary simulations were performed with the FARGO3D hydrodynamical

code in order to better understand the circumstances under which the outward migration of a Jupiter-Saturn resonant system can be effective. These simulations are done in 2-dimensions, with polar cylindrical coordinates $\{x_1, x_2\} = \{r, \phi\}$. The adopted non-rotating reference frame is centred on the central star, which is assumed to have the same mass of the Sun. The disk radius ranges from $R_{min} = 0.4 \ AU$ to $R_{max} = 12.0 \ AU$, with damped outflow boundary conditions implemented both at the inner and other border. This type of boundaries enables the accretion of disk material onto the central star as well as its dissipation due to photoevaporation, stellar winds and radiation pressure. The two planets have the same masses of Jupiter and Saturn and they are assumed to be fully-formed before starting their migration within the gaseous disk. More specifically, the initial positions of the two planets are held fixed until they reach their final masses, when they are released and allowed to migrate. This time enables the system to stabilize itself, in order to avoid problems in the simulation. The initial conditions of the two planets are $a_j = 4 \ AU$ and $a_s = 6 \ AU$, a range of locations that is considered to be highly favorable for giant planet formation due to the presence of the snow-line, being it estimated to be around $3 - 5 \ AU$. The disk is supposed to be locally isothermal, thus providing a good approximation for old disks with low gas density. As a consequence, the cooling, thermal conduction and entropy effects are neglected in these simulations. The surface density is set to $\Sigma = 40 \ g/cm^2$ at $r = 1 \ AU$, a choice which is very similar to the one made by D'Angelo et al. [13], who used a surface density of $\Sigma = 50 \ g/cm^2$. This low density value is in line with the fact that the planets have already formed before starting their migration. The aspect ratio is constant through the disk, being of the order of $h = \frac{H}{r} = 0.05$. This value aligns with those adopted in other simulations, being it equal to $h = 0.04$ in the works conducted by Masset et al. [31] and by D'Angelo et al. [13], while it is set to $h = 0.05$ in the study proposed by Walsh et al. [58]. The viscosity parameter α is supposed to be constant through the disk and it is set to $\alpha = 1 \cdot 10^{-3}$, while the kinematic viscosity is given by $\nu = \alpha \sqrt{r}$. This choice of α well agrees with the value of $\alpha = 6 \cdot 10^{-3}$ used by Masset et al. [31].

By adopting a grid resolution of $N_r = 384$ and $N_\theta = 620$, these preliminary simulations have shown that the resonance capable of driving outward migration for a Jupiter-Saturn pair is indeed the 3:2 mean motion resonance, while the second order 5:3 commensurability is overcome without any problem. The resolution of the grid was then firstly increased by almost a factor of 2, thus setting it to $N_r = 512$ and $N_\theta = 1024$, and subsequently by a factor of 3, with $N_r = 768$ and $N_\theta = 1536$. Surprisingly, the results obtained are different with respect to the low-resolution case. Indeed, in the high resolution case, it is the second-order 5:3 mean motion resonance to drive the outward migration and not the usual 3:2 commensurability. The medium resolution case shows instead an interme-

diate behaviour, with a temporary capture in the 5:3 mean motion resonance and a final arrangement in the 3:2 commensurability. The time evolution of the semi-axes ratio of the two planets in the three grid resolution cases is provided in Fig. 16.
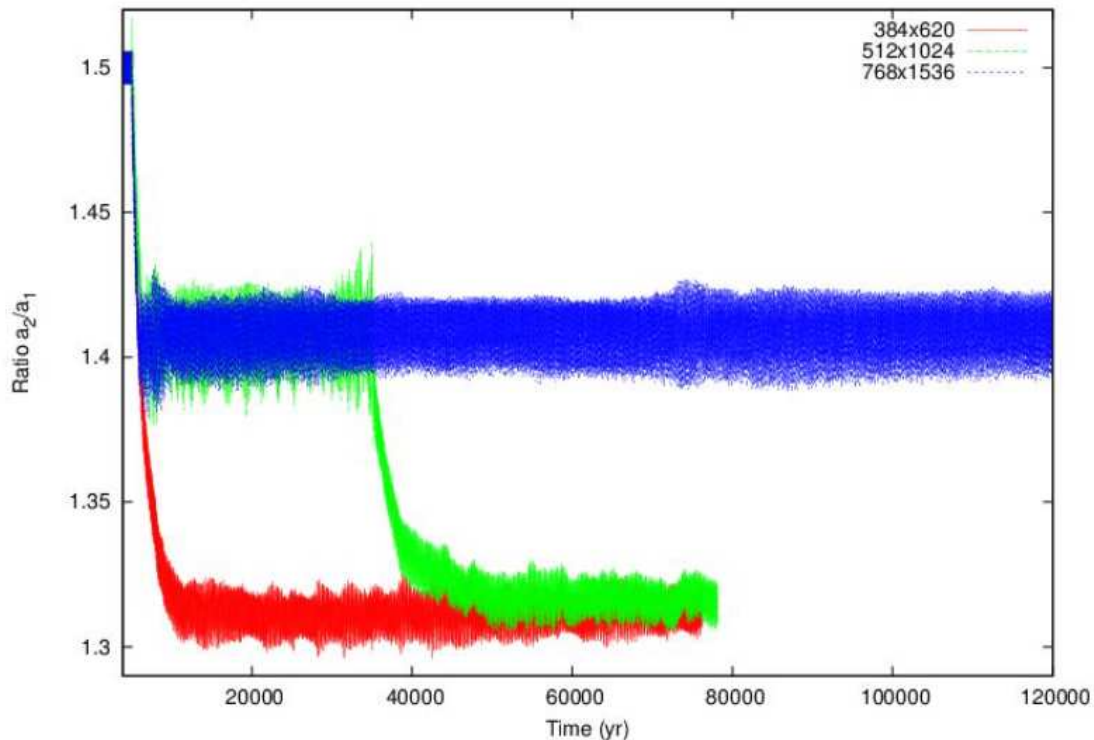

Figure 16: Time evolution of the semi-axes ratio of the two planets in the three grid resolution cases. A ratio of about $a_2/a_1 \approx 1.41$ indicates the occurrence of a 5:3 mean motion resonance, while a ratio of $a_2/a_1 \approx 1.31$ denotes a 3:2 mean motion resonance. Preliminary simulations obtained with the FARGO3D hydrodynamical code.

The obtained results raise several questions regarding whether the observed outcomes are due to an intrinsic issue within the FARGO3D code or if the resolution of the model indeed influences the type of resonance capable of driving the outward planet migration. In order to explore this further, an alternative hydrodynamical code, namely PLUTO, was employed to investigate the coupled evolution of a Jupiter-Saturn pair within its parent protoplanetary disk.

5 The PLUTO Code

PLUTO is a multi-physics, multi-algorithm, high-resolution numerical code, which is specifically designed for handling astrophysical hypersonic flows in the presence of discontinuities [34]. This code is able to integrate a system of conservation laws, i.e. mixed hyperbolic-parabolic systems of partial differential equations, by means of shock-capturing methods and by adopting a conservative discretization based on finite volume or finite difference Godunov-type[12] schemes. In this approach, volume averages are first reconstructed using piecewise monotonic interpolants inside each computational cell. Subsequently, a Riemann problem is solved at each interface with discontinuous left and right states. Finally, the solution is evolved in time [34]. A simplified flow diagram of the strategy followed by the PLUTO code is provided in Fig. 17.
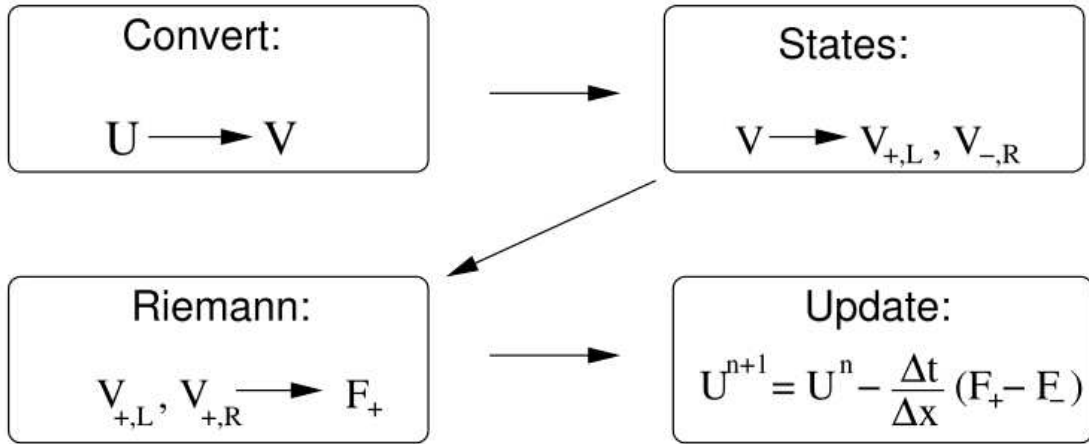

Figure 17: Simplified flow diagram of the reconstruct-solve-average strategy. Firstly, volume averages U are more conveniently mapped into primitive quantities V. Subsequently, left and right states $V_{+,L}$ and $V_{-,R}$ are constructed inside each zone by suitable variable interpolation or extrapolation. A Riemann problem is then solved between $V_{+,L}$ and $V_{+,R}$ to compute the numerical flux function F_+ at cell interfaces. Finally, the solution is advanced in time. From Mignone et al. [34].

It is worth to note that the employment of high-resolution shock-capturing (HRSC) schemes has revealed to be a promising tool to study fluid dynamics in non-linear regimes. In particular, this type of schemes has the ability to accurately simulate strongly supersonic flows, while maintaining robustness and stability. The implementation of HRSC algo-

---

[12]The Godunov scheme is a conservative numerical scheme used to solve partial differential equations. It represents a conservative finite-volume method which solves Riemann problems at each inter-cell boundary. Despite being a first order accurate method in both space and time, it can also be used as a base scheme for developing higher-order methods.

rithms relies on a conservative formulation of the fluid equations, where accurate up-winding is achieved through an exact or approximate solution to the Riemann problem. As it was done for the FARGO3D code, let's denote as U a set of conservative quantities, as $T(U)$ a rank 2 tensor representing the fluxes of each component of U and as $S(U)$ the source terms. It follows that a system of conservation laws is written as:

$$\frac{\partial U}{\partial t} = -\nabla \cdot T(U) + S(U)$$

While the components of U are the main variables being updated, it is more convenient to compute fluxes using a different set of physical quantities. This set will be denoted as the primitive vector V.

The explicit form assumed by all these quantities depends on the particular physics module the user chooses to work with. The possible choices consists of the Newtonian hydrodynamics or HD module, the ideal magnetohydrodynamics or MHD module, the special relativistic hydrodynamics or RHD module, the special relativistic magnetohydrodynamics or RMHD module and the special relativistic magnetohydrodynamics with resistivity or ResRMHD module. Each physics module comprises all the necessary algorithms to calculate the terms involved in the discretization of the right-hand side of the previous system of equations. This should include one or more Riemann solvers, mapping routines for the conversion between primitive and conservative variables, a flux routine that determines the components of $T(U)$ in each direction, a source term function and a routine for computing the maximum and minimum characteristic speeds of the Jacobian matrix.

In order to solve the system of conservation laws, PLUTO adopts a mesh approach, where flow quantities are discretized on a rectangular computational grid enclosed by a boundary. Moreover, guard cells or ghost points are used to implement boundary conditions. It is worth to note that the grid can be either static or dynamically adaptive to the evolution of the flow. In the first case the running of PLUTO requires Python, a C compiler and the make utility, while in the latter one the code relies on the Chombo library for adaptive mesh refinement (AMR). However, in all future simulations the static version of the grid will be adopted.

The PLUTO code can run on both single processors and parallel machines, with the parallel functionality being implemented through the message passing interface (MPI) library. In particular, parallelization is achieved through domain decomposition, where the global domain is divided into subdomains with an equal number of points and each subdomain is assigned to a processor.

5.1 PLUTO Configuration Files

The configuration of PLUTO is stored in five different files:

- The *definitions.h* header file contains all the problem-dependent preprocessor directives required at compilation time.

- The *makefile* is the one needed to compile the code.

- The *pluto.ini* initialization file contains all the run-time parameters.

- The *planet.ini* file defines the initial conditions for the planets present in the simulation.

- The *init.c* file implements the initial and boundary conditions.

The Python script *setup.py* is used to create the first two files, while the latter three must be edited by the user. After these five configuration files are created, PLUTO can be compiled by typing the command *make*. If compilation is successful, the command *./pluto* allows to run the code.

The following subsections will explain the various options accessible through the different configuration files, together with the choices made for the simulations that will be discussed later.

5.2 Definitions.h

As it was said in Sec. 5.1, the header file *definitions.h* is created by the Python script *setup.py* by selecting the *Setup problem* menu. There are different options accessible through this Python script, as it is shown in Tab. 1. In particular:

- *PHYSICS* specifies the fluid equations to be solved. In all future simulations the classical hydrodynamics physics module *HD* described by the Euler equations will be adopted. With this module, PLUTO evolves in time following systems of conservation laws:

$$
\frac{\partial}{\partial t}
\begin{pmatrix} \rho \\ m \\ E_t + \rho\Phi \end{pmatrix}
+ \nabla \cdot
\begin{pmatrix} \rho v \\ mv + pI \\ (E_t + p + \rho\Phi)v \end{pmatrix}^T
=
\begin{pmatrix} 0 \\ -\rho\nabla\Phi + \rho g \\ m \cdot g \end{pmatrix}
$$

In this expression ρ is the mass density, $m = \rho v$ is the momentum density, v is the velocity, p is the thermal pressure, E_t is the total energy density, Φ is the gravitational potential, g is the acceleration vector, while I is the unit tensor. The total

Option	Value
PHYSICS	HD
DIMENSIONS	2
COMPONENTS	2
GEOMETRY	POLAR
BODY_FORCE	NO
COOLING	NO
RECONSTRUCTION	LINEAR
TIME_STEPPING	RK2
DIMENSIONAL_SPLITTING	NO
NTRACER	0
USER_DEF_PARAMETERS	6
NBODY_SYS	YES

Table 1: Options and selected values that are accessible through the *definitions.h* header file.

energy density E_t is related to the gas pressure p by the ideal gas closure [34]:

$$E_t = \frac{p}{\Gamma - 1} + \frac{|m|^2}{2\rho}$$

Primitive variables are defined by $V = (\rho, v, p)^T$ and they are generally more convenient when boundary or initial conditions are assigned.

- *DIMENSIONS* sets the number of spatial dimensions of the problem. In this work it was chosen to deal with two-dimensional hydrodynamics simulations only, so it will always be set equal to 2. The related option *COMPONENTS* is placed equal to 2 as well in order to exclude the z coordinate in the future calculations in the (r, ϕ) coordinates in polar geometry.

- *GEOMETRY* sets the geometry of the problem, which will be in polar cylindrical coordinates $\{x_1, x_2\} = \{r, \phi\}$. As just said, the third dimension x_3 was excluded.

- *BODY FORCE* is used to include a body force in the momentum and energy equations, but this option will not be exploited.

- *COOLING* is used to include optically thin thermal losses, but again it will not be exploited.

- *RECONSTRUCTION* sets the spatial order of integration. In particular, it refers to the process of approximating the values of fluid variables at cell interfaces within the numerical grid. Therefore, it plays a crucial role for accurately calculating fluxes and evolving the solution in time. The reconstruction technique used in PLUTO is

typically based on piecewise polynomial interpolation. This reconstruction aims to estimate the values of the fluid variables at the cell interfaces starting from the values available at the cell centers. The chosen option will be the default *LINEAR* one, which is second order accurate in space and provides a TVD[13] linear reconstruction of the primitive variables. This choice is due to the fact that the linear option handles curvilinear coordinates more correctly than other types of reconstruction.

- *TIME_STEPPING* defines the time increment between two consecutive steps. In this work the second order TVD Runge-Kutta option *RK2* will be used to advance the solution to the next time level. More precisely, if $\Delta t^n = t^{n+1} - t^n$ is the increment between two consecutive steps and $\mathcal{L}$ denotes the discretized spatial operator, the *RK2* option gives:

$$U^* = U^n + \Delta t^n \mathcal{L}^n$$
$$U^{n+1} = \frac{1}{2}(U^n + U^* + \Delta t^n \mathcal{L}^*)$$

  It is worth to note that multi-stage integrators like Runge-Kutta handles non-Cartesian geometries better, especially in the presence of angular coordinates.

- *DIMENSIONAL_SPLITTING* allows to use different numerical integration methods for different physical dimensions, but it will not be exploited in this work.

- *NTRACER* is used to follow the evolution of a specified number of dust grains, but it will not be exploited.

- *USER_DEF_PARAMETERS* sets the number of user-defined parameters that can be changed at runtime. In the future simulations it was chosen to add six user defined parameters. In particular, *M_CO* is the mass of the central star and *ASPECT_RATIO* refers to the scale height of the disk, which is assumed to be a constant. The *ALPHA* parameter gives the selected value for the viscosity parameter α. The other three parameters are related to the superficial density of the disk, whose profile is given by:

$$\Sigma(r) = \Sigma_0 \cdot r^{-\alpha}$$

  In this expression the quantity Σ_0 is the superficial density at $r = 1\ AU$ and its value is provided by the *SIGMA_REF* parameter. The α coefficient is supplied via the *PROFILE_P* parameter, while the *SIGMA_FLOOR* parameter sets a minimum density value. Once being set and labelled in the *definition.h* file as shown in Tab. 2,

---

[13]TVD stands for Total Variational Diminishing and it refers to a type of schemes usually implemented within an unstructured grid finite volume method framework. Note that it is the use of flux limiters, together with an appropriate high resolution scheme, that makes the solutions total variation diminishing.

the values of these six user-defined parameters are selected inside the initialization file *pluto.ini*.

Parameter	Label
M_CO	0
ASPECT_RATIO	1
ALPHA	2
SIGMA_REF	3
SIGMA_FLOOR	4
PROFILE_P	5

Table 2: Setting and labelling of the user-defined parameters in the *definitions.h* file.

- *NBODY_SYS* is used to activate the PLUTO N-body module, which works only in 2-D polar or 3-D spherical coordinates with the RK2 time-stepping algorithm. The user must also define different N-body declarations. In particular, the option *CENTRAL_OBJECT* defines if the disk is centered around a single star in the origin or around the center or mass of a binary. In this work it was chosen to deal with a single star, so it is necessary to provide a user-defined parameter called *M_CO* that must be equal to the mass of the star in code units (as it was done in the *USER_DEF_PARAMETERS* option). The *CO_FEELS_DISK* options was set to *TRUE*, so that the central object is accelerated by the disk. When planets are present in the simulation or when the central object is accelerated by the disk, the coordinate system is accelerated. By setting the *INDIRECT_TERM* option to *YES* a correction term is added to account for this acceleration. The *NO_OF_PLANETS* option defines the number of planets present in the simulation, which will be equal to 2 in all future simulations. Finally, the *PLANET_FORMAT* option was set to *ORBIT* in order to specify the orbital elements of each planet in the *planet.ini* configuration file. The selected N-body declarations are shown in Tab. 3.

Option	Value
CENTRAL_OBJECT	STAR
CO_FEELS_DISK	YES
INDIRECT_TERM	YES
NO_OF_PLANETS	2
PLANET_FORMAT	ORBIT

Table 3: N-body declarations in the *definitions.h* file.

Once the physics module is selected, further options appear in a secondary menu depending on the choice made, as it is shown in Tab. 4. In particular, having selected the *HD* module, the following options are available:

Option	Value
EOS	ISOTHERMAL
ENTROPY_SWITCH	NO
THERMAL_CONDUCTION	NO
VISCOSITY	EXPLICIT
ROTATING_FRAME	NO

Table 4: Physics dependent declarations and correspondent selected values in the *definitions.h* file.

- The *EOS* option selects the equation of state, which will be the isothermal one. In an isothermal gas, the temperature is constant and the pressure is obtained by the following expression:

$$p = \rho c_{iso}^2$$

In this expression c_{iso} represents the isothermal sound speed, which can be either a constant value or a spatially-varying quantity that will be set using the variable *g_isoSoundSpeed* in the *init.c* configuration file. Note that in this case the energy equation is not included.

- The *ENTROPY_SWITCH* option is used to add the entropy equation to the system of conservation laws. However, this option is not available for the isothermal equation of state, so it will not be exploited.

- The *THERMAL_CONDUCTION* option allows to include thermal conduction effects, but again it will not be exploited.

- The *VISCOSITY* option is used to include viscous terms. In this work it was chosen to select the *EXPLICIT* option, which will treat viscosity explicitly. The viscous stresses enter the *HD* equations with two parabolic diffusion terms in the momentum and energy equations, thus giving a mixed hyperbolic/parabolic system of the form:

$$\frac{\partial m}{\partial t} + \nabla \cdot T_h = \nabla \cdot \Pi$$

$$\frac{\partial E_t}{\partial t} + \nabla \cdot F_E = \nabla \cdot (v \cdot \Pi)$$

The quantity Π represents the viscous stress tensor, which for an isotropic viscous stress is given by:

$$\Pi = \nu_1 \left[\nabla v + (\nabla v)^T \right] + \left(\nu_2 - \frac{2}{3}\nu_1 \right) (\nabla \cdot v)$$

In this expression the two coefficients ν_1 and ν_2 are the first (shear) and second

(bulk) parameter of viscosity, respectively.

- The *ROTATING_FRAME* option allows to solve the equations in a reference frame which rotates with constant angular velocity around the vertical polar axis. However, it was chosen to not exploit this option.

It is also possible to manually insert an arbitrary number of user-defined symbolic constants in the header file *definitions.h*. This is important because PLUTO generally works with code units (i.e. non-dimensional units) in order to properly rescale flow quantities. In particular, dimensionalization is necessary when specific length, time or energy scales are introduced in the problem. PLUTO then requires three fundamental units to be specified through the definition of the following constants:

- The *UNIT_LENGTH* L_0 sets the reference length in cm.

- The *UNIT_DENSITY* ρ_0 defines the reference density in gr/cm^3.

- The *UNIT_VELOCITY* v_0 sets the reference velocity in cm/s.

Note that all other units are derived from a combination of these three symbolic constants. Finally, the header file *definitions.h* allows the definition of several user-editable supplementary constants, as it is shown in Tab. 5.

Constant	Value
PRINT_TO_FILE	YES
INTERNAL_BOUNDARY	YES
CHAR_LIMITING	YES
LIMITER	VANLEER_LIM

Table 5: User-editable supplementary constants and selected values in the *definitions.h* file.

Of considerable relevance is the *INTERNAL_BOUNDARY* option, which if set to *YES* enables the control of the solution array at the beginning of every time step inside the computational domain through the *UserDefBoundary()* function defined in the *init.c* configuration file. The *LIMITER* option introduces a flux limiter to restrict the solution gradient near shocks or discontinuities and avoid the spurious oscillations that would otherwise occur with high order spatial discretization schemes due to sharp changes in the solution domain. The selected flux limiter function will be the *VANLEER_LIM* one, which is defined by the following expressions:

$$\phi(r) = \frac{r + |r|}{1 + |r|} \qquad\qquad \lim_{r \to \infty} \phi(r) = 2$$

The supplementary constants *PRINT_TO_FILE* and *CHAR_LIMITING* are instead related to the output of the simulation.

5.3 Makefile

The *makefile* contains instructions to compile the code and produces the executable pluto. When a new *makefile* is created, Python will ask the user to select the appropriate *.defs* file containing the architecture-dependent flags from the *Config* directory. In the future simulations, it will always be the *Linux.gcc.defs* file[14].

The *makefile* is also used to set the headers and objects files. Moreover, it defines the variables *PARALLEL*, *USE_HDF5* and *USE_PNG* to enable parallel mode, support for HDF5 library and support for PNG library, respectively. These variables are available only in the static grid version of PLUTO and in this work they will be set to *TRUE*.

Finally, it allows to add user-defined files to the standard object list created by Python. This will instruct the *makefile* that PLUTO has to be compiled together with these user-supplied files.

5.4 Pluto.ini

The *pluto.ini* input file contains all the runtime information necessary for the computation. This initialization file is divided into different blocks, each of them containing a set of labels and corresponding options:

- The *[Grid]* block controls the grid generation. In the static version of PLUTO, as it will be in this work, it defines the physical domain and generates the whole computation. In particular, for each dimension the first integer defines the number of consecutive adjacent grids that are used to cover the whole physical domain. The following triplet is made of a double precision number, an integer and a character, specifying the leftmost node coordinate value, the number of points and the grid-type, respectively. Finally, the last double precision number defines the rightmost node coordinate value. It is important to note that if a dimension is ignored, then a 1 grid-point only should be assigned to that grid. This is exactly what happens for the third dimension x_3 in the adopted polar geometry. The grid-type entry will be set to *u*, thus constructing a uniform grid patch. By denoting as x_L and x_R the leftmost and rightmost points of the patch, the grid spacing will be:

$$\Delta x = \frac{x_R - x_L}{N}$$

---

[14]The argument *gcc* stands for GNU Compiler Collection, which is a C compiler originally written for the GNU operating system.

The adopted grids for future simulations are shown in Tab. 8, Tab. 6 and Tab. 7. With respect to the low-resolution case, the resolution of the grid is increased by a factor of 2 in the medium-resolution case and by a factor of 3 in the high-resolution case.

Dimension	N° of grids	Left node	N° of points	Grid type	Right node
X1-grid	1	0.4	128	u	12.0
X2-grid	1	0.0	256	u	6.28318531
X3-grid	1	0.0	1	u	1.0

Table 6: Low-resolution grid implemented in the Grid block of the *pluto.ini* initialization file.

Dimension	N° of grids	Left node	N° of points	Grid type	Right node
X1-grid	1	0.4	256	u	12.0
X2-grid	1	0.0	512	u	6.28318531
X3-grid	1	0.0	1	u	1.0

Table 7: Medium-resolution grid implemented in the Grid block of the *pluto.ini* initialization file.

Dimension	N° of grids	Left node	N° of points	Grid type	Right node
X1-grid	1	0.4	384	u	12.0
X2-grid	1	0.0	768	u	6.28318531
X3-grid	1	0.0	1	u	1.0

Table 8: High-resolution grid implemented in the Grid block of the *pluto.ini* initialization file.

- The *[Chombo Refinement]* block controls the grid refinement if PLUTO was compiled with the Chombo library. Since a static version of the grid will always be adopted in the future simulations, this block will be ignored.

- The *[Time]* block specifies some adjustable time-marching parameters. In particular, the *CFL* parameter represents the Courant[15] number, which controls the time step length of the simulation. By denoting as N_{dim} the number of spatial dimensions, the Courant number must satisfy the following condition:

$$CFL \leq \frac{1}{N_{dim}}$$

Since in this work $N_{dim} = 2$, this means that $CFL \leq 0.5$. However, it seems that a second order Runge-Kutta algorithm requires $CFL \leq 0.4$ for stability reasons

---

[15]The Courant number is a dimensionless value that represents the time a particle stays in one cell of the mesh. It must be below 1, otherwise the time step is too large to see the particle in one cell.

and this is the value that will be adopted. The *CFL_max_var* parameter defines the maximum time step growth between two consecutive steps. The *tstop* parameter sets the time at which the integration must end, while the *first_dt* parameter defines the initial time step. The selected values of all these parameters for the future simulations are shown in Tab. 9.

Parameter	Value
CFL	0.4
CFL_max_var	1.1
tstop	10000000
first_dt	1.e-6

Table 9: Time block parameters and selected values in the *pluto.ini* initialization file.

- The *[Solver]* block selects the Riemann solver for flux computation. In this work it was chosen to deal with the Harten, Lax, Van Leer approximate Riemann solver[16]. It is selected by using the *hll* string and represents one of the least accurate but most diffusive solver options.

- The *[Boundary]* block is used to specify the boundary conditions that must be applied in the ghost zones of the computational domain. In this work it was chosen to set the *userdef* option along the radial direction, in order to use dumped outflow boundary conditions that were not available in the code. This type of boundary condition will always be used at the inner border of the disk, while at the outer border both a damped outflow and a reflective boundary will be employed. Concversely, the *periodic* option was adopted along the azimuthal direction. Note that user-supplied boundary conditions must be implemented in the *UserDefBoundary()* function defined in the *init.c* configuration file. A graphical representation of the boundary blocks used in this work is provided in Tab. 10.

Dimension	Option	Dimension	Option
X1-beg	userdef	X1-beg	userdef
X1-end	userdef	X1-end	reflective
X2-beg	periodic	X2-beg	periodic
X2-end	periodic	X2-end	periodic
X3-beg	periodic	X3-beg	periodic
X3-end	periodic	X3-end	periodic

Table 10: Boundary block and selected options in the *pluto.ini* initialization file.

---

[16]The HLL solver, developed by Ami Harten, Peter Lax and Bram Van Leer, gives an approximate solution to the Riemann problem. It is based on the integral form of the conservation laws and the largest and smallest signal velocities at the interface.

- The *[Static Grid Output]* block controls the output in the static grid version of PLUTO. In particular, the *uservar* option defines additional variables that must be written in the disk, with an integer representing the number of such variables. The *output_dir* option sets the name of the directory where the output files will be written (it must already exist at runtime or an error will occur). The subsequent options assign the output intervals for different data types. For each line, the first field specifies the time interval in code units between two consecutive outputs, with a negative value used to suppress the output for a specific format. The second field gives the number of steps and in this case negative values will be ignored. Finally, the last field can be set either to *single_file* in order to have one single output containing all the variables, or to *multiple_files* to have different variables written in different files. Note that the string *dbl* refers to double precision (8 bytes) binary data, while *flt* to single precision (4 bytes) ones. The last line defines instead the call frequency of the *Analysis()* function present in the *init.c* configuration file. The values adopted in this work are shown in Tab. 11.

Option	Value
uservar	0
output_dir	./out

Option	Time interval	N° of steps	Output
dbl	100.0	-10000	single_file
flt	-1.0	-1	single_file
analysis	-1.0	10	

Table 11: Static grid output block options and selected values in the *pluto.ini* initialization file.

- The *[Parameters]* block is used to provide user-defined input parameters, which will be read at runtime. The six parameters used in this work were already presented in the *definitions.h* subsection, where they were set and labelled. The selected values of these parameters are shown in Tab. 12, which will be used in the low and high density regimes, respectively.

5.5 Planet.ini

It was said in the *definitions.h* subsection that the *NBODY_SYS* option is used to activate the PLUTO N-body module. The initial conditions for the planets present in the simulation are stored in the *planet.ini* configuration file. In particular, since the option *PLANET_FORMAT* was set to *ORBIT* in the *definitions.h* file, the user must specify the orbital elements of each planet.

Parameter	Value	Parameter	Value
M_CO	1.0	M_CO	1.0
ASPECT_RATIO	0.05	ASPECT_RATIO	0.05
ALPHA_SIGMA	1.e-3	ALPHA_SIGMA	1.e-3
SIGMA_REF	40.0	SIGMA_REF	1500.0
SIGMA_FLOOR	1.0e-6	SIGMA_FLOOR	1.0e-6
PROFILE_P	1.0	PROFILE_P	1.0

Table 12: User-defined parameters and selected values in the parameters block of the *pluto.ini* inizialization file.

The required orbital elements are the mass of the planet, the semi-major axis, the eccentricity, the inclination, the longitude of the ascending node, the argument of periapsis, the true anomaly and the disk feedback. All these quantities are shown in Tab. 13, together with the correspondent values used in this work.

m	a	e	i	Omega	omega	f	Feedback
9.546e-4	4.0	0.0	0.0	4.7123893+00	3.141593e+00	0	1
2.858e-4	6.0	0.0	0.0	0.0	0.0	0	1

Table 13: Values of the orbital elements used in the *planet.ini* initialization file.

Note that the N-body module writes the following files to the disk:

- The *nbody_com.dat* file contains the Cartesian coordinates of the center of mass of the central object and the center of mass of all objects (i.e. the central object and the planets).

- The *nbody_coordinates.dat* file contains the Cartesian coordinates of all objects.

- The *nbody_orbital_elements.dat* file contains the orbital elements of the objects in Jacobian coordinates.

The output frequency of these three files is the same as the output frequency of the PLUTO *Analysis()* function defined in the *[Static Grid Output]* block in the *pluto.ini* initialization file.

5.6   Init.c

The source file *init.c* provides a set of functions that are used to define the fluid configuration for a specific problem. In particular, the following functions are included:

- The *Init()* function is used to assign the fluid initial conditions as functions of the spatial coordinates. By denoting as v a pointer to a vector of primitive quantities

and as $x1, x2, x3$ the coordinates x_1, x_2, x_3 of the computational cell where v is initialized, the required syntax is:

$$void\ Init\ (double\ *v,\ double\ x1,\ double\ x2,\ double\ x3)$$

Note that the expression for the azimuthal velocity of the disk takes into account the presence of a pressure gradient that decreases its value.

- The *UserDefBoundary()* function sets user-defined boundary conditions at the physical boundary sides of the computational domain if the option *userdef* is chosen inside the *pluto.ini* configuration file. Moreover, as already said in the *definitions.h* subsection, this function can be used to control the solution array at the beginning of every time step inside the computational domain if the *INTERNAL_BOUNDARY* option is set to *YES*. Thanks to this feature it is possible to adjust the value of selected variables inside a specific region rather than at the boundaries. The syntax required from this function is:

$$void\ UserDefBoundary\ (const\ Data\ *d,\ RBox\ *box,\ int\ side,\ Grid\ *grid)$$

In this expression $*d$ is a pointer to the PLUTO data structure, which contains a four-index array of primitive variables defined at the cell center[17]. The argument $*box$ is a pointer to the RBox structure and it defines the rectangular portion of the domain over which ghost zone values should be assigned. However, the use of the box structure is not mandatory and the two options *X1_BEG_LOOP()* and *X1_END_LOOP()* may be employed. The argument $side$ specifies on which side of the physical domain user-defined values should be prescribed. Possible values are *X1_BEG* and *X1_END* in order to assign boundary conditions in the ghost zones at the beginning and end of the physical domain in the x_1 direction. The value 0 instead controls the solution inside the domain and it can be used only if the *INTERNAL_BOUNDARY* option is set to *TRUE* in the *definitions.h* configuration file. Finally, the argument $*grid$ is a pointer to the grid structure that contains all the relevant grid information. In the present work, this function is exploited to implement damped outflow boundary conditions at the borders of the disk.

- The *Analysis()* function is used to perform run-time data analysis in order to save input or output data for the post-processing phase. The call frequency of this function is set in the *[Static Grid Output]* block of the *pluto.ini* initialization file.

---

[17]The syntax is $d \rightarrow Vc\ [nv][k][j][i]$, where the integer nv labels the variable, while k, j, i are the indices of the x_3, x_2, x_1 directions, respectively.

- The *BodyForceVector()* function and the textitBodyForcePotential() functions define the vector components of the acceleration and the gravitational potential. However, in this work it was decided to not enable the *BODY_FORCE* flag in the *definitions.h* file, so these functions will not be exploited.

5.7 Comparison between PLUTO and FARGO3D

While PLUTO and FARGO3D are both hydrodynamical codes used for simulating fluid dynamics, they have some differences in their features and focus areas.

The main distinction between the two codes is based on the fact that they use different numerical methods to solve the equations of fluid dynamics. In particular, PLUTO employs a Godunov-type shock-capturing scheme using the finite volume formalism. Within this context, volume averages are first reconstructed employing piecewise monotonic interpolants inside each computational cell. Subsequently, a Riemann problem is solved at each interface and the solution is evolved in time. This approach is well-suited for capturing highly supersonic flows in the presence of strong discontinuities.

Conversely, FARGO3D is based on a finite-difference method that employs operator splitting and upwind techniques. Instead of using the Riemann problem to evaluate the fluxes at each interface, it exploits the staggering of the velocity field to express the flux in a simpler way. This code is specifically designed for modeling accretion disks in astrophysical contexts. As a result, it is highly compatible with the study of planet-disk interactions and planet migration.

It is worth to note that the construction of codes based on Godunov's methods, such as the PLUTO code, involves some notable differences compared to staggered mesh codes, like the FARGO3D code. In particular, let's consider the following salient points:

- The computational cost of performing a full time-step using a staggered mesh code is considerably lower compared to that of employing Godunov's method.

- Codes that employ the Godunov's method, where a Riemann's problem is used to compute the fluxes at the cell interfaces, automatically ensure the conservation of the physical quantities. Conversely, the FARGO3D code lacks such conservation properties, which must be addressed separately.

- Unlike Godunov's methods, staggered mesh codes do not encounter difficulties when handling steady flows with source terms. This fact is important in numerous scenarios within protoplanetary disks, where it is crucial to accurately capture the vertical and rotational equilibrium of the unperturbed disk, as well as the equilibrium of the envelope surrounding embedded planets.

57

- Codes utilizing Godunov's method typically employ fluxes of total energy, thus ensuring the energy conservation with high precision. On the other hand, staggered mesh codes employ fluxes of internal energy and they do not achieve machine-accurate conservation of energy. While this may initially appear as a drawback, it is not the case. In fact, protoplanetary disks often exhibit large Mach numbers, which causes the kinetic energy to surpass the internal energy by two or three orders of magnitude. As a consequence, truncation errors affecting the kinetic energy can propagate to the internal energy budget, thus amplifying the relative error. This challenge is commonly referred to as the high Mach number problem [49]. Since many problems involving planet-disk interactions necessitate precise entropy advection in the co-orbital region of the planet, it is preferable to treat the internal energy separately.

- The inclusion of new processes within the code typically involves a more extensive effort when using Godunov's method, often requiring the rewriting of the Riemann solver. Conversely, it is comparatively easier to introduce new or different physics in staggered mesh codes by employing the operator splitting technique.

It is safe to conclude that the choice between PLUTO and FARGO3D depends on the specific simulation requirements and scientific objectives related to the study of fluid dynamics, with PLUTO offering a more general-purpose and flexible framework, while FARGO3D providing specialized capabilities for accretion disk simulations.

6 Results

As it was anticipated in Sec. 4.1, it was chosen to investigate the coupled evolution of a Jupiter-Saturn pair within its parent protoplanetary disk by using the PLUTO hydrodynamical code. This was done in order to understand whether the observed outcomes obtained by the preliminary simulations performed with the FARGO3D code are due to an intrinsic issue within the code or if the resolution of the model influences the type of resonance capable of driving the outward planet migration.

The setup conditions of the simulations are the same used with the FARGO3D code. The 2-dimensional hydrodynamic simulations are done in polar cylindrical coordinates $\{x_1, x_2\} = \{r, \phi\}$. The adopted non-rotating reference frame is centred on the central star, which is assumed to have the same mass of the Sun. The disk is supposed to be locally isothermal and its radius ranges from $R_{min} = 0.4\ AU$ to $R_{max} = 12.0\ AU$. The surface density is set to $\Sigma = 40\ g/cm^2$ at $r = 1\ AU$, while the aspect ratio is constant through the disk and it is equal to $h = \frac{H}{r} = 0.05$. The two planets have the same masses of Jupiter and Saturn and their initial conditions are $a_j = 4\ AU$ and $a_s = 6\ AU$. More specifically, they are assumed to start with zero mass, which linearly increases until it reaches its final value. At that point, the entire system begins to evolve. The viscosity parameter α is supposed to be constant through the disk and it is set to $\alpha = 1 \cdot 10^{-3}$, while the kinematic viscosity is given by $\nu = \alpha \sqrt{r}$.

6.1 Medium-Resolution Simulations

It was firstly chosen to implement damped outflow boundary conditions at both the inner and outer border of the disk, as it was done with the FARGO3D code. The adopted grid resolution is $N_r = 256$ and $N_\theta = 512$.

As it was said in Sec. 3.1, a planet exerting its gravitational force to the disk has the ability to initiate waves at Lindblad resonances, whose combination results in the formation of a spiral density wave with a single-arm pattern, namely the wake. The inner part of the spiral wave rotates faster than the planet, thus exerting a positive gravitational torque on it. This tends to accelerate the planet, which is forced to migrate outwards. Conversely, the outer part of the spiral wave rotates slower than the planet, thus leading to a negative gravitational torque that tends to slow it down and causing an inward migration. Generally, the sum of the two torques is negative and causes an overall inward migration. This mechanism, called type I migration, acts until a gap is created in the disk. At that point, type II migration takes place when a gap forms around the orbit of the massive planet, leading to a migration which is coupled to the viscous evolution of the disk. As evidence

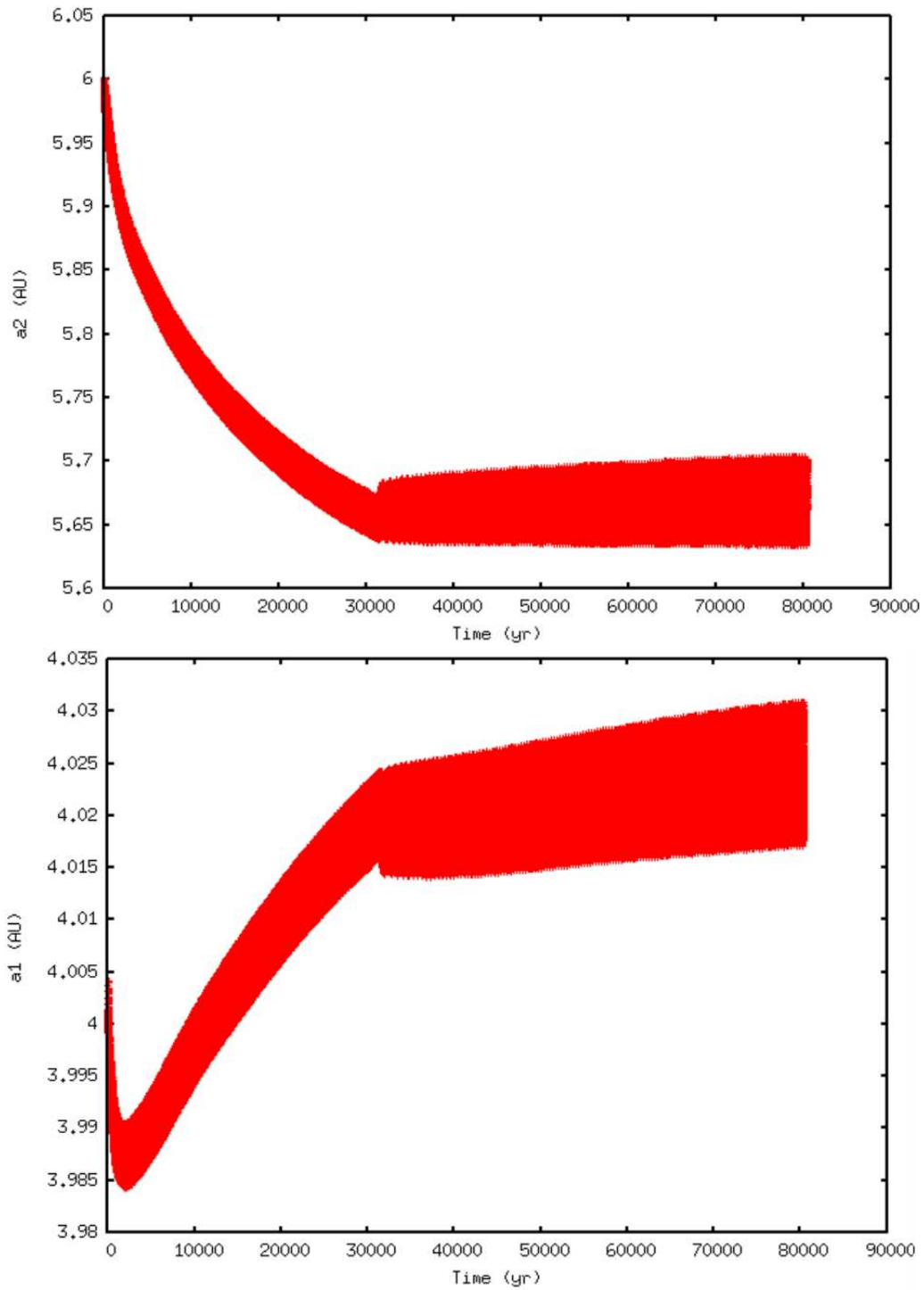of this behaviour, Fig. 18 provides the time evolution of the semi-major axes of Saturn and Jupiter.

Figure 18: Time evolution of the semi-major axis for the external (top panel) and internal planet (bottom panel). The simulation is made with PLUTO, using a grid resolution of 256 x 512 and damped outflow boundaries at both the inner and outer border of the disk.

It is observed that the inner planet firstly migrates inward with a speed progressively de-

creasing as it opens a gap in the gas around its orbit and thus leading to a type II migration, which follows the viscous evolution of the disk. In the meanwhile, the less massive outer planet undergoes a faster inward migration, since it only opens a partial gap in the disk, leading to a convergent migration of the two planets. However, it does not take long for Saturn to start perturbing the outer part of the Jupiter's spiral wave. As a consequence, the positive torque exerted by the inner part of the spiral wave dominates on the other and Jupiter begins to migrate outwards. This leads to an even faster convergent migration, which drives the planets into resonance. After about $3 \cdot 10^4 \ yr$, the two planets successfully merge their gaps and they start migrating together. Since the inner planet is more massive than the outer one, the positive torque exerted by the inner disk overtakes the negative torque exerted by the outer disk, thus forcing the planets to migrate outwards. However, it can be observed that the migration occurs at a very slow pace, with the two planets being almost stationary in their positions.

The resonance lock of the two planets is proven by the fact that the ratio of their semi-major axes remains constant over time, as it is observed in Fig. 19.
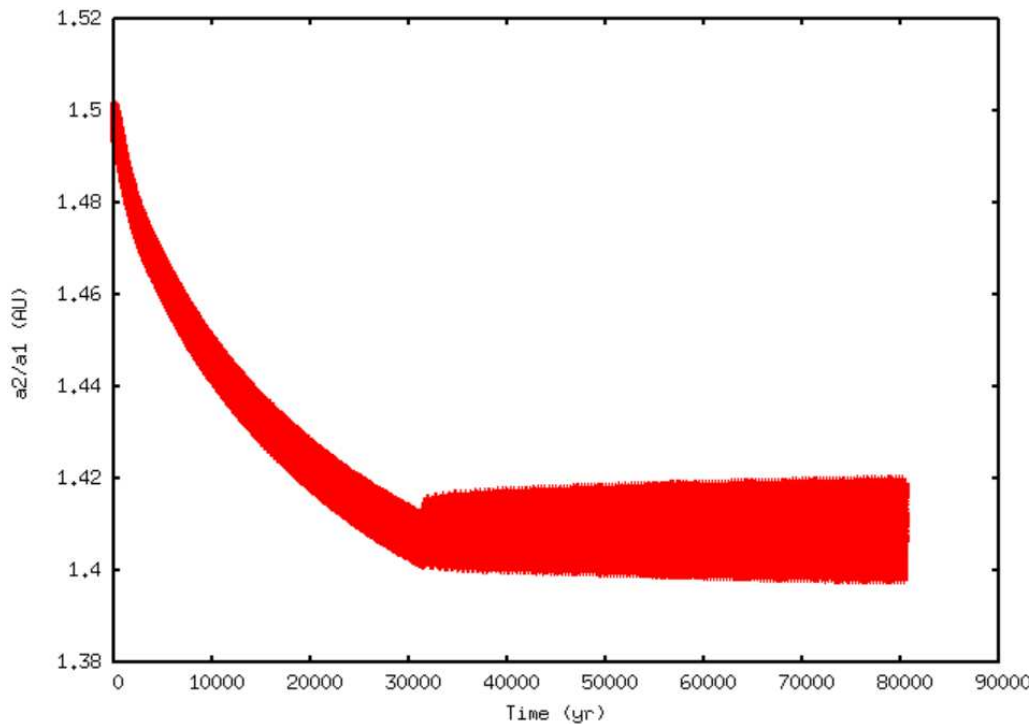
Figure 19: Time evolution of the ratio between the semi-major axes of the two planets. The simulation is made with PLUTO, using a grid resolution of 256 x 512 and damped outflow boundaries at both the inner and outer border of the disk.

Although the model resolution is not very high, the simulation already shows that the resonance capable of driving the outward migration for a Jupiter-Saturn pair is the second order 5:3 mean motion resonance and not the usual first order 3:2 commensurability. This

is illustrated in Fig. 20, which displays the libration of the resonant argument associated with the 5:3 mean motion resonance.
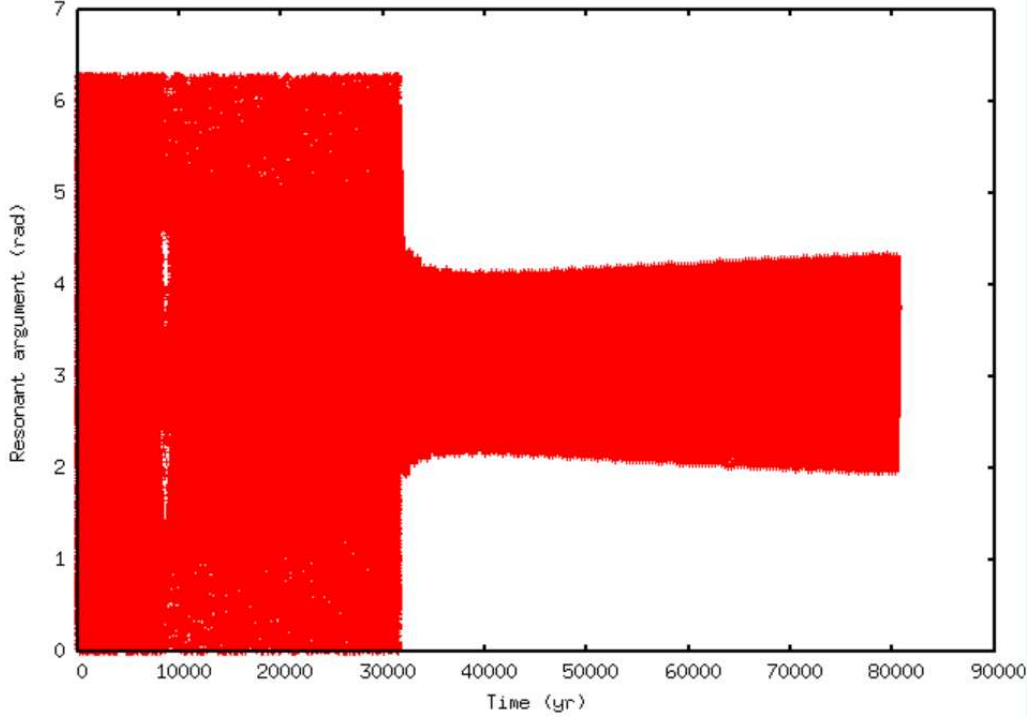

Figure 20: Time evolution of the resonant argument associated with the 5:3 mean motion resonance. The simulation is made with PLUTO, using a grid resolution of 256 x 512 and damped outflow boundaries at both the inner and outer border of the disk.

It is interesting to note that the two-planet system attempted to enter both the first order 2:1 and 3:2 resonances at the beginning of the simulation, but eventually crossed these types of commensurability and continued its evolution until the final capture in the 5:3 mean motion resonance. This behaviour is shown in Fig. 21, which provides the resonant arguments related to the 2:1 and 3:2 mean motion resonances.

As it was said in Sec. 3.4, there are two angles describing the capture in resonance of two planets. If a system is considered to be in a $p + q : p$ mean motion resonance, they are given by:

$$\phi_{1,2} = (p + q)\lambda_2 - p\lambda_1 - q\bar{\omega}_{1,2}$$

In this expression, λ_1 and λ_2 denote respectively the mean longitudes of the inner and outer planets, while $\bar{\omega}_1$ and $\bar{\omega}_2$ refer to the longitude of their pericentres.

Typically, a stable resonance capture implies the libration of both the resonant angles ϕ_1 and ϕ_2, as it happens fort the 5:3 mean motion resonance. Nevertheless, it may occur that the presence of dissipative terms within the N-body simulation causes the libration of only one of them. This is exactly what comes out from the analysis of the time evolution of the resonant arguments associated to the 2:1 and 3:2 mean motion resonances. The system

is only temporarily captured in resonance and, after crossing these commensurabilities, it continues its evolution.
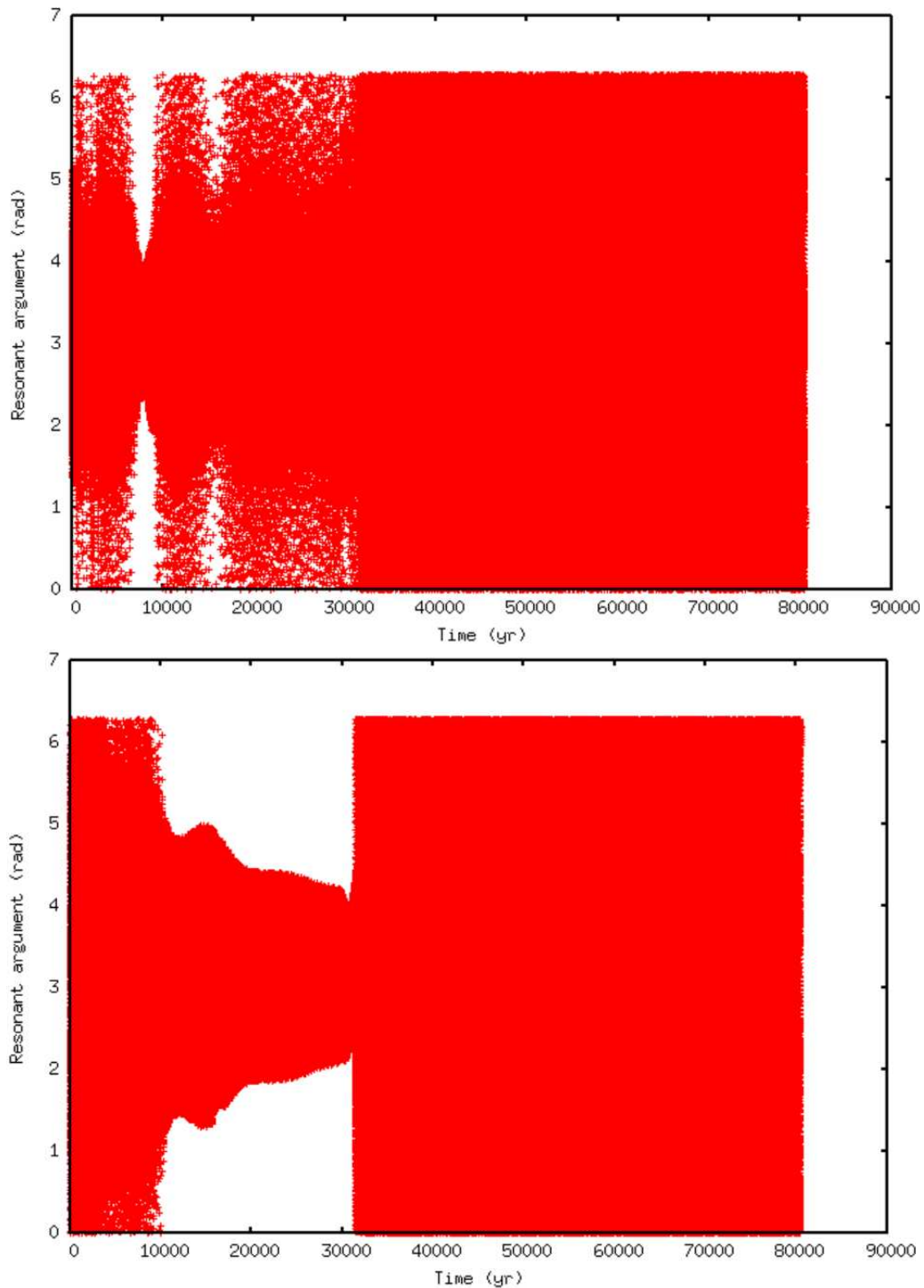

Figure 21: Time evolution of the resonant arguments associated with the 2:1 (top panel) and 3:2 (bottom panel) mean motion resonances. The simulation is made with PLUTO, using a grid resolution of 256 x 512 and damped outflow boundaries at both the inner and outer border of the disk.

The time-evolution of the superficial density of the disk is illustrated by the six snapshots provided in Fig. 22. Let's refer for simplicity to simulation times, which in PLUTO
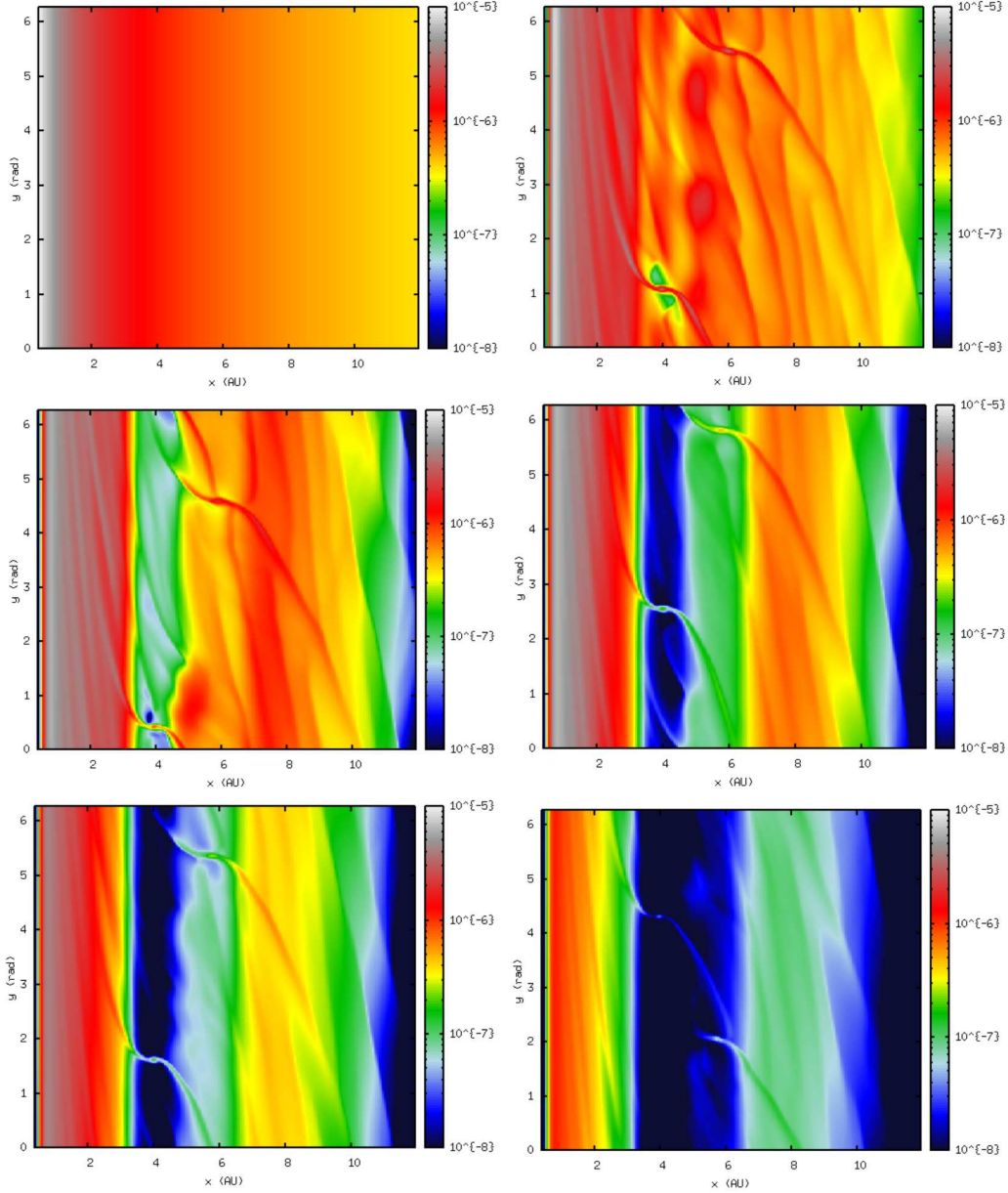
Figure 22: 3-dimensional snapshots of the superficial density of the disk at simulation times $t = 0\ syr$, $t = 10^3\ syr$, $t = 10^4\ syr$, $t = 10^5\ syr$, $t = 2 \cdot 10^5\ syr$ and $t = 5 \cdot 10^5\ syr$. The density is given in code units, being it a factor $8 \cdot 10^6$ smaller than the real value in g/cm^2. The simulation is made with PLUTO, using a grid resolution of 256 x 512 and damped outflow boundaries at both the inner and outer border of the disk.

are related to real times by a factor of 2π (1 $simulation\ year = 1\ syr = 2\pi\ yr$). At time $t = 0\ syr$ (top left panel), the superficial density has a value of $\Sigma_0 = 40\ g/cm^2$ at $r = 1\ AU$ and its profile is given by $\Sigma(r) = \Sigma_0 \cdot r^{-1}$. At time $t = 10^3\ syr$ (top right panel), the presence of the two planets has ignited the propagation of several density

waves through the disk. At time $t = 10^4\ syr$ (middle left panel), Jupiter is starting to open a gap in the disk. At time $t = 10^5\ syr$ (middle right panel), Jupiter has already opened a deep gap in the disk, while Saturn has only created a partial one. At $t = 2 \cdot 10^5\ syr$ (bottom left panel), the two planets have merged their gap into a single one and they are starting to migrate together. Finally, at $t = 5 \cdot 10^5\ syr$ (bottom right panel), the disk has already considerably dissipated, with the common gap being almost devoid of material. Let's now analyze the choice of using damped outflow boundary conditions at both the inner and outer border of the disk. At the inner border this type of boundary simulates the accretion of disk material onto the central star with good accuracy. On the other hand, at the outer border, the dissipation of material seems to be too high possibly due to the formation of waves which drive the gas out of the outer border, with the disk being truncated at roughly $r = 10\ AU$ after around $5 \cdot 10^5\ syr$. In order to avoid such high mass dissipation, it was chosen to run a simulation with a damped outflow boundary condition at the inner border of the disk and a reflective boundary at the outer border. All the other simulation parameters are kept the same as in the previous setup.
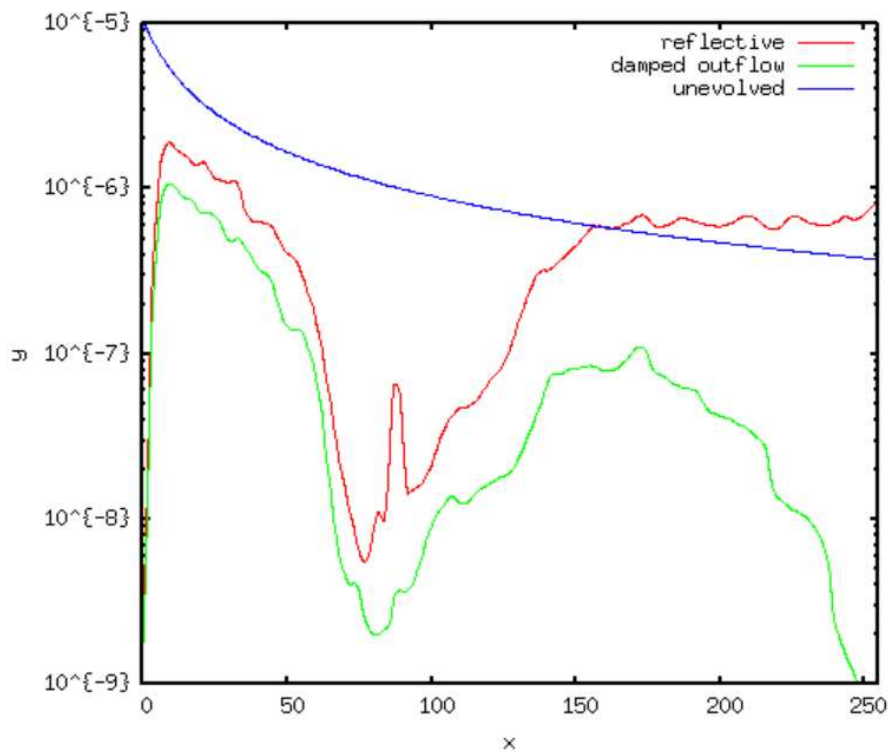

Figure 23: 2-dimensional plot of the superficial density of the disk. The x-axis represents the radial distance from the star, given in terms of the grid resolution. The y-axis expresses the superficial density in code units. The red and green profiles are both computed at a simulation time $t = 5 \cdot 10^5\ syr$, while the blue profile gives the initial superficial density of the disk. The simulations are made with PLUTO, using a grid resolution of 256 x 512 and a damped outflow boundary condition at the inner border of the disk.

As it is shown in Fig. 23, in this case the disk is able to retain significantly more material compared to the previous scenario. This fact is also observed in the 3-dimensional representations of the superficial density of the disk. As it was previously done, Fig. 24 provides six snapshots evaluated at the simulation times $t = 0\ syr$, $t = 10^3\ syr$, $t = 10^4\ syr$, $t = 10^5\ syr$, $t = 2 \cdot 10^5\ syr$ and $t = 5 \cdot 10^5\ syr$.
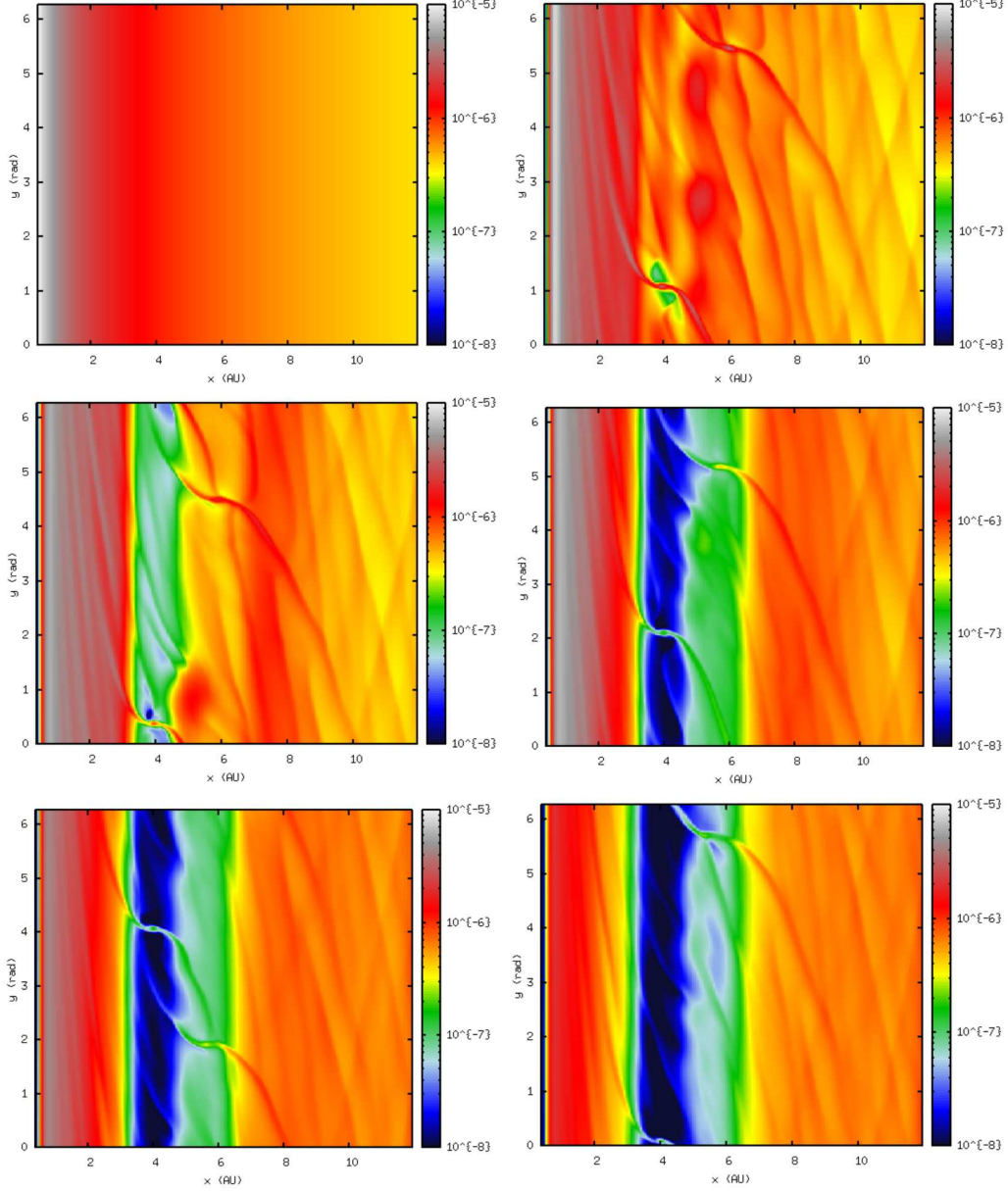
Figure 24: 3-dimensional snapshots of the superficial density of the disk at simulation times $t = 0\ syr$, $t = 10^3\ syr$, $t = 10^4\ syr$, $t = 10^5\ syr$, $t = 2 \cdot 10^5\ syr$ and $t = 5 \cdot 10^5\ syr$. The density is given in code units, being it a factor $8 \cdot 10^6$ smaller than the real value in g/cm^2. The simulation is made with PLUTO, using a grid resolution of 256 x 512 and damped outflow boundaries at inner border of the disk, while a reflective boundary is implemented at the outer border.

It is straightforward to notice how the outer edge of the disk has a higher surface density compared to the case in which the damped outflow boundary condition was implemented. However, this does not seem to affect the simulation results. In Fig. 25 it is given the time evolution of the semi-major axis of the two planets (green curves) superimposed to the results obtained previously (red curves).
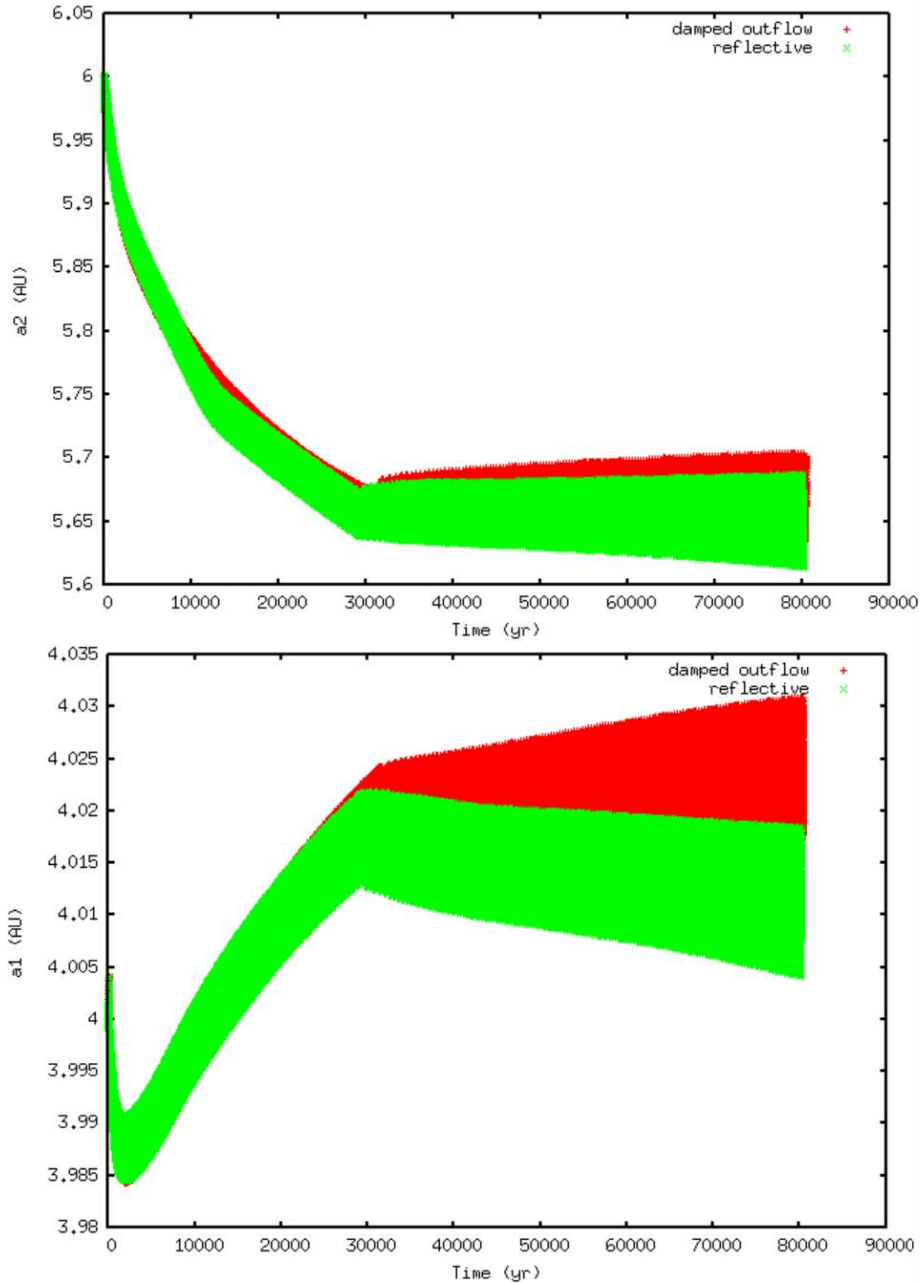

Figure 25: Time evolution of the semi-major axis for the external (top panel) and internal planet (bottom panel). The simulations are made with PLUTO, using a grid resolution of 256 x 512 and damped outflow boundaries at the inner border of the disk. The green curve refers to the case in which a reflective boundary is used at the outer border, while the red curve represents the results obtained previously with the damped outflow condition.

The migration of both Jupiter and Saturn within their parent protoplanetary disk is very similar in the two simulations, leading always to a capture in resonance after about $3 \cdot 10^4 \ yr$ from the start of their evolution. Once the two planets have merged their gaps, they start migrating together at a very slow pace.

It is clear from the figures that the two simulations involve the same type of resonance capture for the Jupiter-Saturn system. This fact is particularly evident in Fig 26, which shows the time evolution of the ratio between the semi-major axes of the two planets.
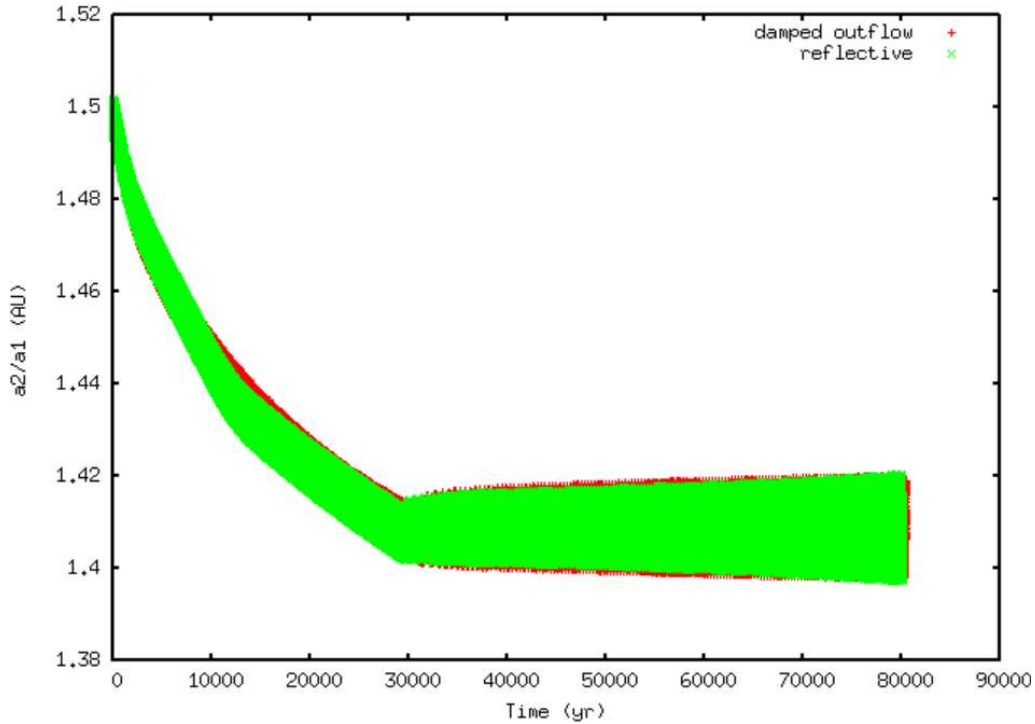

Figure 26: Time evolution of the ratio between the semi-major axes of the two planets. The simulations are made with PLUTO, using a grid resolution of 256 x 512 and damped outflow boundaries at the inner border of the disk. The green curve refers to the case in which a reflective boundary is used at the outer border, while the red curve represents the results obtained previously with the damped outflow condition.

Therefore, the resonance capable of driving the outward migration for a Jupiter-Saturn pair is again the second order 5:3 mean motion resonance, whose resonant argument's libration is provided in Fig. 27. Also in this case, the system attempts to enter the first order 2:1 and 3:2 mean motion resonances at the beginning of its evolution, quickly crossing them only to be finally captured in the 5:3 mean motion resonance.

6.2 Low-Resolution Simulations

The medium resolution case discussed in Sec. 6.1, based on a grid with $N_r = 256$ and $N_\theta = 512$, found that the resonance with the ability to induce an outward migration for a
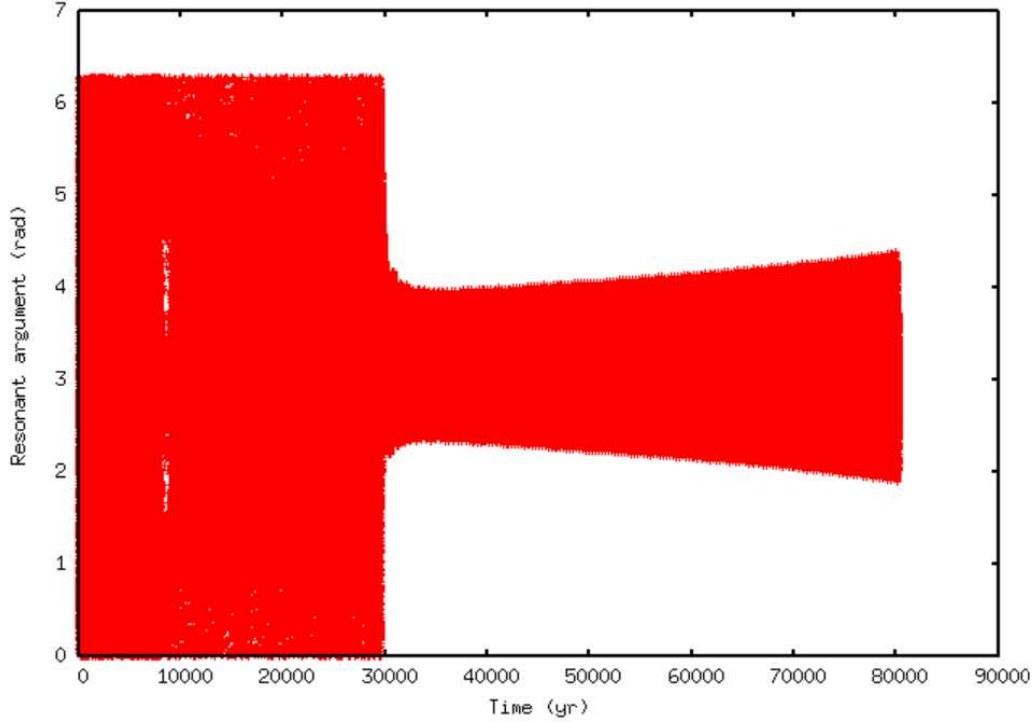
Figure 27: Time evolution of the resonant argument associated with the 5:3 mean motion resonance. The simulation is made with PLUTO, using a grid resolution of 256 x 512 and damped outflow - reflective boundaries at the inner and outer border of the disk, respectively.

Jupiter-Saturn pair is the second order 5:3 mean motion resonance and not the usual 3:2 commensurability.

In order to understand if the resolution of the model influences the type of resonance capable of driving the outward planet migration, it was chosen to run two simulations with a grid resolution of $N_r = 128$ and $N_\theta = 256$. This choice corresponds to the low-resolution case, having a resolution of one order of magnitude lower than the medium-resolution case. The setup conditions of the two simulations are the same used with the FARGO3D code and in Sec. 6.1. Both the simulations adopt a damped outflow boundary condition at the inner border of the disk. The first one uses a damped outflow boundary also at the outer border, while the second one implements a reflective boundary condition. In other words, it was decided to recreate the same simulations previously conducted, but at a lower resolution.

As it is shown in Fig. 28, in these new simulations the capture in resonance of the two planets occurs at a slightly longer time compared to the medium-resolution case. In particular, it takes place at a time of the order of $t = 4 \cdot 10^4 \ yr$, with a small difference based on the boundary condition implemented at the outer border of the disk. Nevertheless, the ratio's value of about $a_2/a_1 \approx 1.41$ again indicates that the two-planet system experiences

69

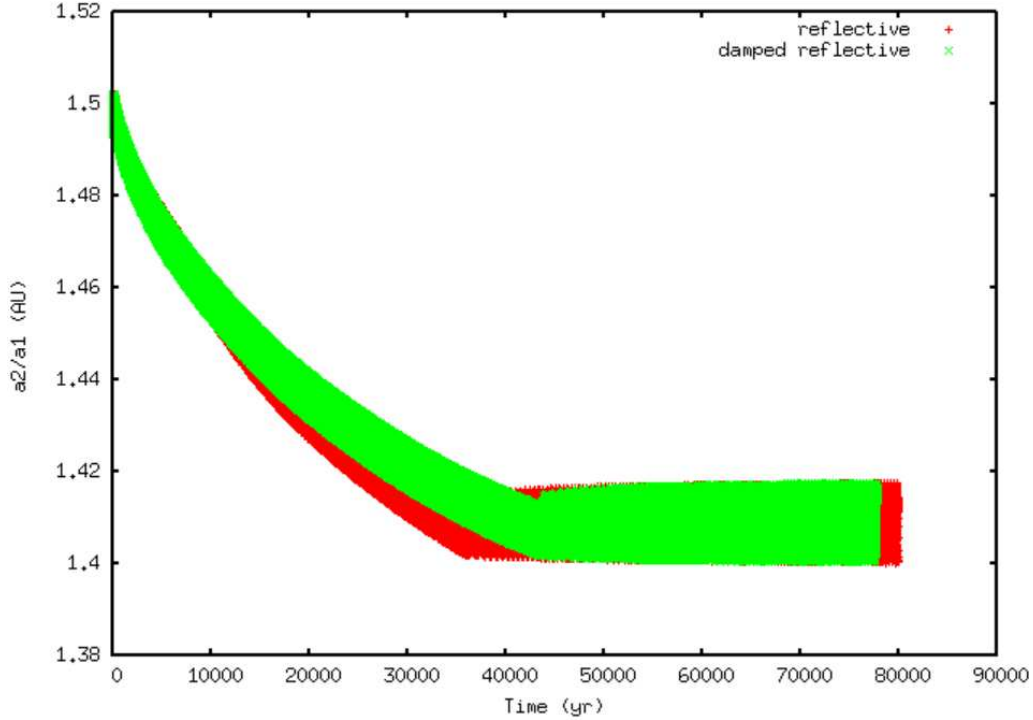a second order 5:3 mean motion resonance.

Figure 28: Time evolution of the ratio between the semi-major axes of the two planets. The simulations are made with PLUTO, using a grid resolution of 128 x 256 and damped outflow boundaries at the inner border of the disk. The red curve refers to the case in which a reflective boundary is used at the outer border, while the green curve represents the results obtained with the damped outflow condition.

This fact is also confirmed by the libration of both the resonant arguments associated to the 5:3 mean motion resonance, whose time evolution in the two different simulations is provided in Fig. 29.

As previously observed in the medium-resolution case, the system attempts to enter the first order 2:1 and 3:2 mean motion resonances at the beginning of its evolution, but it is again able to surpass these types of commensurability and to reach the final capture in the 5:3 mean motion resonance.

6.3 High-Resolution Simulations

To conclude the investigation about the influence of the model resolution on the resonance capable of driving the outward migration for a Jupiter-Saturn pair, it was decided to run a simulation with a grid resolution of $N_r = 384$ and $N_\theta = 768$. This way, the resolution of the grid is increased by a factor of 3 compared to the low-resolution case. Damped outflow boundaries are used at both the inner and outer border of the disk.

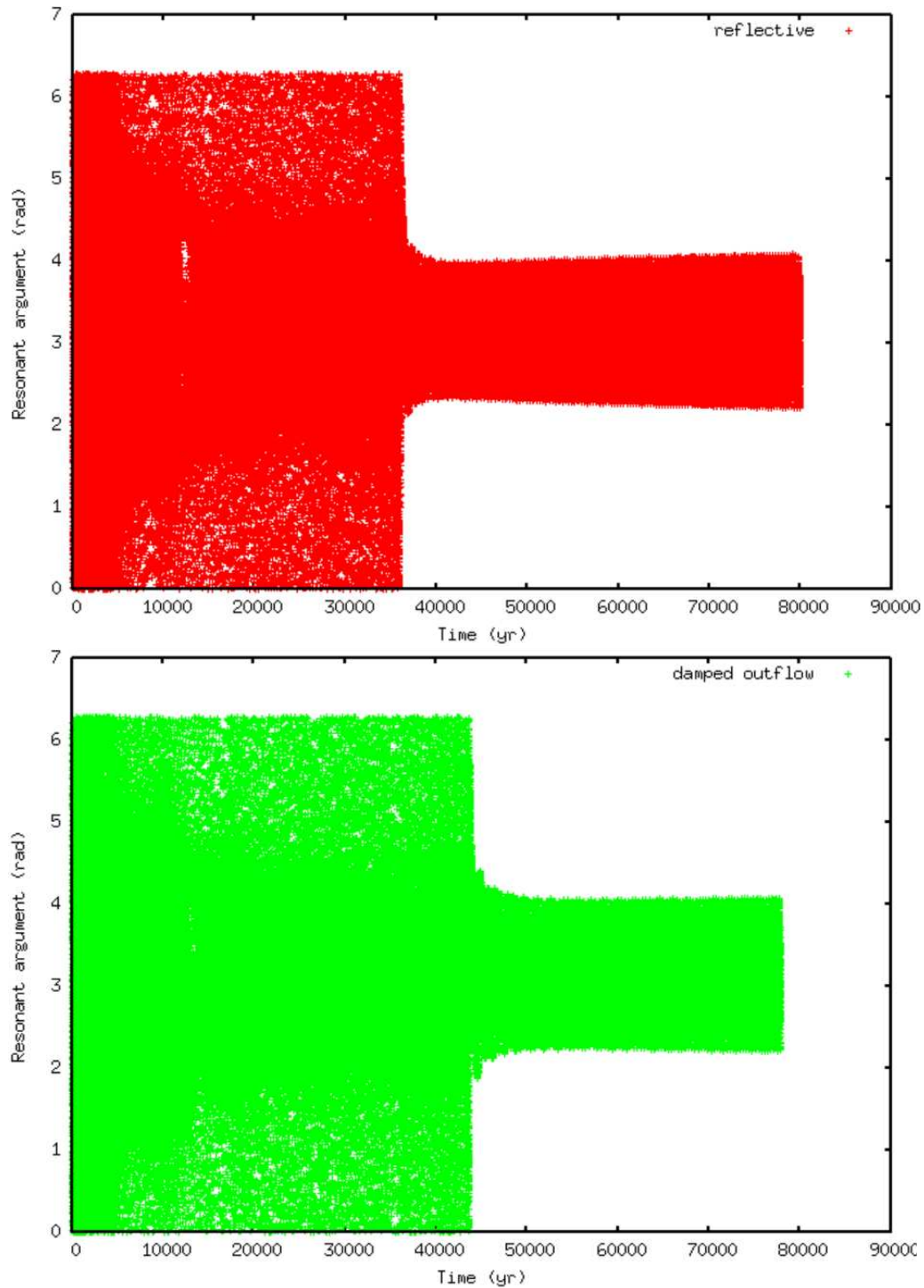The time evolution of the ratio between the semi-major axes of the two planets and of the

Figure 29: Time evolution of the resonant argument associated with the 5:3 mean motion resonance. The simulations are made with PLUTO, using a grid resolution of 128 x 256 and damped outflow boundaries at the inner border of the disk. The red curve (top panel) refers to the case in which a reflective boundary is used at the outer border, while the green curve (bottom panel) represents the results obtained with the damped outflow condition.

resonant argument associated to the 5:3 mean motion resonance are given in Fig. 30 and Fig. 31, respectively.
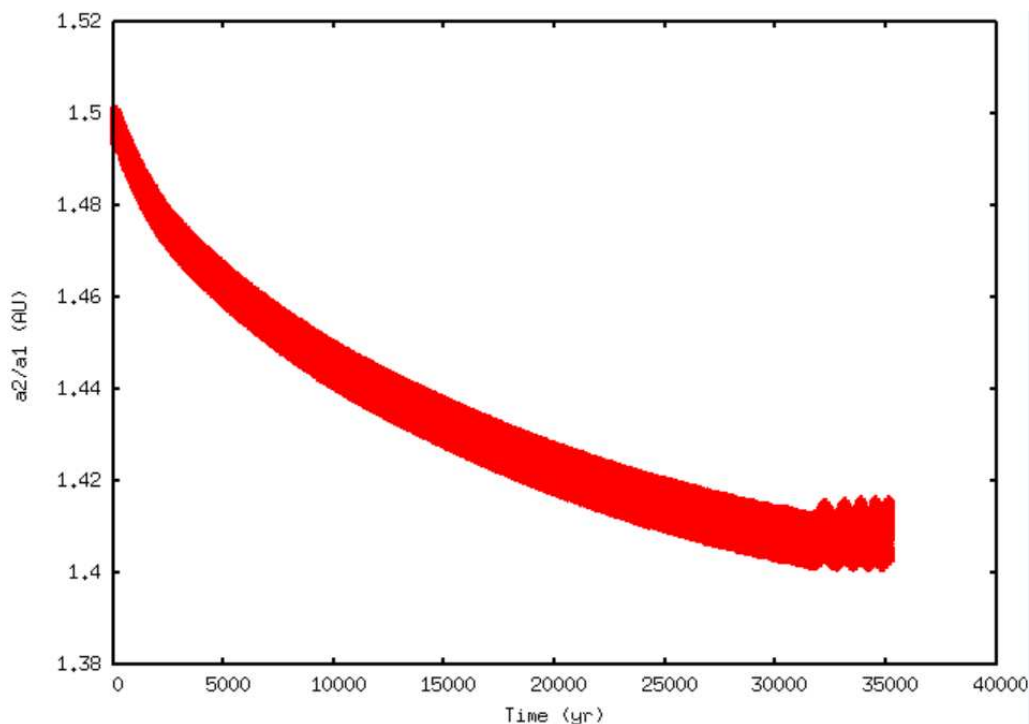

Figure 30: Time evolution of the ratio between the semi-major axes of the two planets. The simulation is made with PLUTO, using a grid resolution of 384 x 768 and damped outflow boundaries at both the inner and outer border of the disk.

It is immediate to note that they show the same results already obtained at lower resolutions. Independently on the model resolution, PLUTO finds that the resonance capable of driving the planets outward migration is the 5:3 mean motion resonance. The usual 3:2 commensurability is only approached at the beginning of the simulation as well as the 2:1 mean motion resonance, but they are easily surpassed by the Jupiter-Saturn system.

6.4 High Density Simulations

Historically, the first order 3:2 mean motion resonance was found using numerical programs with very high superficial densities, being them of the order of $\Sigma = 1000 - 1500 \ g/cm^2$ at $r = 1 \ AU$. However, the formation of planets was taken into account in this study, resulting in a lower superficial density. In particular, its value was set to be equal to $\Sigma = 40 \ g/cm^2$ at $r = 1 \ AU$, according to the study conducted by D'Angelo et al. [13].

In order to investigate the ability of PLUTO in handling the study of planet-disk interactions and planet migration, it was chosen to run a high density simulation, expecting to
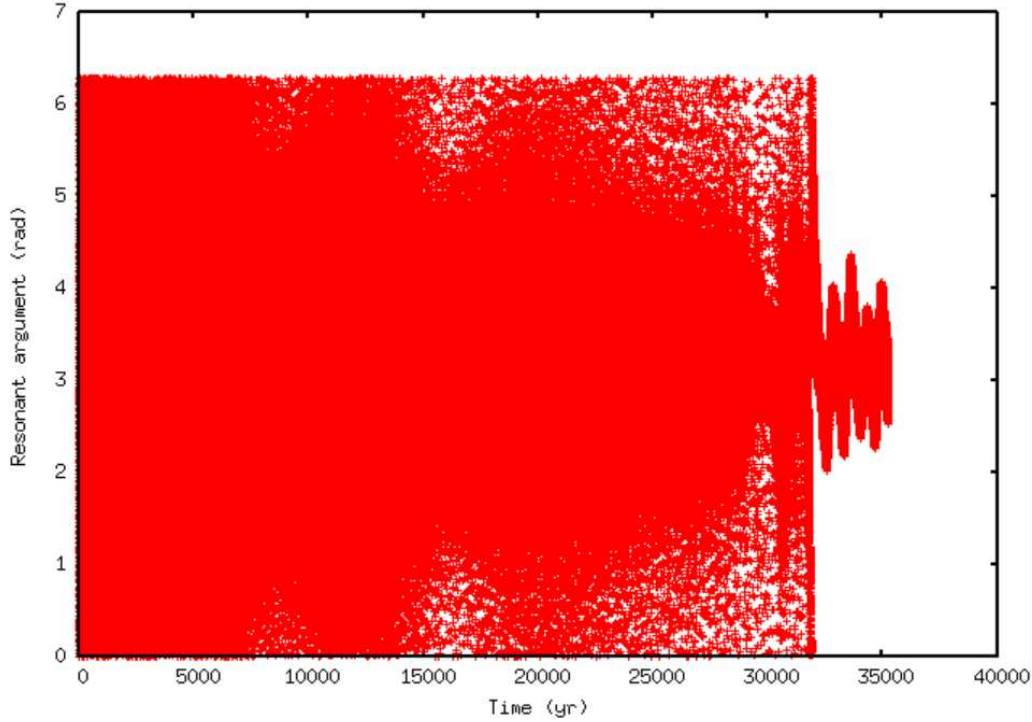
Figure 31: Time evolution of the resonant argument associated with the 5:3 mean motion resonance. The simulation is made with PLUTO, using a grid resolution of 384 x 768 and damped outflow boundaries at both the inner and outer border of the disk.

find the common 3:2 mean motion resonance. The adopted grid resolution is $N_r = 256$ and $N_\theta = 512$, while the superficial density is set to $\Sigma = 1500 \ g/cm^2$ at $r = 1 \ AU$. A damped outflow boundary condition is implemented at the inner border of the disk, while a reflective boundary is used at the outer border. The other setup parameters are the same used in all the previous simulations.

In Fig. 32, it is shown the time evolution of the semi-major axes of Saturn and Jupiter. In this high density case, the inward migration rate experienced by the two planets is much higher compared to the results obtained in the low-density case. Furthermore, the system covers a larger radial distance before being captured in resonance. By comparing the two density regimes, Saturn undergoes an inward migration of $r = 0.35 \ AU$ when $\Sigma_0 = 40 \ g/cm^2$, while it reaches a radial displacement of the order of $r = 1.4 \ AU$ when $\Sigma_0 = 1500 \ g/cm^2$. Jupiter's inward migration switches instead from $r = 0.015 \ AU$ to a value of $r = 0.65 \ AU$, without reversing the direction of its motion in the high density regime.

The time evolution of the ratio between the semi-major axes of Saturn and Jupiter is provided in Fig. 33. The capture in resonance of the two planets starts with a certain degree of instability early on in the simulation and then it progressively stabilizes over time. This happens much earlier with respect to the results obtained previously, when it was found a

73

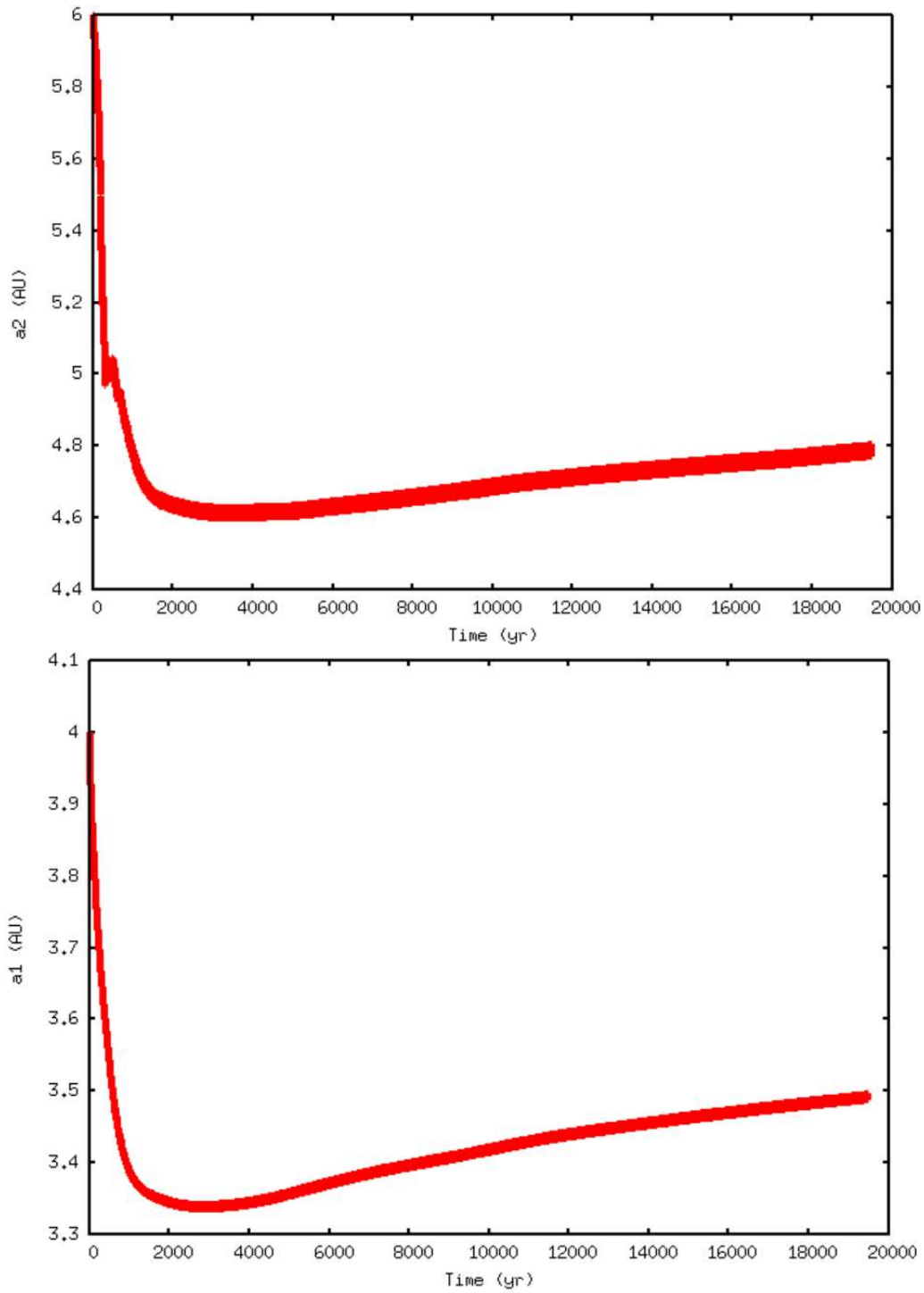Figure 32: Time evolution of the semi-major axis for the external (top panel) and internal planet (bottom panel). The simulation is made with PLUTO, using a grid resolution of 256 x 512 and a superficial density of $\Sigma = 1500 \ g/cm^2$ at $r = 1 \ AU$. A damped outflow boundary condition is implemented at the inner border of the disk, while a reflective boundary is used at the outer border.

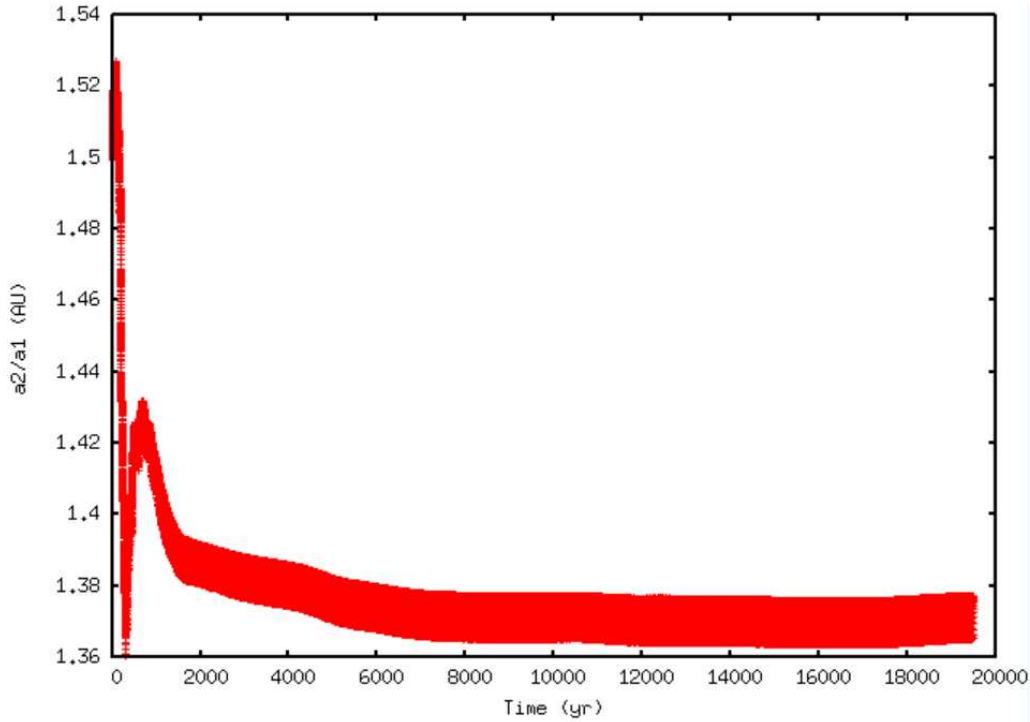capture in resonance after about $t = 3 \cdot 10^4 \ yr$.

Figure 33: Time evolution of the ratio between the semi-major axes of the two planets. The simulations are made with PLUTO, using a grid resolution of 256 x 512 and a superficial density of $\Sigma = 1500 \ g/cm^2$ at $r = 1 \ AU$. A damped outflow boundary condition is implemented at the inner border of the disk, while a reflective boundary is used at the outer border.

Fig. 34 provides instead the time evolution of the resonant argument associated with the first order 3:2 mean motion resonance. The libration of this angle demonstrates the capability of the PLUTO code to find the commonly accepted mean motion resonance that drives the planets' outward migration in the case of high superficial density. As a consequence, it is possible to conclude that PLUTO is able of effectively studying planet-disk interactions and specifically planet migration.

6.5 Discussion

As it was anticipated in Sec. 4.1, the hydrodynamical code PLUTO was used to analyze the results obtained in the preliminary simulations conducted with the FARGO3D code. In these 2-dimensional simulations, performed in the low-density regime, it was found that the type of commensurability capable of driving the outward migration for a Jupiter-Saturn pair changes depending on the model resolution.

In particular, it was observed that by increasing the grid resolution by a factor of 3, it is the second-order 5:3 mean motion resonance to drive the planet outward migration and
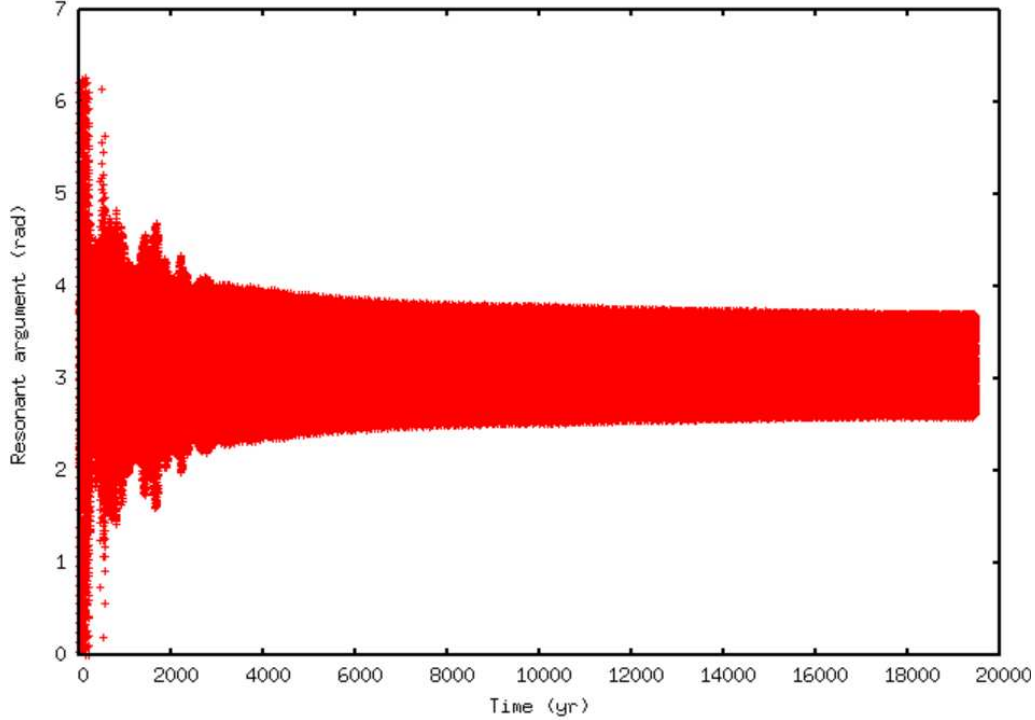
Figure 34: Time evolution of the resonant argument associated with the 3:2 mean motion resonance. The simulations are made with PLUTO, using a grid resolution of 256 x 512 and a superficial density of $\Sigma = 1500 \ g/cm^2$ at $r = 1 \ AU$. A damped outflow boundary condition is implemented at the inner border of the disk, while a reflective boundary is used at the outer border.

not the usual 3:2 commensurability. Therefore, the aim of this work was to investigate whether the observed outcomes were due to an intrinsic issue within the FARGO3D code or if the resolution of the model indeed influences the type of resonance capable of driving the outward migration.

In order to verify which of the two solutions is correct, it was chosen to run several simulations with the PLUTO code, by adopting the same setup conditions that were used with the FARGO3D code. More specifically, simulations covering three orders of magnitude in grid resolution have been executed, ranging from $N_r = 128$ and $N_\theta = 256$ to $N_r = 384$ and $N_\theta = 768$. It was chosen to use a damped outflow boundary condition at the inner border of the disk, which enables the accretion of disk material onto the central star. At the outer border, it was decided to employ both a damped outflow boundary and a reflective boundary. The low-density condition implies a superficial density of the order of $\Sigma = 40 \ g/cm^2$ at $r = 1 \ AU$, a value that takes into account the time required for the formation of planets within the protoplanetary disk.

Independently of the model resolution, all the results obtained suggest that the resonance capable of driving the outward migration for a Jupiter-Saturn pair is the second order 5:3

mean motion resonance. The two-planet system attempts to enter both the first order 2:1 and 3:2 resonances at the beginning of the simulation, but eventually crosses these commensurabilities and it continues its evolution until its final capture in the 5:3 mean motion resonance.

It was then decided to investigate the ability of PLUTO in handling the study of planet-disk interactions and planet migration. Historically, the 3:2 mean motion resonance was found using numerical programs with much higher densities, i.e. without taking into account planet formation within the disk. For this reason, it was chosen to run a simulation with a superficial density of the order of $\Sigma = 1500 \ g/cm^2$ at $r = 1 \ AU$, expecting to find the common 3:2 commensurability. This is precisely what comes out of the simulation, thus confirming that PLUTO is effectively able to study this type of problems.

In Sec. 5.7, it was pointed out that while PLUTO and FARGO3D are both hydrodynamical codes used for simulating fluid dynamics, they have some differences in their features and focus areas. In particular, the main distinction between the two codes is based on the different numerical methods used to solve the equations of fluid dynamics. PLUTO exploits a Godunov-type shock-capturing scheme using the finite volume formalism. Within this context, volume averages are first reconstructed employing piecewise monotonic interpolants inside each computational cell. Subsequently, a Riemann problem is solved at each interface and the solution is evolved in time. This approach is well-suited for capturing highly supersonic flows in the presence of strong discontinuities.

Conversely, FARGO3D is based on a finite-difference method that employs operator splitting and upwind techniques. Instead of using the Riemann problem to evaluate the fluxes at each interface, it exploits the staggering of the velocity field to express the flux in a simpler way. This code is specifically designed for modeling accretion disks in astrophysical contexts and it is highly compatible with the study of planet-disk interactions and planet migration.

Both PLUTO and FARGO3D are capable of achieving similar levels of numerical precision. However, PLUTO is a more versatile hydrodynamical code, offering many capabilities that can contribute to obtain accurate simulations of planet migration. On the other hand, FARGO3D is specifically designed for modeling accretion disks, but it provides a simpler treatment of the fluxes.

Based on this information and on the results obtained from the performed simulations, it is possible to conclude that PLUTO seems to handle the study of planet migration more precisely. In fact, it provides the same results achieved with the FARGO3D code when using a very dense grid even in the case of low resolution. In other words, it appears to be comparable to the use of FARGO3D with a higher grid resolution. The resonance capable of driving the outward migration for a Jupiter-Saturn pair in the low-density regime seems

to be the second order 5:3 mean motion resonance and not the usual 3:2 commensurability. This fact is independent on the model resolution, which implies that the question arising from the preliminary simulations conducted with FARGO3D is due to an intrinsic issue within the code.

7 Conclusions

In this work, it was chosen to use numerical modeling in order to investigate the outward migration of a Jupiter-Saturn pair in resonance within a circumstellar disk. The aim was to understand the effects of model resolution on the migration behaviour and to compare the performances of two hydrodynamical codes, namely FARGO3D and PLUTO, in handling planet-disk interactions.

The 2-dimensional preliminary simulations conducted with FARGO3D in the low-density regime revealed that the type of resonance capable of driving the planet outward migration changes depending on the model resolution. Specifically, the low-resolution case exhibited the usual 3:2 commensurability, while increasing the resolution by a factor of 3 resulted in the second-order 5:3 mean motion resonance driving the migration.

To verify the validity of these findings and explore the role of model resolution further, 2-dimensional hydrodynamical simulations were conducted using the PLUTO code with different grid resolutions. In particular, it was chosen to use a 128 x 256 grid for the low-resolution case, a 256 x 512 grid for the medium-resolution case and a 384 x 768 grid for the high resolution case. It was also decided to use different boundary conditions at the outer border of the disk, implementing both a damped outflow and a reflective boundary. All the results consistently showed that the second order 5:3 mean motion resonance is the driving force behind the outward migration of a Jupiter-Saturn pair in the low-density regime. The first order 3:2 commensurability is only crossed at the beginning of the simulation, as well as the 2:1 mean motion resonance, but they are surpassed by the two-planet system. This outcome is achieved regardless of the model resolution, thus suggesting that the question arising from the preliminary simulations is due to an intrinsic issue within the FARGO3D code.

Additionally, by performing simulations in the high-density regime, it was proved that PLUTO is capable of accurately studying planet migration and handling planet-disk interactions. This follows from the fact that the 3:2 mean motion resonance was historically discovered by using numerical models that did not account for planet formation within the disk and used high values for the gas surface density. Since PLUTO effectively finds this type of commensurability under the above mentioned conditions, it means that the code has the ability to treat this type of problems.

PLUTO's versatility and numerical precision make it a valuable tool for investigating complex phenomena in astrophysical contexts. While FARGO3D is specifically designed for modeling accretion disks, PLUTO offers comparable results that are not influenced by the resolution of the model. Until the issue encountered within the FARGO3D code is fixed, it is safe to conclude that PLUTO offers a more accurate and reliable approach to the study of the outward migration of two planets in resonance.

In conclusion, the investigation of resonant migration between two planets is a fascinating area for future research, thanks primarily to increasingly available computational power. By refining our understanding of planetary dynamics and of the complex interactions within planetary systems, future studies can explore the mechanisms and consequences of resonant migration in greater detail. Exploring different scenarios, boundary conditions and numerical models can contribute to a more comprehensive understanding of this phenomenon. Furthermore, advancements in observational techniques and data analysis will also contribute to the validation of theoretical predictions and to the improvement of present-day models. This way, it will be possible to obtain new insights into the formation and evolution of planetary systems.

References

[1] Simon Albrecht et al. "Obliquities of Hot Jupiter Host Stars: Evidence for Tidal Interactions and Primordial Misalignments". In: *The Astrophysical Journal* 757.1, 18 (Sept. 2012), p. 18. DOI: `10.1088/0004-637X/757/1/18`.

[2] C. Baruteau et al. "Planet-Disk Interactions and Early Evolution of Planetary Systems". In: *Protostars and Planets VI*. University of Arizona Press, 2014. DOI: `10.2458/azu_uapress_9780816531240-ch029`.

[3] K. Batygin and A. Morbidelli. "Analytical treatment of planetary resonances". In: *Astronomy & Astrophysics* 556 (July 2013), A28. DOI: `10.1051/0004-6361/201220907`.

[4] Steven V. W. Beckwith et al. "A Survey for Circumstellar Disks around Young Stellar Objects". In: *The Astronomical Journal* 99 (Mar. 1990), p. 924. DOI: `10.1086/115385`.

[5] Pablo Benıtez-Llambay and Frédéric S. Masset. "FARGO3D: A New GPU-oriented MHD Code". In: *The Astrophysical Journal Supplement Series* 223.1, 11 (Mar. 2016), p. 11. DOI: `10.3847/0067-0049/223/1/11`.

[6] B. Bitsch and W. Kley. "Evolution of inclined planets in three-dimensional radiative discs". In: *Astronomy & Astrophysics* 530 (May 2011), A41. DOI: `10.1051/0004-6361/201016179`.

[7] B. Bitsch and W. Kley. "Orbital evolution of eccentric planets in radiative discs". In: *Astronomy & Astrophysics* 523 (Nov. 2010), A30. DOI: `10.1051/0004-6361/201014414`.

[8] B. Bitsch et al. "Highly inclined and eccentric massive planets". In: *Astronomy & Astrophysics* 555 (July 2013), A124. DOI: `10.1051/0004-6361/201220310`.

[9] J. Blum and G. Wurm. "The growth mechanisms of macroscopic bodies in protoplanetary disks." In: *Annual Rewiew of Astronomy and Astrophysics* 46 (Sept. 2008), pp. 21–56. DOI: `10.1146/annurev.astro.46.060407.145152`.

[10] Sourav Chatterjee and Jonathan C. Tan. "Inside-out Planet Formation". In: *The Astrophysical Journal* 780.1, 53 (Jan. 2014), p. 53. DOI: `10.1088/0004-637X/780/1/53`.

[11] A. Crida and A. Morbidelli. "Cavity opening by a giant planet in a protoplanetary disc and effects on planetary migration". In: *Monthly Notices of the Royal Astronomical Society* 377.3 (May 2007), pp. 1324–1336. DOI: `10.1111/j.1365-2966.2007.11704.x`.

[12]   A. Crida, A. Morbidelli, and F. Masset. "On the width and shape of gaps in proto-planetary disks". In: *Icarus* 181.2 (Apr. 2006), pp. 587–604. DOI: `10.1016/j.icarus.2005.10.007`.

[13]   Gennaro D'Angelo and Francesco Marzari. "Outward Migration of Jupiter and Saturn in Evolved Gaseous Disks". In: *The Astrophysical Journal* 757.1 (Sept. 2012), p. 50. DOI: `10.1088/0004-637x/757/1/50`.

[14]   J. Drazkowska and Y. Alibert. "Planetesimal formation starts at the snow line". In: *Astronomy & Astrophysics* 608 (Dec. 2017), A92. DOI: `10.1051/0004-6361/201731491`.

[15]   N. Dzyurkevich et al. "Trapping solids at the inner edge of the dead zone: 3-D global MHD simulations". In: *Astronomy & Astrophysics* 515 (June 2010), A70. DOI: `10.1051/0004-6361/200912834`.

[16]   Stephen M. Fendyke and Richard P. Nelson. "On the corotation torque for low-mass eccentric planets". In: *Monthly Notices of the Royal Astronomical Society* 437.1 (Oct. 2013), pp. 96–107. DOI: `10.1093/mnras/stt1867`.

[17]   P. Goldreich and S. Tremaine. "Disk-satellite interactions." In: *The Astrophysical Journal* 241 (Oct. 1980), pp. 425–441. DOI: `10.1086/158356`.

[18]   P. Goldreich and S. Tremaine. "The excitation of density waves at the Lindblad and corotation resonances by an external potential." In: *The Astrophysical Journal* 233 (Nov. 1979), pp. 857–871. DOI: `10.1086/157448`.

[19]   Erik Gullbring et al. "The Structure and Emission of the Accretion Shock in T Tauri Stars. II. The Ultraviolet-Continuum Emission". In: *The Astrophysical Journal* 544.2 (Dec. 2000), pp. 927–932. DOI: `10.1086/317253`.

[20]   Lee Hartmann, Gregory Herczeg, and Nuria Calvet. "Accretion onto Pre-Main-Sequence Stars". In: *Annual Rewiew of Astronomy and Astrophysics* 54 (Sept. 2016), pp. 135–180. DOI: `10.1146/annurev-astro-081915-023347`.

[21]   J. Henrard and A. Lemaitre. "A Second Fundamental Model for Resonance". In: *Celestial Mechanics* 30.2 (June 1983), pp. 197–218. DOI: `10.1007/BF01234306`.

[22]   P. B. Ivanov and J. C. B. Papaloizou. "On the tidal interaction of massive extrasolar planets on highly eccentric orbits". In: *Monthly Notices of the Royal Astronomical Society* 347.2 (Jan. 2004), pp. 437–453. DOI: `10.1111/j.1365-2966.2004.07238.x`.

[23]   A. Johansen and A. Youdin. "Protoplanetary Disk Turbulence Driven by the Streaming Instability: Nonlinear Saturation and Particle Concentration". In: *The Astrophysical Journal* 662.1 (June 2007), pp. 627–641. DOI: `10.1086/516730`.

[24] Scott J. Kenyon and Benjamin C. Bromley. "Terrestrial Planet Formation. I. The Transition from Oligarchic Growth to Chaotic Growth". In: *The Astronomical Journal* 131.3 (Mar. 2006), pp. 1837–1850. DOI: 10.1086/499807.

[25] W. Kley, J. Peitz, and G. Bryden. "Evolution of planetary systems in resonance". In: *Astronomy & Astrophysics* 414.2 (Jan. 2004), pp. 735–747. DOI: 10.1051/0004-6361:20031589.

[26] Eiichiro Kokubo and Shigeru Ida. "Oligarchic Growth of Protoplanets". In: *Icarus* 131.1 (1998), pp. 171–178. DOI: https://doi.org/10.1006/icar.1997.5840.

[27] Jacques Laskar and Philippe Robutel. "Stability of the Planetary Three-Body Problem. I. Expansion of the Planetary Hamiltonian". In: *Celestial Mechanics and Dynamical Astronomy* 62.3 (July 1995), pp. 193–217. DOI: 10.1007/BF00692088.

[28] D. N. C. Lin and John Papaloizou. "On the Tidal Interaction between Protoplanets and the Protoplanetary Disk. III. Orbital Migration of Protoplanets". In: *The Astrophysical Journal* 309 (Oct. 1986), p. 846. DOI: 10.1086/164653.

[29] Wladimir Lyra, Sijme-Jan Paardekooper, and Mordecai-Mark Mac Low. "Orbital Migration of Low-mass Planets in Evolutionary Radiative Models: Avoiding Catastrophic Infall". In: *The Astrophysical Journal Letters* 715.2 (June 2010), pp. L68–L73. DOI: 10.1088/2041-8205/715/2/L68.

[30] Francesco Marzari. *Planetary Astrophysics*. 2023.

[31] F. Masset and M. Snellgrove. "Reversing type II migration: resonance trapping of a lighter giant protoplanet". In: *Monthly Notices of the Royal Astronomical Society* 320.4 (Feb. 2001), pp. L55–L59. DOI: 10.1046/j.1365-8711.2001.04159.x.

[32] F. S. Masset. "Planet Disk Interactions". In: *EAS Publications Series*. Ed. by M. -J. Goupil and J. -P. Zahn. Vol. 29. EAS Publications Series. Jan. 2008, pp. 165–244. DOI: 10.1051/eas:0829006.

[33] Michel Mayor and Didier Queloz. "A Jupiter-mass companion to a solar-type star". In: *Nature* 378.6555 (Nov. 1995), pp. 355–359. DOI: 10.1038/378355a0.

[34] A. Mignone et al. "PLUTO: A Numerical Code for Computational Astrophysics". In: *The Astrophysical Journal Supplement Series* 170.1 (May 2007), pp. 228–242. DOI: 10.1086/513316.

[35] A. Morbidelli et al. "Building giant-planet cores at a planet trap". In: *Astronomy & Astrophysics* 478.3 (Nov. 2007), pp. 929–937. DOI: 10.1051/0004-6361:20078546.

[36] Alessandro Morbidelli. *Modern celestial mechanics : aspects of solar system dynamics*. 2002.

[37] C. D. Murray and S. F. Dermott. *Solar system dynamics*. 1999.

[38] Alexander J. Mustill and Mark C. Wyatt. "A general model of resonance capture in planetary systems: first- and second-order resonances". In: *Monthly Notices of the Royal Astronomical Society* 413.1 (May 2011), pp. 554–572. DOI: `10.1111/j.1365-2966.2011.18201.x`.

[39] M. Nagasawa, S. Ida, and T. Bessho. "Formation of Hot Planets by a Combination of Planet Scattering, Tidal Circularization, and the Kozai Mechanism". In: *The Astrophysical Journal* 678.1 (May 2008), pp. 498–508. DOI: `10.1086/529369`.

[40] R. P. Nelson. "On the orbital evolution of low mass protoplanets in turbulent, magnetised disks". In: *Astronomy & Astrophysics* 443.3 (Nov. 2005), pp. 1067–1085. DOI: `10.1051/0004-6361:20042605`.

[41] Richard P. Nelson and John C. B. Papaloizou. "Possible commensurabilities among pairs of extrasolar planets". In: *Monthly Notices of the Royal Astronomical Society* 333.2 (June 2002), pp. L26–L30. DOI: `10.1046/j.1365-8711.2002.05506.x`.

[42] G. I. Ogilvie and S. H. Lubow. "On the wake generated by a planet in a disc". In: *Monthly Notices of the Royal Astronomical Society* 330.4 (Mar. 2002), pp. 950–954. DOI: `10.1046/j.1365-8711.2002.05148.x`.

[43] Yasuhiro Ohta, Atsushi Taruya, and Yasushi Suto. "The Rossiter-McLaughlin Effect and Analytic Radial Velocity Curves for Transiting Extrasolar Planetary Systems". In: *The Astrophysical Journal* 622.2 (Apr. 2005), pp. 1118–1135. DOI: `10.1086/428344`.

[44] C. W. Ormel and H. H. Klahr. "The effect of gas drag on the growth of protoplanets". In: *Astronomy & Astrophysics* 520 (Sept. 2010), A43. DOI: `10.1051/0004-6361/201014903`.

[45] S. -J. Paardekooper et al. "A torque formula for non-isothermal type I planetary migration - I. Unsaturated horseshoe drag". In: *Monthly Notices of the Royal Astronomical Society* 401.3 (Jan. 2010), pp. 1950–1964. DOI: `10.1111/j.1365-2966.2009.15782.x`.

[46] S.-J. Paardekooper and J. C. B. Papaloizou. "On disc protoplanet interactions in a non-barotropic disc with thermal diffusion". In: *Astronomy & Astrophysics* 485.3 (May 2008), pp. 877–895. DOI: `10.1051/0004-6361:20078702`.

[47] J. C. B. Papaloizou and J. D. Larwood. "On the orbital evolution and growth of protoplanets embedded in a gaseous disc". In: *Monthly Notices of the Royal Astronomical Society* 315.4 (July 2000), pp. 823–833. DOI: 10.1046/j.1365-8711.2000.03466.x.

[48] P. Pinilla, M. Benisty, and T. Birnstiel. "Ring shaped dust accumulation in transition disks". In: *Astronomy & Astrophysics* 545 (Sept. 2012), A81. DOI: 10.1051/0004-6361/201219315.

[49] Dongsu Ryu et al. "A Cosmological Hydrodynamic Code Based on the Total Variation Diminishing Scheme". In: *The Astrophysical Journal* 414 (Sept. 1993), p. 1. DOI: 10.1086/173051.

[50] Zsolt Sandor, Wladimir Lyra, and Cornelis P. Dullemond. "Formation of planetary cores at type I migrations traps". In: *The Astrophysical Journal* 728.1 (Jan. 2011), p. L9. DOI: 10.1088/2041-8205/728/1/19.

[51] G. Schneider et al. "NICMOS Coronagraphic Observations of the GM Aurigae Circumstellar Disk". In: *The Astronomical Journal* 125.3 (Mar. 2003), pp. 1467–1479. DOI: 10.1086/367596.

[52] M. D. Snellgrove, J. C. B. Papaloizou, and R. P. Nelson. "On disc driven inward migration of resonantly coupled planets with application to the system around GJ876". In: *Astronomy & Astrophysics* 374.3 (Aug. 2001), pp. 1092–1099. DOI: 10.1051/0004-6361:20010779.

[53] James M. Stone and Michael L. Norman. "ZEUS-2D: A Radiation Magnetohydrodynamics Code for Astrophysical Flows in Two Space Dimensions. I. The Hydrodynamic Algorithms and Tests". In: *The Astrophysical Journal Supplement Series* 80 (June 1992), p. 753. DOI: 10.1086/191680.

[54] Genya Takeda and Frederic A. Rasio. "High Orbital Eccentricities of Extrasolar Planets Induced by the Kozai Mechanism". In: *The Astrophysical Journal* 627.2 (July 2005), pp. 1001–1010. DOI: 10.1086/430467.

[55] Hidekazu Tanaka, Taku Takeuchi, and William R. Ward. "Three-Dimensional Interaction between a Planet and an Isothermal Gaseous Disk. I. Corotation and Lindblad Torques and Planet Migration". In: *The Astrophysical Journal* 565.2 (Feb. 2002), pp. 1257–1274. DOI: 10.1086/324713.

[56] Hidekazu Tanaka and William R. Ward. "Three-dimensional Interaction between a Planet and an Isothermal Gaseous Disk. II. Eccentricity Waves and Bending Waves". In: *The Astrophysical Journal* 602.1 (Feb. 2004), pp. 388–395. DOI: 10.1086/380992.

[57] Peggy Varniere, A. C. Quillen, and Adam Frank. "The Evolution of Protoplanetary Disk Edges". In: *The Astrophysical Journal* 612.2 (Sept. 2004), pp. 1152–1162. DOI: 10.1086/422542.

[58] Kevin J. Walsh et al. "A low mass for Mars from Jupiter's early gas-driven migration". In: *Nature* 475.7355 (July 2011), pp. 206–209. DOI: 10.1038/nature10201.

[59] W. R. Ward. "Horsehoe Orbit Drag". In: *Lunar and Planetary Science Conference*. Vol. 22. Lunar and Planetary Science Conference. Mar. 1991, p. 1463.

[60] William R. Ward. "Protoplanet Migration by Nebula Tides". In: *Icarus* 126.2 (Apr. 1997), pp. 261–281. DOI: 10.1006/icar.1996.5647.

[61] S. J. Weidenschilling et al. "Accretional Evolution of a Planetesimal Swarm". In: *Icarus* 128.2 (Aug. 1997), pp. 429–455. DOI: 10.1006/icar.1997.5747.

[62] Stuart J. Weidenschilling and Francesco Marzari. "Gravitational scattering as a possible origin for giant planets at small stellar distances". In: *Nature* 384.6610 (Dec. 1996), pp. 619–621. DOI: 10.1038/384619a0.

[63] A. Zsom et al. "The outcome of protoplanetary dust growth: pebbles, boulders, or planetesimals?" In: *Astronomy & Astrophysics* 513 (Apr. 2010), A57. DOI: 10.1051/0004-6361/200912976.